NUREG/CR-5261
BNL-NUREG-52174

Safety Evaluation of MHTGR Licensing Basis Accident Scenarios

Prepared by P.G. Kroeger

Brookhaven National Laboratory

Prepared for
U.S. Nuclear Regulatory
Commission

AVAILABILITY NOTICE

Availability of Reference Materials Cited in NRC Publications

Most documents cited in NRC publications will be available from one of the following sources:

1. The NRC Public Document Room, 2120 L Street, NW, Lower Level, Washington, DC 20555

2. The Superintendent of Documents, U.S. Government Printing Office, P.O. Box 37082, Washington, DC 20013-7082

3. The National Technical Information Service, Springfield, VA 22161

Although the listing that follows represents the majority of documents cited in NRC publications, it is not intended to be exhaustive.

Referenced documents available for inspection and copying for a fee from the NRC Public Document Room include NRC correspondence and internal NRC memoranda; NRC Office of Inspection and Enforcement bulletins, circulars, information notices, inspection and investigation notices; Licensee Event Reports; vendor reports and correspondence; Commission papers; and applicant and licensee documents and correspondence.

The following documents in the NUREG series are available for purchase from the GPO Sales Program: formal NRC staff and contractor reports, NRC-sponsored conference proceedings, and NRC booklets and brochures. Also available are Regulatory Guides, NRC regulations in the *Code of Federal Regulations*, and *Nuclear Regulatory Commission Issuances*.

Documents available from the National Technical Information Service include NUREG series reports and technical reports prepared by other federal agencies and reports prepared by the Atomic Energy Commission, forerunner agency to the Nuclear Regulatory Commission.

Documents available from public and special technical libraries include all open literature items, such as books, journal and periodical articles, and transactions. *Federal Register* notices, federal and state legislation, and congressional reports can usually be obtained from these libraries.

Documents such as theses, dissertations, foreign reports and translations, and non-NRC conference proceedings are available for purchase from the organization sponsoring the publication cited.

Single copies of NRC draft reports are available free, to the extent of supply, upon written request to the Office of Information Resources Management, Distribution Section, U.S. Nuclear Regulatory Commission, Washington, DC 20555.

Copies of industry codes and standards used in a substantive manner in the NRC regulatory process are maintained at the NRC Library, 7920 Norfolk Avenue, Bethesda, Maryland, and are available there for reference use by the public. Codes and standards are usually copyrighted and may be purchased from the originating organization or, if they are American National Standards, from the American National Standards Institute, 1430 Broadway, New York, NY 10018.

NUREG/CR-5261
BNL-NUREG-52174
R1, R7, R8

Safety Evaluation of MHTGR Licensing Basis Accident Scenarios

Manuscript Completed: October 1988
Date Published: April 1989

Prepared by
P.G. Kroeger

Brookhaven National Laboratory
Upton, NY 11973

Prepared for
Division of Regulatory Applications
Office of Nuclear Regulatory Research
U.S. Nuclear Regulatory Commission
Washington, DC 20555
NRC FIN A3827

ABSTRACT

The safety potential of the Modular High-Temperature Gas Reactor (MHTGR) was evaluated, based on the Preliminary Safety Information Document (PSID), as submitted by the U.S. Department of Energy to the U.S. Nuclear Regulatory Commission.

The relevant reactor safety codes were extended for this purpose and applied to this new reactor concept, searching primarily for potential accident scenarios that might lead to fuel failures due to excessive core temperatures and/or to vessel damage, due to excessive vessel temperatures.

The design basis accident scenario leading to the highest vessel temperatures is the depressurized core heatup scenario without any forced cooling and with decay heat rejection to the passive Reactor Cavity Cooling System (RCCS). This scenario was evaluated, including numerous parametric variations of input parameters, like material properties and decay heat. It was found that significant safety margins exist, but that high confidence levels in the core effective thermal conductivity, the reactor vessel and RCCS thermal emissivities and the decay heat function are required to maintain this safety margin.

Severe accident extensions of this depressurized core heatup scenario included the cases of complete RCCS failure, cases of massive air ingress, core heatup without scram and cases of degraded RCCS performance due to absorbing gases in the reactor cavity. Except for no-scram scenarios extending beyond 100 hr, the fuel never reached the limiting temperature of 1600°C, below which measurable fuel failures are not expected. In some of the scenarios, excessive vessel and concrete temperatures could lead to investment losses but are not expected to lead to any source term beyond that from the circulating inventory.

Several future extensions of the current work are suggested.

EXECUTIVE SUMMARY AND CONCLUSIONS

In support of the safety evaluations of the MHTGR concept by the NRC, performance evaluations of the conceptual design were performed at BNL. These efforts are documented in this report.

This summary section follows the sequence of accident scenarios as presented in the body of the report, beginning with depressurized core heatup transients, which are still considered to be design basis events, and continuing, thereafter, with more severe accident scenarios. Ultimately a summary of the suggested future work is given.

Safety Evaluation of the MHTGR During Depressurized Core Heatup Transients with Functioning RCCS

The scenarios considered in this section assume that scram, depressurization, and loss of all forced circulation occur at the beginning of the accident, with conduction and radiation heat transfer from the core to the passive RCCS, which continues to function normally. Corresponding events are considered in Chapter 15 of the PSID, specifically in DBE-11 and SRDC-6 to 11.

During normal full power operation the RCCS continually removes about 0.8 MW from the reactor vessel. In the early phases of the accident scenario the decay heat exceeds the heat removal by the RCCS, and the excess energy is stored in the core, resulting in a gradual core heatup. After 60 to 70 hr the RCCS heat removal exceeds the decay heat, and the system begins to cool down. In the best estimate case, a peak fuel temperature of about 1370°C is reached after 55 hr and a peak vessel temperature of about 425°C occurs after 91 hr. These best estimate temperatures are lower than those cited in the more conservative PSID evaluations. Typical results of reactor temperatures and heat flows for such a transient are shown in Figures 3.1 and 3.2.

The major emphasis of our analysis was to independently verify the PSID evaluations and to identify the parameters which, within their uncertainty bounds, could have a significant safety effect on the accident transient. Peak fuel and vessel temperatures during the transient were the output parameters of primary concern.

Excessive fuel temperatures can lead to fission product release. Current DOE data appear to indicate that very few, if any, fuel failures are likely to occur in the 1600 to 1800°C temperature range. Nevertheless, a value of 1600°C has frequently been cited as the threshold below which one is assured of no additional fuel failures, and no fission product releases beyond the circulating and plated out inventory. At temperatures of 2200°C and above, massive fuel failures would be expected.

Vessel temperatures in excess of the maximum allowable ASME code values could prevent future reuse of the pressure vessel. A maximum permissible temperature of 480°C was considered during this study. Since completion of this work, the vendor has decided to apply for an ASME code extension to 540°C as maximum permitted vessel temperature.

To establish the effect of various uncertainties in the input data on the

peak fuel and vessel temperatures, a large number of parametric evaluations were made. Many of these variations, such as in-core gaps between fuel elements, initial graphite irradiation damage, air inlet temperature to the RCCS, as well as thermal emissivities of the reactor and RCCS materials had no major impact on the peak fuel temperatures. The vessel and RCCS thermal emissivities did have a significant effect on the vessel temperatures, indicating that this parameter should be controlled during manufacture and operation, primarily by avoiding any polishing or painting of the steel surfaces.

The two parameters having the most significant impact on the fuel and vessel temperatures were the decay heat and the effective thermal conductivity of the fuel elements and reflector blocks. Parametric evaluations were performed in order to establish the effect of these two parameters on peak fuel and vessel temperatures.

The results of Figures 3.12 and 3.13 show that a 30% increase in decay heat or a 37% reduction in effective thermal conductivity would be required before peak fuel temperatures of 1600°C would be reached. Significantly larger margins exist before the 2200°C threshold would be reached. A 27% increase in decay heat was found to cause peak vessel temperatures of 480°C, the value beyond which the restart capability of the vessel might be compromised.[1] Thus, during depressurized core heatup scenarios with functioning RCCS, significant performance margins exist before fuel failures and additional fission product release would be expected. However, the evaluations show that a high confidence in the decay heat function and effective core thermal properties is required to assure that vessel temperatures do remain within safe bounds.

Safety Evaluation of the MHTGR During Depressurized Core Heatup Transients Without Functioning RCCS

The passive RCCS has a very low failure probability, and even in case of catastrophic failures, only parts of the system would be likely to fail, resulting in partial flow blockages and/or partial loss of draft. Parametric evaluations of RCCS performance have shown it to be highly "self-adjusting" (large increases in flow resistance lead to some flow reduction and higher air exit temperatures, with a relatively small loss in total energy removed). Nevertheless, as a limiting case, depressurized core heatup without any cooling by the RCCS is being considered in this section.

In order to protect the surrounding concrete surfaces, the RCCS design includes thermal insulation. Additional shielding and thermal insulation are provided at the top and the bottom of the reactor cavity. This thermal insulation is the most significant heat transfer barrier in any heatup scenarios without functioning RCCS. The failure assumed here is a most unlikely case, in that it postulates a worst case combination of:

1. Eliminating all air flow by blocking all flow passages completely, while

2. keeping all thermal insulation in place.

[1] The corresponding margin to 540°C is 55%.

Adding more conservatism, for our Base Case evaluation, a concrete of relatively low thermal conductivity and a poorly conducting soil (clay) were assumed. Several parametric variations in concrete/soil properties and configurations were evaluated. A corresponding case is considered in Appendix G, Section G.2 of the PRA report for the MHTGR.

Our analyses found that the peak core temperatures exceeded those for the corresponding cases with RCCS by about 35°C only, and were essentially independent of concrete and soil conditions, since these structures were still relatively cool at 78 hr, when the core temperatures peaked. However, the vessel temperatures eventually reached levels between 700 and 800°C, typically peaking between 400 and 1,200 hr, i.e., weeks after the onset of the accident. Poorer concrete and soil conditions affected the peak vessel temperatures slightly, but greatly slowed down the ultimate cooldown. Several regions of the concrete walls of the reactor silo reached temperatures as high as 700°C. Thus, at least partial failure of these structures, weeks after the onset of the accident, is not precluded.

Parametric variations of decay heat and core effective thermal conductivity (with RCCS failed) gave only slightly smaller margins than the corresponding cases with RCCS as shown in Figures 4-14 and 4-16: a 27% increase in decay heat and a 33% reduction of the core effective thermal conductivity were required to reach peak fuel temperatures of 1600°C. However, unacceptable vessel and concrete temperatures are possibly reached. A 40% increase in decay heat brings the peak vessel temperature to 1000°C (however, only after 6 weeks). While there is no specific vessel failure temperature or failure mode, mechanistic accident scenarios can be envisioned here, during which some fuel failures occur around 100 hr, and subsequent vessel failures occur after several weeks, when core temperatures have already returned to the 1200 to 1300°C range.

To establish whether the reactor cavity could be designed to withstand even these core heatup accidents without functioning RCCS, an evaluation was made for a case of best estimate rather than conservative concrete and soil properties, and without the thermal insulation within the RCCS (this insulation is not really required for the RCCS to function properly under normal or accident conditions). In this case, the vessel temperatures peaked about 100°C lower than in the preceding cases, and the peak concrete temperatures at critical areas peaked near 250°C. One local peak concrete temperature at the side wall surface reached 560°C. Thus, a "hardened" reactor silo design with significantly lower vessel and concrete temperatures may be achievable with appropriate design modifications, i.e., elimination or reduction in insulation and proper concrete selection.

In summary, the decay heat and thermal conductivity margins for fuel failures are very close to the corresponding cases with RCCS functioning. However, higher decay heat levels can significantly impact on the peak vessel and concrete temperatures, and some structural failures of these components at very long times are possible.

Evaluation of Large Air Ingress Scenarios

For significant amounts of air to enter the core large failures of the primary loop pressure vessel system must be postulated. These could be either

in the form of multiple reactor vessel failures, or in the form of a cross duct double-guillotine break. The latter was assumed here.

In either case, the total gas flow through the core after such a break was found to be limited by the friction pressure drop through the 16 mm diameter and approximately 12 m long coolant holes in the core.

Assuming an unlimited supply of pure air and no recirculation between the gasses exiting and entering the vessel at the break, the core inlet flow ranged from an initial value of 700 kg/hr to about 260 kg/hr for most of the 10 day transient evaluated (for 50 volume % mixtures of helium and air the flow rates were about one third of the above values). Varying the chemical reaction rates and the gas species diffusion coefficients by several orders of magnitude, it was found that in virtually all conditions all the air entering will oxidize, exiting almost exclusively as carbon monoxide, and any uncertainty in reaction rates or diffusion coefficients will only affect the length of the reaction zone. The corresponding graphite oxidation rate was about 60 kg/hr for most of the transient. The thermal contribution from this exothermal graphite-air reaction to the core heatup was small, amounting to only about 10% of the nuclear decay heat.

As the air volume in the reactor and steam generator cavities is generally limited, significant air inflow could last but a few hours, with the inflow being originally a helium air mixture, gradually being replaced by a $He/CO/N_2$ atmosphere. Early during such a scenario, local burning of the exiting CO in the reactor cavity is not impossible, and this could possibly continue for a few hours. For the graphite oxidation to proceed to the point that structural damage inside the core would become possible, an unlimited air supply would have to be available for many days. It should be noted that the air flow into the core and the corresponding amount of graphite reacted, as given here, are larger than those reported by the DOE team. This is apparently due to our use of a finer nodalization in the computation of the downward flowing gas temperatures at the core barrel. While our conclusions are relatively insensitive to these differences in air flow rates, it appears that our results would be the more accurate ones.

Evaluation of Moderate Water Ingress Scenarios

Considering the moderate steam generator break of SRDC-6 (single off-set tube rupture) the long term consequences of graphite oxidation during the subsequent depressurized core heatup transient were evaluated.

Subsequent to the shutdown of HTS and/or SCS, their respective flow valves are in a closed position. If they were hermetically closed, only internal in-core recirculation of the He/H_2O mixture of about 18 volume % H_2O would be possible, resulting in very small in-core flow rates of about 0.5 kg/hr. As both valves are designed to permit some bypass flow in their closed position, initial estimates indicate a net circulation between steam generator and core of about 3 kg/hr, which is very minor. However, after the first few hours, the core temperatures are sufficiently high that all H_2O entering the core will react (endothermic), oxidizing about 1 kg/hr of graphite.

The gas exiting the core would have a 30 volume % concentration of water gas (CO + H2). However, it could leave the primary loop only after passing

through the steam generator and relief valve train, where it would be strongly diluted. Therefore, it is very unlikely that any combustible mixture could enter the reactor building.

Thus, no serious safety consequences from this accident scenario have been identified. Extension of this work to include large water ingress rates is planned.

Depressurized Core Heatup Accident Scenarios Without Forced Cooling and Without Scram

The case of a depressurization accident without scram and without any forced cooling, but with functioning RCCS was investigated, using the reactivity feedback coefficients from the PSID for an EOC condition and best estimate cross section data supplied by GA. A similar case is presented in Section G.1 of Volume 2 of the PRA report for the MHTGR.

The reactor was found to shut down within about two minutes, due to the negative Doppler feedback coefficients. The power generated during this initial period amounted to about 40 full power seconds, resulting in an average active core temperature rise of about 100°C.

Recriticality due to Xenon decay was observed at about 50 hr, with power spikes occurring about one per hour, with an initial peak of 17 MW, decaying to a final steady level of about 1.2 MW.

Beyond about 120 hr an equilibrium condition was observed, where the positive reactivity due to low Xenon concentration just balances negative reactivity due to elevated fuel temperatures.

The peak core temperatures for this best estimate evaluation reached 1600°C at about 60 hr and peaked at 1760°C at about 120 hr, prevailing at this level for hundreds of hours rather than decaying moderately fast, as in the corresponding accident with scram. Thus some fuel damage and fission product release after 60 hr must be expected. Vessel temperatures of about 550°C would preclude reutilization of the vessel.

Further investigations will consider the case without functioning RCCS, and the sensitivity of the results to variations in the core and reflector temperature coefficients and the cross section data, in particular since in these accident scenarios the peak core temperature is strongly dependent on the Doppler feedback coefficients.

Reduction in Reactor Cavity Heat Transfer due to H_2O and/or CO_2 Accumulation

Water vapor, carbon dioxide and, to a lesser extent, carbon monoxide can reduce the heat transfer via radiation from the reactor vessel to the RCCS panels.

Water vapor could reach the reactor cavity in accident scenarios involving massive failures of the secondary loop, such as a main steam line break in the steam generator cavity. Significant accumulations of CO_2 would require prior massive ingress scenarios and chemical reactions in the primary loop, and therefore is of much lower probability.

A preliminary gas radiation heat transfer model was used to estimate the effects of such CO_2 and H_2O accumulations in the reactor cavity. The results show that with maximum possible water vapor concentrations in the reactor cavity the heat transfer in the cavity could be reduced by up to 33% for a given set of vessel and RCCS temperatures, resulting in a compensating vessel temperature rise of about 40°C for nominal operating conditions and an increase in peak vessel temperatures of about 50°C during a depressurized core heatup accident scenario.

Temperature Transients Subsequent to a Collapse of the Core Support Structure

Initial estimates of the effect of a collapse of the core support structure on the subsequent core heatup scenarios considered approximate models for single fuel elements reaching the vessel surfaces and even the concrete. It was pointed out that such scenarios are extremely unlikely, since all fuel elements are surrounded by several layers of reflector elements.

Considering various geometric and thermal resistance configurations, it was found that the peak fuel temperatures of such scenarios were always lower than those in an intact core which retains a higher power density and the minimum possible heat transfer surface envelope. However, fuel elements resting on the vessel surface can cause hot spots on the vessel with surface temperatures in the range from 660 to 950°C, at which level further local vessel failures could not be ruled out.

Future Work

The results reported here represent the current state of our ongoing independent analyses. Several further extensions of this work are planned, and others may be added as additional items of concern are identified.

In particular, fission product transport during blowdown, as well as during long term transients, should be modelled. The releases occurring during blowdown can be evaluated based on blowdown transient calculations using the RATSAM code. For the long term transients the ATMOS code has been used to evaluate the gas exchange between the various reactor building cavities. The corresponding fission product transport models should be added to this code to evaluate the potential fission product release from the reactor building.

To evaluate partial restoration of RCCS cooling after 36 hr, as suggested in the NRC Bounding Event Sequence 3 (BES-3), our THATCH modelling of this scenario should be extended to include the effect of reduced buoyancy in the RCCS due to heatup of the downflow channel and the surrounding structures prior to restoration of cooling.

The air ingress evaluations should be extended to consider the effects of higher chemical reactivity of the Stackpole 2020 graphite in the lower plenum and bottom reflector regions. These regions are at lower temperatures and have less exposed graphite surface. However, preferential oxidation here, if it were to be observed, could result over a long time in weakening of the core support structure.

Our evaluations of water ingress scenarios should be extended to more massive ingress scenarios, like the ones of BES-4.

The case of core heatup without scram is to be extended to investigate the effect of uncertainties in the reactivity and cross section data currently supplied by DOE and to consider the case without RCCS cooling.

The more detailed model of banded gas radiation is to be coded and applied to obtain a firmer assessment of the negative effects of H_2O and CO_2 on reactor cavity heat transfer and the resulting higher peak vessel temperatures.

TABLE OF CONTENTS

LIST OF FIGURES

LIST OF FIGURES (Continued)

LIST OF FIGURES (Continued)

LIST OF FIGURES (Continued)

LIST OF TABLES

ACKNOWLEDGEMENTS

During the execution of this work, the author had numerous helpful and valuable discussions with Drs. Gregory J. Van Tuyle and Hsiang-Shou Cheng of Brookhaven National Laboratory (BNL) and with Dr. Peter Williams of the U. S. Nuclear Regulatory Commission (NRC).

A draft of the report was reviewed by Drs. James G. Guppy and Gregory J. Van Tuyle at BNL and Dr. Peter Williams at the NRC.

Early drafts of the report were typed by Mrs. Amalia Ruggiero. The final draft and final report were typed by Mrs. Linda Hanlon.

The author gratefully acknowledges all of the help and support he received.

1. INTRODUCTION

The conceptual design of the Modular High Temperature Gas-Cooled Reactor (MHTGR), currently being developed under DOE sponsorship has been submitted to the NRC in a Preliminary Safety Information Document (PSID). In support of the Safety Evaluation Report to be issued by the NRC, initial safety evaluations of this concept were conducted at BNL, in part to validate the vendors performance claims, and in other cases extending the analyses to more remote and more severe accident scenarios.

The starting point for our efforts were the codes developed and used in the Source Term Study for the 2240 MW HTGR (Reilly et al., 1984). In several areas significant code extensions were required, including models for the passive air cooled Reactor Cavity Cooling System (RCCS), adding a point kinetics model, and including initial models for graphite oxidation during water and air ingress scenarios.

A brief design description and an overview of the codes used in the analysis is given in Section 2. The initial analyses for the conceptual design are presented in Section 3 to 9, while Section 10 outlines the required code extensions for future evaluations as the design progresses to the preliminary and final design stages.

Some details of the models are described in the appendices.

2. DESIGN DESCRIPTION AND OUTLINE OF REACTOR SAFETY CODES

The reactor vessel and the steam generator are located in two adjacent cavities of an underground silo as shown in Figure 2-1. A schematic of the reactor with steam generator is shown in Figure 2-2. Further details of the design of the MHTGR are given, for instance, in a concept description report [Bechtel National, 1986]. Power is generated in a ceramic graphite moderated core using inert helium as the primary coolant for energy transfer to the steam generator. The active core fuel elements are arranged in an annular cylinder, surrounded in the center and on all sides by graphite reflector elements. Helium flow is normally provided by the main circulator. In case the main circulator or any other steam generator component is not available for service, the reactor would be scrammed, and a shutdown cooling system, located at the bottom of the reactor vessel would generally be used for decay heat removal.

A third heat removal system, which comprises one of the inherent safety features of the MHTGR is a passive air cooling system, the Reactor Cavity Cooling System (RCCS). It is shown schematically in Figure 2-3. In case neither of the above forced flow cooling systems is available, the reactor will be scrammed and heat rejection is then predominantly by conduction and radiation from the active core via the side reflectors and the reactor vessel, across the reactor cavity to the RCCS cooling panels. Inside the cooling panel an airflow is created by natural circulation assisted by the outlet stack.

The reactor vessel is not thermally insulated and during normal power operation a parasitic heat loss to the RCCS of about 0.9 MW (0.25% of 350 MW_{th} design power) is allowed. Thus, the RCCS is a completely passive system, without valves, damper or other active components. It is always in operation, self activated, whenever there is a heat flow from the reactor vessel.

The analysis of the basic depressurized core heatup transients was performed with the THATCH code, analyzing transient conduction and radiation in the reactor vessel, coupled with the PASCOL code, which analyzes quasi-static RCCS flow and heat transfer conditions.

The THATCH code is a general purpose reactor code, which was applied here to the MHTGR reactor vessel geometry. It solves the conduction equation for all major solid capacitances, as nodalized by the user, applying an Alternating Direction Implicit numerical method, using prescribed temperature dependent property functions for all reactor components.

Heat transfer across internal gaps can be modelled as conduction, convection, and one-dimensional radiation, or any combination of these, as specified by the user. For larger internal volumes, multi-dimensional radiation modelling will provide better results and can be employed as a code option. It is used here in the upper and lower plena. During normal reactor operation, the thermal conductivity of all the core graphite and some of the reflector graphite decreases due to irradiation damage. During the relatively slow core

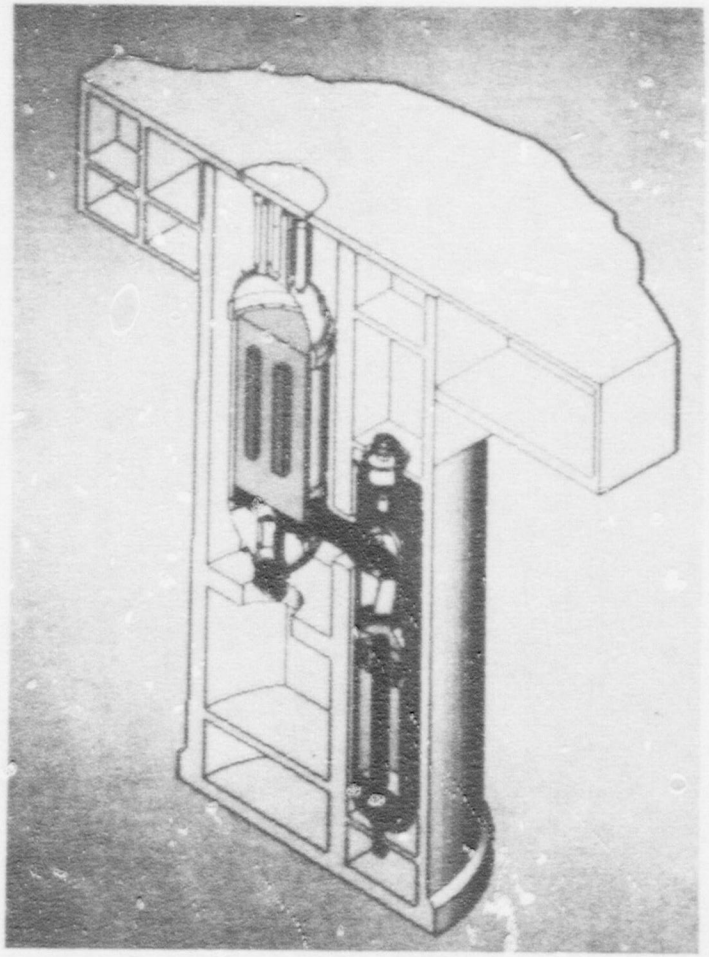

Figure 2-1 MHTGR in Undergroud Site (Bechtel, 1986)

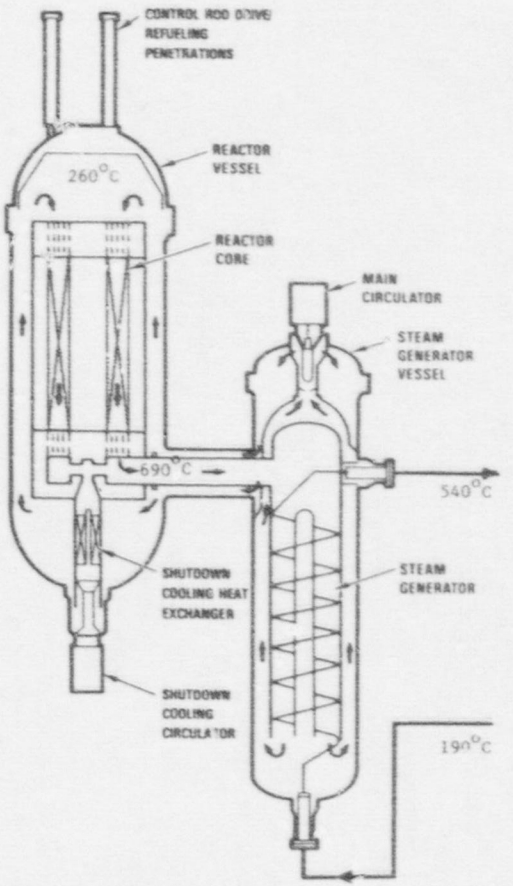

Figure 2-2 Schematic of MHTGR Primary Loop (Bechtel, 1986)

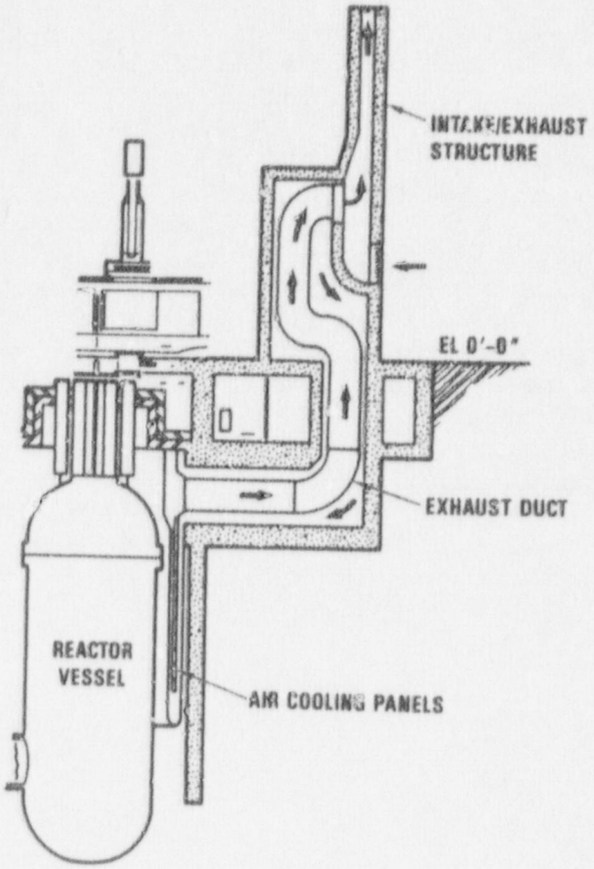

Figure 2-3 Passive Decay Heat Removal System
(Bechtel, 1986)

heatup accident scenarios, annealing will occur, with the original, undamaged thermal conductivity being restored. The material then remains annealed during the subsequent cooldown. Such a core thermal property model, requiring the thermal conductivity to be specified at each location as function of temperature and temperature history is also included in the code.

At the prevailing temperature levels and dimensions, heat transfer from the reactor vessel across the reactor cavity to the RCCS panels is predominantly by radiation, with turbulent natural convection contributing about 5 to 10% of the total heat transfer. Heat transfer within the RCCS up-flow channel is by conduction and radiation to its internal fins and the back panel, and by convection from all metal surfaces to the upflowing air. The PASCOL code models, at each elevation, either this combined conduction/convection/radiation heat transfer, or uses a prescribed fin effectiveness coefficient in computing local heat transfer from the panels to the coolant, using local panel temperatures. Sample evaluations have shown that detailed local fin conduction and radiation solutions are not warranted, since for a given design the fin effectiveness does not vary significantly in space or time during a transient. Constant user supplied fin effectiveness data, developed in a separate parametric study, where therefore generally applied here. Coupled with the axially nodalized heat transfer analysis, the PASCOL code also solves a one-dimensional quasi-steady momentum equation for the RCCS air flow, including ducting losses and stack effect.

Further details regarding the modelling, material properties and design data are given in Appendices A and B. Both codes have been verified extensively by comparison to available transient data and by application with simplified geometries and material properties to cases where exact solutions are available.

3. PARAMETRIC EVALUATION OF DEPRESSURIZED CORE HEATUP SCENARIOS WITH FUNCTIONING RCCS

Of the accidents scenarios covered in Chapter 15 of the MHTGR PSID, the depressurized core heatup transients without forced flow cooling by either the HTS or the SCS, result in the highest core and vessel temperatures. Under these conditions decay heat removal is predominantly by conduction and radiation from the core to the passive RCCS, and from there by convection to the environment. The RCCS constitutes the only safety-grade decay heat removal system.

To establish confidence in the capability of the MHTGR to achieve reactor cooldown via the passive RCCS, such transients are evaluated in this section. The first evaluation constitutes a base case, using predominantly best estimate data. Numerous parametric variations in design and operating data were applied thereafter, to establish the available safety margins, and to identify possible sensitivities to uncertainties in input data and modelling assumptions. These results are presented in this section.

The reactor transients were modelled using the THATCH code, which computes the temperature field in the reactor, internally coupled with the PASCOL code, which evaluates the passive air cooling module, i.e., the RCCS.

The reactor and RCCS input data are based on the PSID descriptions and the core material properties and other design data provided by DOE [GA, 1987-01]. The nominal decay heat used for most evaluations, is also based on DOE submittals [GA, 1986-01]. The most important model data and material properties are summarized in Appendix A.

Parametric evaluations of RCCS performance and its sensitivity to various design and operating parameters are summarized in Appendix B. As indicated there, the RCCS was found to be extremely fault tolerant. That is, an increase for instance in the ducting flow resistance would result in a slight flow reduction, but slightly higher air exit temperatures, with essentially unchanged total energy removal. This establishes the RCCS as a passive system, that is relatively insensitive to many variations in design selections and operating conditions.

3.1 Best Estimate Case for Depressurized Core Heatup Transient with Functioning RCCS

A best estimate "Base Case" of a depressurized core heatup transientwill be presented here, to be compared below with several parametric variations, to identify the most important variables that can effect the critical parameters during such core heatup transients. The main interest is in the peak fuel and vessel temperatures. Excessive fuel temperatures lead to fuel failure and fission product release. Excessivevessel temperatures could compromise structural integrity of the vessel, as well as adherence to ASME code limits for reusability of the vessel subsequent to any such accident scenario.

The Base-Case used the "nominal" decay heat data submitted by DOE [GA, 1986-01]. The radial and axial distribution of after heat was assumed to follow the full power profiles, as given in the PSID.

In-core gaps between adjacent fuel elements were modelled as 1 mm wide in horizontal direction, and 0.5 mm in axial direction.

All active core graphite was assumed to be fully irradiated. For the reflector blocks adjacent to the core a relatively conservative partial irradiation damage was assumed as summarized in Table 3-1. During the transient, graphite annealing is assumed to occur between 1000 and 1300°C, with the annealed material retaining its recovered properties in any subsequent cooldown.

The RCCS was assumed to operate at 20°C air inlet temperature, with the reactor vessel and the RCCS panels having a nominal thermal emissivity of 0.8.

Typical results for this case are shown in Figures 3-1 through 3-6. Following loss of forced cooling from full power operation, with scram and loss of primary loop pressure, the core begins to heat up. Initially, the decay heat exceeds the heat transfer out of the core, resulting in temporary energy storage in the core. Core temperatures peak at 1320°C at about 60 hr into the transient. At about the same time, heat transfer out of the active core begins to exceed the decay heat, thus resulting in a net cooldown for the active core. The reactor vessel temperatures peak at 89 hr at 425°C. Beyond 73 hr the net heat transfer to the RCCS exceeds the decay heat resulting in a net cooldown of the reactor. The RCCS air flow peaks at 12.8 kg/s, and the air outlet temperature at 123°C, both around 90 hr, with a heat removal rate of 1.33 MW. (It should be noted that the above temperatures are significantly lower than results previously reported and also lower than the PSID data. This is mainly due to the use of nominal decay heat data, while previous investigations used the more conservative PSID data or LTR-4 data [Sund, 1973]). Implementation of a full annealing model (see Appendix A), which presents the actual physical processes more correctly than a simple temperature dependence of core properties, also contributed to this effect).

The plots of gas inventory in the reactor vessel and in the reactor cavity indicate that only very small fractions of the respective gas inventories are expected to be exchanged with gas in connected cavities.

3.2 Parametric Variation of Major Design and Operating Parameters

To identify any potential sensitivities of the main output parameters of our analyses - peak fuel and vessel temperatures - to variations in input parameters or modelling assumptions a large number of design and operating parameters were varied parametrically. The various cases are compared against the Base Case in Table 3-2.

The Base Case used as radial decay heat distribution the corresponding power profile given in PSID for normal operation. In contrast, a uniform radial power profile was applied in Case 2. The result was about 50°C higher peak fuel temperature, and virtually no change in vessel temperature. As a radially uniform decay heat distribution is not only more conservative but also apparently closer to actual conditions, one might consider Case 2 a more

Table 3-1 Assumed Base Case Reflector Irradiation

	Percent of Saturation Irradiation Damage
Central Reflector:	
Reflector element row adjacent to core	95
Next reflector element row	60
Replaceable Side Reflectors:	
2/3 of reflector element row adjacent to core	95
Remainder (i.e., 1 1/3 rows)	60
Top Reflector:	
1/2 of reflector element height	100
Bottom Reflector:	
1/2 of reflector element height	82

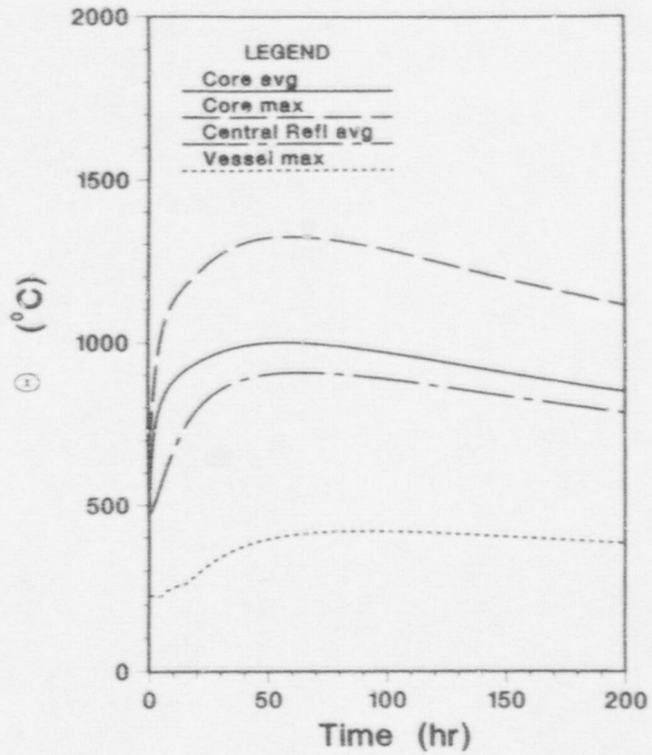

Figure 3-1 Core and Vessel Temperature During a Depressurized Core Heatup Transient with RCCS Cooldown (Base Case)

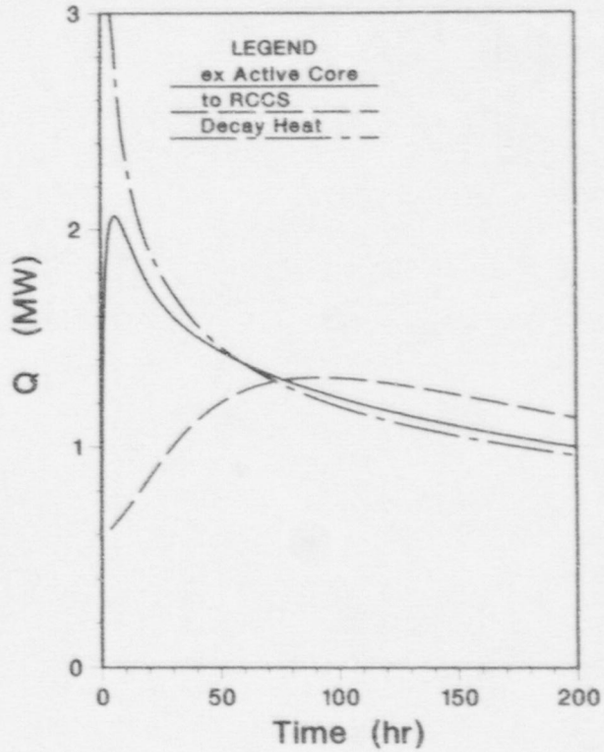

Figure 3-2 Decay Heat and Heat Flows During a Depressurized Core Heatup Transient with RCCS Cooldown (Base Case)

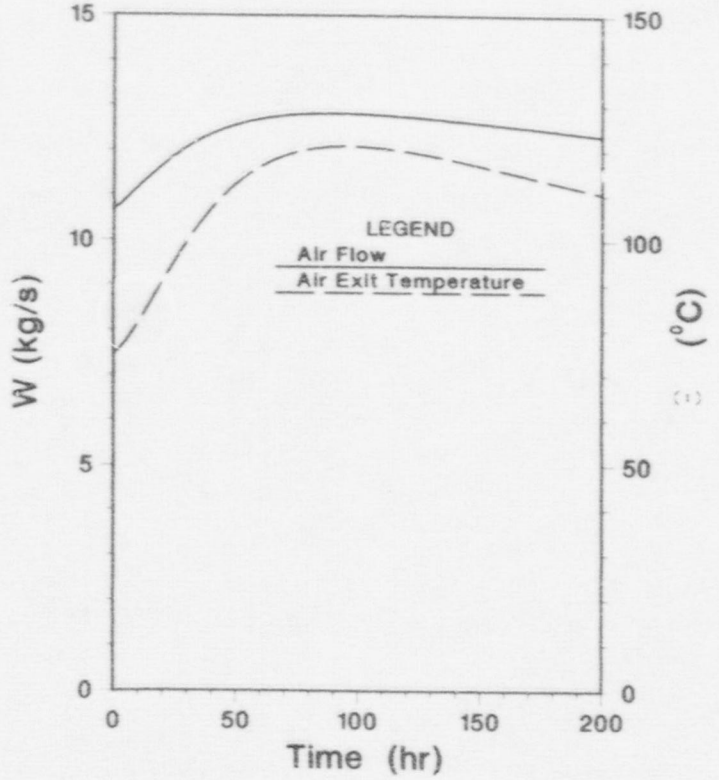

Figure 3-3 RCCS Performance During a Depressurized Core Heatup Transient with RCCS Cooldown (Base Case)

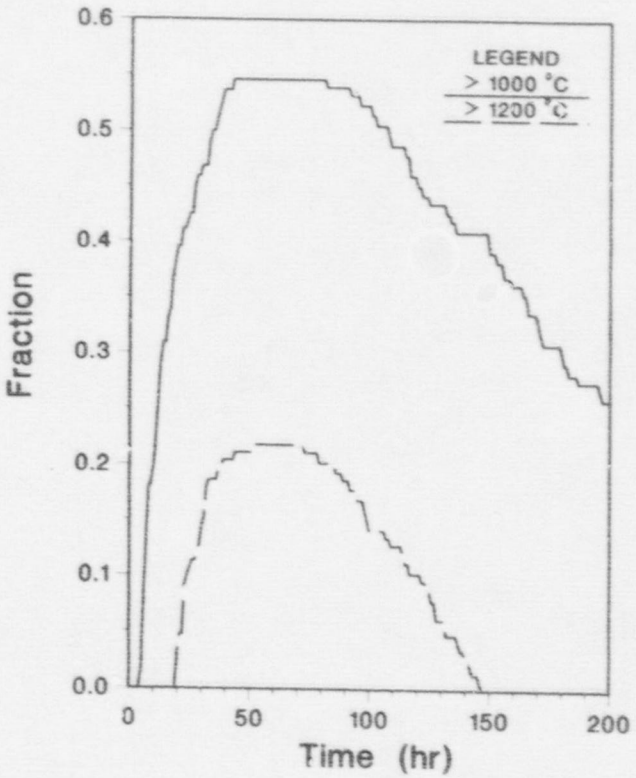

Figure 3-4 Fractions of Active Core Exceeding Specified Temperature Limits During a Depressurized Core Heatup Transient with RCCS Cooldown (Base Case)

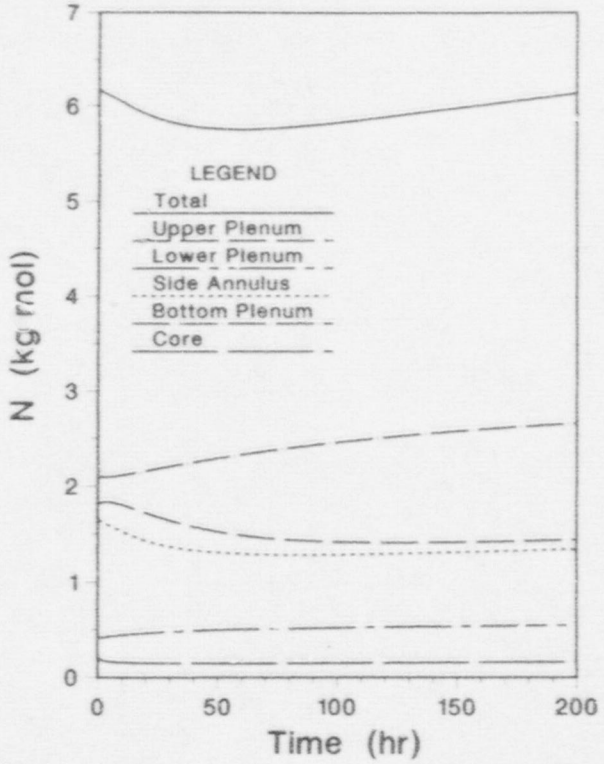

Figure 3-5 Reactor Vessel Gas Inventory During a Depressurized Core Heatup Transient with RCCS Cooldown (Base Case)

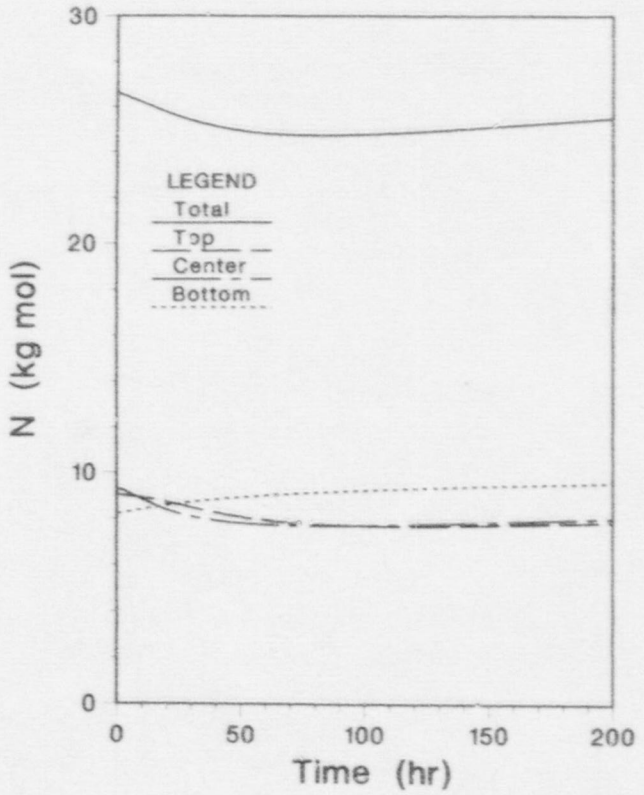

Figure 3-6 Reactor Cavity Gas Inventory During a Depressurized Core Heatup Transient with RCCS Cooldown (Base Case)

Table 3-2 Parametric Comparison of Depressurized Core Heatup Transients with Operating RCCS

Case No.	Description	Peak Fuel Temperature			Peak Vessel Temperature			Vessel Cross Over Time* hr
		Value °C	At Time hr	Variation From Base Case °C	Value °C	At Time hr	Variation From Base Case °C	
1	Base Case	1320	58	----	425	89	----	73
2	Uniform Radial After-Heat Profil:	1366	55	+46	424	91	-1	74
3	LTR-4 decay heat	1522	70	+202	489	100	+64	91
4a	Without Any In-Core Gaps	1272	56	-48	433	82	+8	66
4b	In-Core Gap Widths Doubled	1339	59	+19	423	92	-2	76
5a	All Reflector Graphite Unirradiated	1261	54	-59	421	83	-4	68
5b	All Replaceable Side Reflectors Plus One Row Each of Top and Bottom Reflectors Irradiated to Saturation	1354	63	+34	427	95	+2	78
6	RCCS Air Inlet Temperature 43°C	1321	59	+1	436	90	+11	75
7	RCCS and Vessel Emmissivity 0.6	1324	61	+4	474	97	+49	82
8	Suppress Graphite Annealing	1405	67	+85	423	92	-2	74
9	Maximize Fuel Temperature (LTR Decay Heat; Uniform Radial After-Heat; RCCS Air Inlet Temperature 43°C)	1579	67	+259				93
10	Maximize Vessel Temperature (LTR Decay Heat; w/o In-Core Gaps; Unirradiated Reflector Graphite; RCCS Air Inlet Temperature 43°C)				502	88	+77	81

*Time at which heat leaving vessel exceeds decay heat, i.e., net cooldown of reactor vessel and internals begins.

appropriate best estimate transient than the Base Case.[2] Thus, our best estimate at this time indicates peak fuel temperatures of about 1370°C at 55 hr, and peak vessel temperatures of about 425°C at 90 hr. Some of the results for this case are given in Figures 3-7 through 3-10. Use of the axial power profile of the PSID during a decay heat transient is conservative, as it creates higher local peak power densities and fuel temperatures than would actually be expected under decay heat conditions. Therefore, the axial after heat distribution was not varied here.

In Case 3, the LTR-4 decay heat function [Sund, 1973] was used. This results in about 28% more energy being generated in the core during the first 100 hr. As anticipated, the peak fuel temperatures increased significantly, by 202°C, and the peak vessel temperature increased by 64°C.

The in-core gaps between adjacent fuel elements present a heat transfer resistance which, depending on gap size and graphite temperatures, can be dominated by radiation or conduction. The Base Case used best estimate values of 1 mm gaps in radial direction and 0.5 mm in axial direction. The effect of these gaps on fuel and vessel temperatures is shown by arbitrarily eliminating them. As the in-core heat transfer improves without gaps, peak fuel temperatures decrease by 48°C and the peak vessel temperature increases by 8°C. While this case without gaps is not practically possible, it shows the overall effect of the in-core gaps, and also indicates that a temporary and/or locally improved thermal contact between blocks cannot cause any significant hot spots on the vessel. Wider gaps will not produce significantly higher fuel temperatures as radiation across the gaps generally dominates in the hottest regions of the core. Another run with radial and axial gap sizes of twice the Base Case gap dimensions demonstrated this, resulting in a peak fuel temperature of 1339°C, i.e., only 20°C higher than for the Base Case. Thus, the results are more sensitive to the physical presence of these gaps, than to their actual width.

With irradiation damage, the thermal conductivity of core graphite is significantly reduced (see Appendix A). While the active core will, in general, be irradiated to saturation, only a relatively small layer of the reflectors adjacent to the active core will have incurred a sufficient fast fluence to show significant irradiation damage. For the Base Case a relatively high irradiation damage in the reflector was assumed, as shown above.

Lesser irradiation damage would generally tend to reduce fuel temperatures and increase vessel temperatures. As shown in Table 3-2, for the case of completely unirradiated reflectors, Case 5a, fuel temperatures dropped by 59°C. However, unexpectedly, the peak vessel temperature also dropped slightly. Looking at the details of the transients one finds that around 30 to 60 hr when the core temperatures peaked, the vessel was indeed about 5°C hotter than in the Base Case. But with more heat transferred earlier to the RCCS, the vessel temperature peaked slightly earlier, and at 4°C below the Base Case value.

Thus, the main effect of reflector irradiation damage is an increase in

[2]For this reason, uniform radial after heat was used as Base Case in later evaluations, as shall be noted; but most of the work of this section uses in its Base Case the PSID radial power profile.

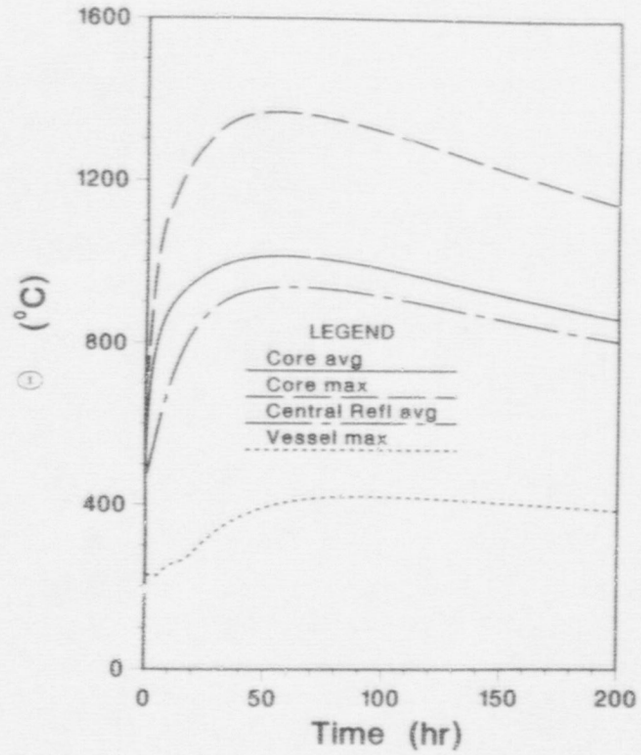

Figure 3-7 Core and Vessel Temperature During a Depressurized Heatup Transient with RCCS Cooldown (Case of Uniform Radial After Heat Profile)

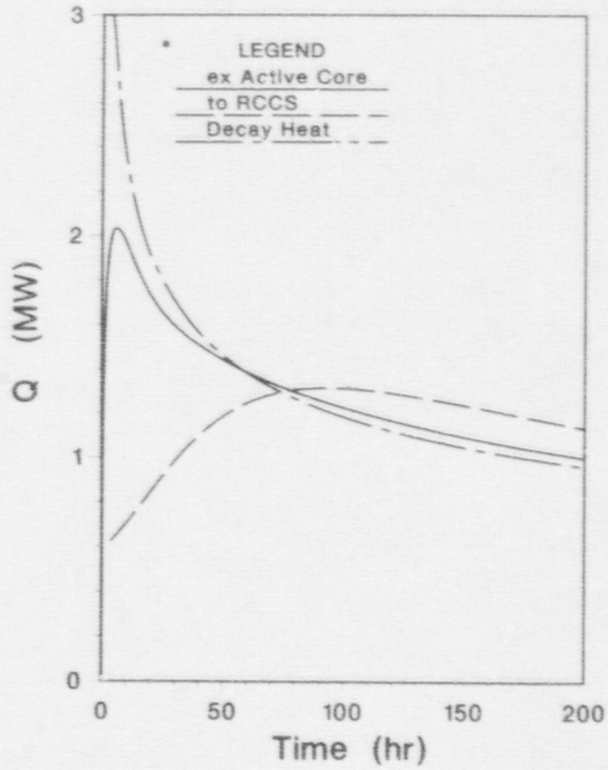

Figure 3-8 Decay Heat and Heat Flows During a Depressurized Core Heatup Transient with RCCS (Case of Uniform Radial After Heat Profile)

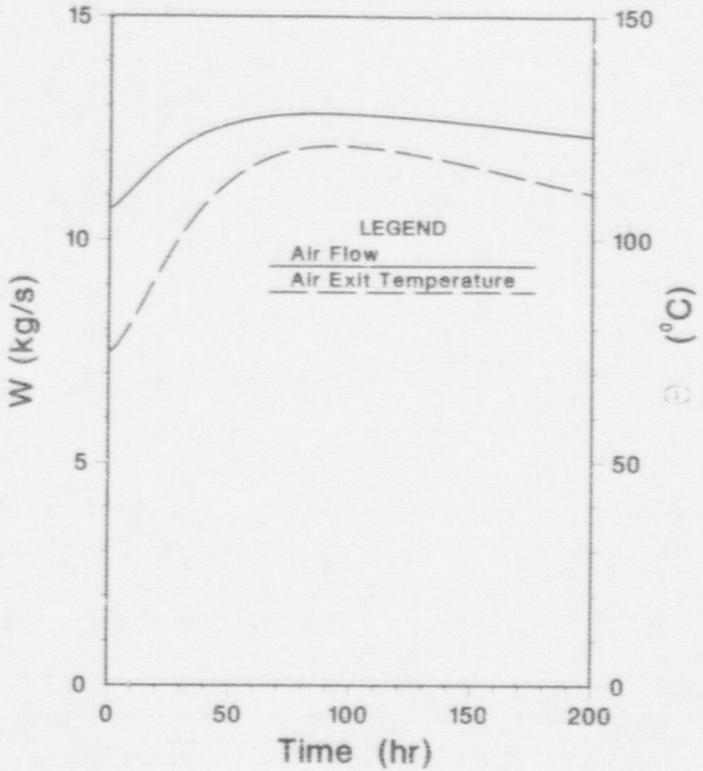

Figure 3-9 RCCS Performance During a Depressurized Core Heatup Transient with RCCS Cooldown (Case of Uniform Radial After Heat Profile)

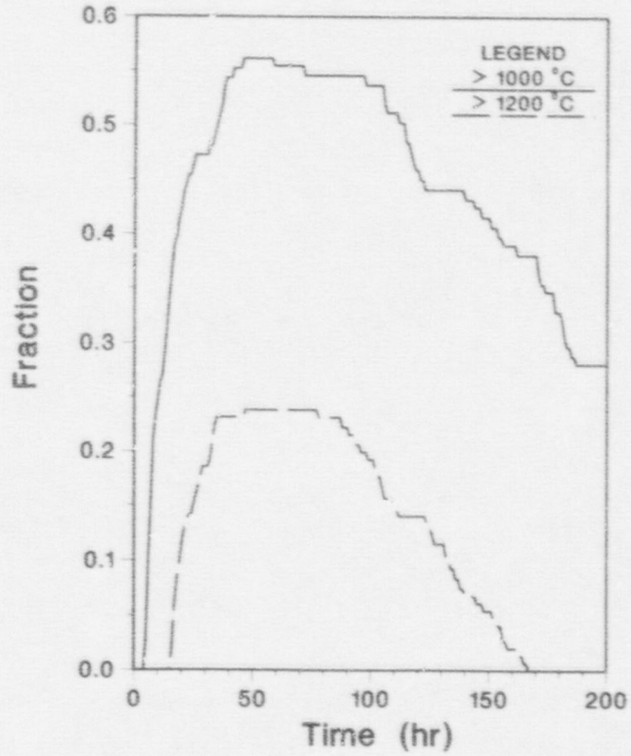

Figure 3-10 Fractions of Active Core Exceeding Specific Temperature Limits During a Depressurized Core Heatup Transient with RCCS Cooldown (Case of Uniform Radial After Heat Profile)

the peak fuel temperature. While the damage values currently being used are considered to be conservative, another run was made as Case 5b, with all replaceable side reflectors at the active core level, and one upper and lower reflector element row fully irradiated to saturation. The peak fuel temperature for this run was 1354°C, i.e. 34°C higher than for the Base Case. Thus, even with this maximum theoretical irradiation damage, fuel temperatures did not increase dramatically.

In Cases 6 and 7, some of the RCCS operating and design parameters were varied. Using a conservative RCCS air inlet temperature of 43°C (110°F) rather than the best estimate value of 20°C (68°F), peak core temperatures rose by only 1°C, an insignificant amount. However, the vessel temperature was affected, rising by 11°C. Arbitrarily reducing the vessel and RCCS panel thermal emissivity from a base value of 0.8 to 0.6, again the effect on core temperature was minor, increasing the peak temperature by only 4°C. However, the effect on the vessel was quite significant with a rise in peak temperature of 49°C. As steel surface emissivities can vary widely, based on surface quality and amount of oxidation, the vessel and RCCS panel emissivities should be controlled during manufacturing as well as in operation, most practically via a technical specification.

Finally, to illustrate the effect of annealing, a run was made suppressing its effect in the core and in the reflectors. It should be noted that this is a non-physical condition being imposed, just to show the effect of annealing during a core heatup transient. In this artifical case, the fuel temperatures rose by 85°C, while the vessel temperatures were hardly impacted.

In a further run several of the above variations, which tend to raise core temperatures were imposed simultaneously, namely: a 1) conservative after-heat, a 2) uniform radial after-heat distribution, and a 3) conservative RCCS air inlet temperature. This run, designated Case 9, should be considered as a conservative upper limit on peak fuel temperatures. The combined conservatisms resulted in a peak core heat temperature of 1579°C, i.e., 260°C above the Base Case.

It is interesting to note that the sum of the temperature increases for using LTR decay heat (+202°C), uniform radial after heat (+46°C) and increased RCCS air inlet temperature (+1°C) is only 249°C, whereas imposing the three effects together resulted in a peak core temperature rise of 259°C, i.e., more than the addition of the individual effects. As the effect of increased RCCS air inlet temperature was very minor, this indicates that at higher core temperatures the effect of a uniform radial decay heat profile is more pronounced than at the Base Case temperature levels.

In order to maximize the vessel temperatures, a run was made, designated Case 10, with LTR decay heat, no in-core gaps, unirradiated reflector graphite, and an RCCS air inlet temperature of 43°C. The resulting peak vessel temperature was 502°C, i.e., about 80°C above the Base Case. This value exceeds the maximum PSID value of 482°C. A vessel temperature of 500°C during a depressurized core heatup transient might be of concern, in particular with respect to restart capability after such an accident. However, this run is also very conservative, particularly regarding use of the 28% higher LTR-4 de-

cay heat function.[3]

As an additional parameter, the effective thermal emissivity inside the reactor vessel and the core barrel was varied. Since these runs inadvertently used a uniform radial power profile and an air inlet temperature of 43°C, they cannot be compared directly to the runs in Table 3-2. As the effect was found to be minor, rerunning of these cases, and inclusion in the above table was not warranted at this time. The results were as follows:

Internal Reactor Vessel and Core Barrel Emissivity	Peak Core Temperature °C	Peak Vessel Temperature °C
0.5	1377	427
0.8	1369	433
1.0	1367	436

As the gap thermal resistance decreases with increasing emissivity, the peak fuel temperatures decrease and the vessel temperatures increase. However, the range of temperature changes is only about 10°C since the core barrel gaps are not the controlling heat transfer resistances.

Further variations of the reactor vessel and RCCS thermal emissivities were made, again using a constant radial decay heat profile. The emissivities were varied between 0.5 and 1.0. As mentioned above, the effect on fuel temperature were very minor, but the effect on the peak vessel temperature was significant. It is shown in Figure 3-11, again indicating that the vessel and panel emissivities ought to be controlled.

Thus, in summary, with operating RCCS it appears to be almost impossible to reach fuel temperatures of 1600°C, above which some fuel failure and fission product releases can occur, even with very conservative assumptions.

Under normal transient conditions, the peak vessel temperatures will remain below 450°C. However, under very conservative assumptions (in particular with 28% raise in decay heat or greater reduced vessel and) vessel temperatures of 500°C can be reached, and could be reason for concern.

3.3 Variation of Key Parameters to Establish Safety Margins

The results of Section 3.1 indicated that core decay heat removal via RCCS can be achieved without approaching fuel failures or excessive vessel temperatures. In Section 3.2 it was shown that reasonable variations in most parameters did not raise significant safety concerns. However, these results were based on DOE supplied decay heat data and core graphite properties. In

[3] It should be noted that our peak vessel temperatures are those of the hottest inside node of two radial vessel nodes. Those of the PSID are an average value at the hottest cross section. With a temperature gradient of about 25°C across the vessel our values are about 6°C higher than those of the PSID just due to the different definition of peak vessel temperature.

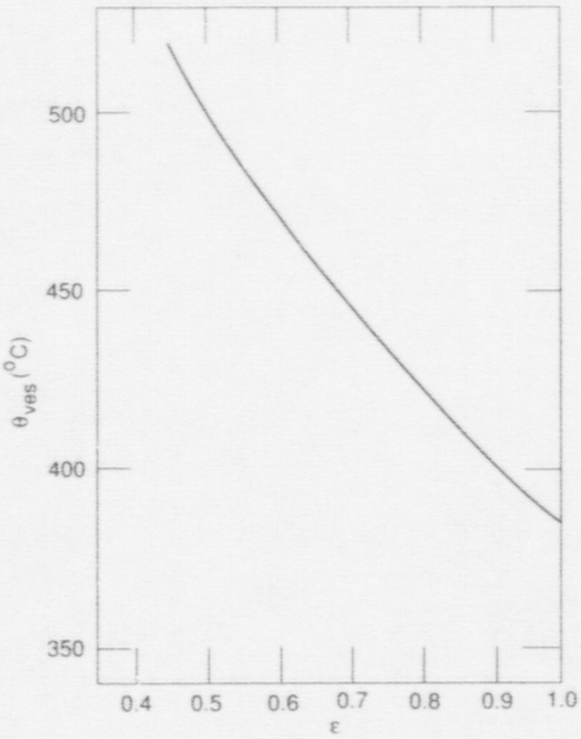

Figure 3-11 Effect of Vessel and RCCS Emissivities (ε) on Peak Vessel Temperature (θ_v) During Depressurized Core Heatup Transients with RCCS Cooldown

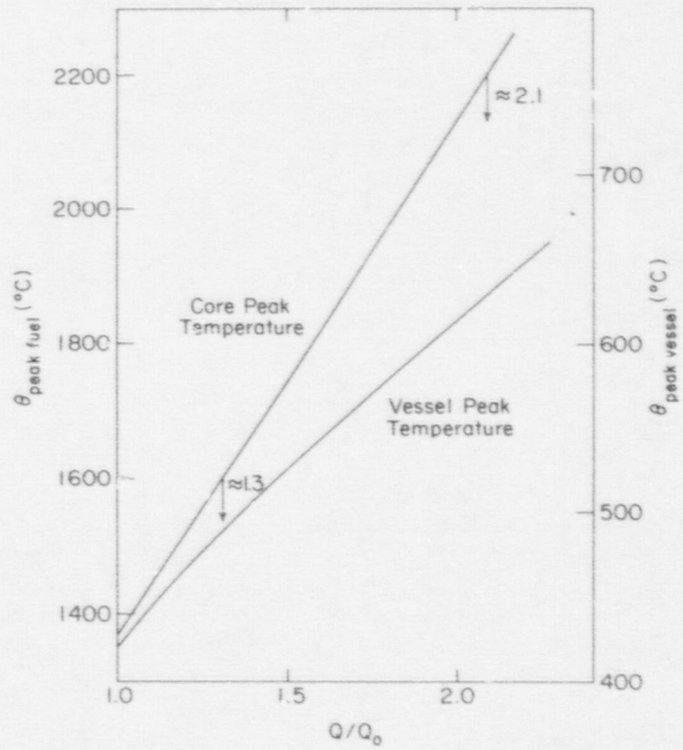

Figure 3-12 Peak Fuel and Vessel Temperatures as Function of Increased Decay Heat Generation

this section an evaluation is made to establish what magnitude of change in decay heat and core graphite properties can be tolerated before fuel failures and excessive vessel temperatures must be expected.

All runs in this section use a radially uniform decay heat profile. The results are summarized in Table 3-3 and in Figures 3-12 and 13.

It should be noted that the graphite properties for H451 and Stackpole 2020 are based on DOE supplied data, which are given only up to 1527°C and 800°C respectively. Linear extrapolations were used beyond the data base, which was the practice in previous studies as well, as there do not appear to be any data for higher temperatures. While such extrapolations may be reasonable up to peak core temperatures of 1700°C, their use beyond that remains open to question.

In raising the core decay heat beyond the best estimate values of [GA, 1986-01] the total decay heat curve was raised by the indicated factor Q/Q_o. Figure 3-2 shows that a peak fuel temperature of 1600°C, often considered as the point where some fission product release may become noticeable, is reached if the actual decay heat were 30% above the best estimate values. To reach peak fuel temperatures of 2200°C, where massive fuel failures are expected, one would have to stipulate an increase in decay heat of ì10%. The vessel temperatures also increases with decay heat levels, and an increase of 27% would be required to reach a peak vessel temperature of of 480°C.

In varying the core thermal conductivities the whole active core and all replaceable reflector blocks of H451 were varied by the indicated factor, k/ko. Figure 3-13 shows that the core thermal conductivity would have to be 63% of it best estimate values before a peak fuel temperature of 1600°C would be observed. At only 30% of its best estimate value, 2200°C would be reached, the level of massive fuel failures. As the in-core temperature gradients increase with reduced thermal conductivities, the peak vessel temperatures decrease slightly for lower thermal conductivities.

Table 3-3 includes one case of increased core thermal conductivities. As expected it results in lower peak fuel temperatures. And while the early vessel temperatures of this case are slightly higher than those of the Base Case, due to larger heat removal to the RCCS at earlier times, the ultimate peak vessel temperature remains very slight below that of the Base Case. I.e., higher core thermal conductivities do not raise any concerns with respect to vessel temperature.

It was further observed that variations in decay heat had little influence on the times of peak fuel temperatures which occurred between 55 and 57 hr or peak vessel temperatures (occurring around 86 to 92 hr). However, with decreasing core conductivity, peak fuel and vessel temperatures were reached later, ranging from 55 to 140 hr for the fuel and from 92 to 166 hr for the vessel.

In summary, there are margins of 30% in decay heat and 37% in core thermal conductivity before fuel temperatures of 1600°C are reached, and significantly higher margins before the bulk fuel failure temperature level of 2200°C is reached. However, these evaluations do emphasize that a high confidence in decay heat data and effective core thermal property data, including the

Table 3-3 Peak Fuel and Vessel Temperatures as Function of Decay Heat and Reactor Graphite Thermal Conductivity

Case No.	Description	Peak Fuel Temperature	Peak Vessel Temperature
1	Base Case	1360	422
	Increase in Decay Heat Q/Qo		
11	1.2	1516	466
12	1.5	1740	526
13	2.0	2128	614
	Change in Core Thermal Conductivity k/ko		
26	1.25	1283	421
21	0.75	1500	422
22	0.50	1747	417
23	0.375	1967	412
24	0.263	2317	403
25	0.250	2377	401

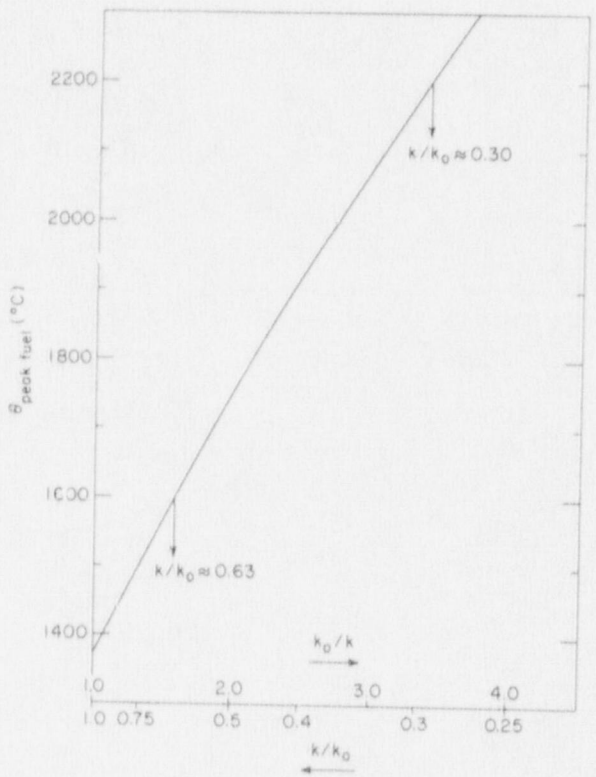

Figure 3-13 Peak Fuel Temperature as Function of Reduced In-Core Effective Thermal Conductivity

graphite annealing model, is required in order to accept the current best estimate reactor temperature transients.

4. PARAMETRIC EVALUATION OF DEPRESSURIZED CORE HEATUP TRANSIENTS WITHOUT OPERATING RCCS ("EARTH HEATUP")

It is recognized that the passive RCCS has a very low failure probability, and that even in case of catastrophic failures, only parts of the system would generally be lost, with partial flow blockages and/or partial loss of draft. Nevertheless, as a limiting case, depressurized core heatup without any cooling by the RCCS is being considered in this section. Depending on the initiator for this extremely severe accident scenario, the reactor silo walls or the RCCS panels may collapse, and the system geometry could be affected. The same could apply to the reactor vessel and/or its supports. One could speculate endlessly at the low probability level of such scenarios concerning the post accident geometry. For this evaluation it is assumed, non-mechanistically, that all below ground structures remain intact but that all air flow through the RCCS has ceased. To protect the surrounding concrete surfaces, the RCCS includes thermal insulation. At the top and at the bottom of the reactor cavity, shielding and additional thermal insulation are provided. This thermal insulation is the most significant heat transfer barrier in core heatup scenarios without RCCS cooling.

The failure assumed here is a most conservative case, in that it assumes a very "organized" event which:

1. eliminates all air flow, blocking all flow passages completely, while

2. keeping all thermal insulation in place.

In all practically conceivable accident scenarios of this kind, large parts of the air flow passages, but not 100% of them, would be blocked; and even 90% blockage with some remaining air flow would completely alter the accident scenario, providing significant cooling. At the same time it is assumed that this severely destructive event leaves all reactor cavity thermal insulation in place, while one would expect that an event of this severity would cause some of the insulated panels to collapse, leading to better heat removal and lower ultimate reactor and cavity temperatures.

In some initial computations it was established that the reactor cavity wall surface area was an important parameter for such core heatup scenarios. Furthermore, heat losses from the top and bottom of the vessel, while being only 10% of the total heat loss from the vessel, still had a significant effect on when and at which temperature level peak fuel and vessel temperatures were reached.

Thus, the two-dimensional THATCH model for this accident scenario includes top and bottom structures. As can be seen in Figure 4-1, most of the reactor cavity is surrounded by 1.5 m concrete walls leading to side cavities and to the steam generator cavity. Less than one third of the vessel surface "see" directly the 0.9 m outer concrete wall of the silo with earth behind it. Our model assumed peripheral symmetry, with either geometry prevailing all around. The results did not differ significantly, and an average of these two cases would represent the actual transient. To identify potential local vessel hot spots, one might want to expand this analysis at a later design stage to include the actual three-dimensional effects.

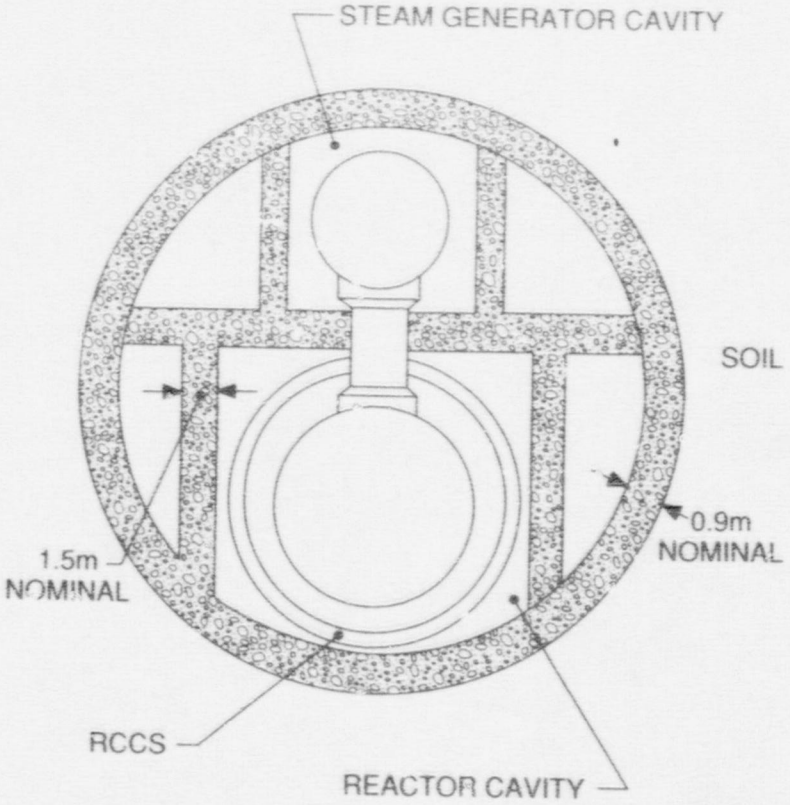

Figure 4-1 Cross Section of Reactor Silo (Cut Above Reactor Vessel)

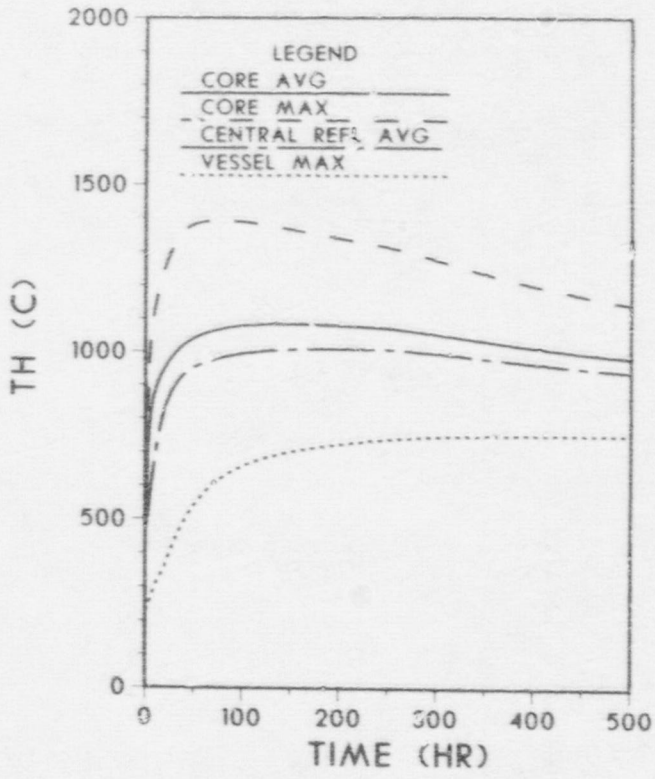

Figure 4-2 Core and Vessel Temperatures During a Depressurized Core Heatup Accident Without Operating RCCS (Base Case)

Upon suggestions by the DOE team, a two-dimensional radiation model was applied for the heat transfer across the reactor cavity, from the vessel to the RCCS structures. While runs made with this current 2-D radiation model were not identical to the earlier runs using a 1-D radiation model, the results seem to indicate that the inclusion of the more physical 2-d radiation model did not affect the peak temperatures very much.

4.1 Best Estimate Depressurized Core Heatup Transient Without Operating RCCS

For the Base Case, the nominal decay heat function was used assuming a uniform radial decay heat distribution. The heat transfer at the side was modelled as conduction across the RCCS insulation into 1.5 m of concrete, then by radiation and convection across a 2 m wide cavity, then conduction across 0.9 m of the outer silo concrete wall, and ultimately conduction to clay soil. The initial reflector irradiation and other data are equivalent to those of the Base Case with functioning RCCS, described in Section 3.1.

The results are relatively sensitive to the concrete material properties as well as to those of the thermal insulation in the RCCS. For the thermal insulation, conductivities of .0462 W/mk at 38°C and .104 W/mk at 482°C were provided by GA [GA, 1987-01]. Our model interpolates and extrapolates from these two points. As the insulation temperatures rarely exceed 650°C, the degree of extrapolation may be acceptable, given the larger uncertainties in the concrete properties.

Concrete properties vary widely, depending on local conditions, such as the cement and aggregate composition, as well as the final concrete density and its moisture content. For this work the values cited in GA-A15000 were used [GA, 1978]. Its thermal conductivity as function of temperature in °C is:

$$k = 1.945 * \left[1 - .0563 * \left(\frac{\theta}{100}\right)\right] \frac{W}{mK}$$

This relation gives the following values:

θ [°C]	100	300	700
k [W/mK]	1.84	1.62	1.18

Other typical data for normal concrete vary between 1.3 and 2.6 W/mK at room temperatures, and the above function is possibly higher than average since it was originally intended for an especially dense PCRV concrete (see for instance Figure 13 of Schneider, 1981). Concrete thermal conductivities typically descrease with temperature as drying occurs, and some of the physically bound water evaporates. Therefore, a more conservative thermal conductivity was selected for our Base Case, using the above function up to 200°C and a dry concrete conductivity of 0.5 above 400°C, with linear transition between these two models for temperatures between 200 and 400°C. Our Base Case results are therefore also more conservative than the corresponding DOE evaluations of Appendix G of DOE-HTGR-86-011, Rev. 4.

Our assumption of clay as the surrounding soil, with a relatively low thermal conductivity (k = 1.28 W/m K), is not really a best estimate, but a fairly conservative value. When these evaluations were initiated, it was felt

that conservative properties should be assumed, since the current DOE plan is not to consider the surrounding soil or the concrete thermal properties in the design of the reactor cavity.

Results for the Base Case transient are shown in Figures 4-2 through 4-6. The peak fuel temperature of 1393°C is reached at 78 hr, as compared to 1366° at 55 hr for the corresponding case with functioning RCCS (see Section 3). At the time of peak core temperatures the surrounding concrete structures have been little affected, and concrete/soil properties and configurations have had virtually no effect on peak core temperatures. But concrete and soil can have an effect on the speed of the subsequent cooldown. The vessel reaches its peak temperature of 754°C at 425 hr. However, this maximum is very flat, and vessel temperatures remain within 10°C of this value from 270 hr to 800 hr. The final cooldown proceeds very slowly, and at 1500 hr (2 months) the maximum core temperature has reached 910°C, and the maximum vessel temperature is still 710°C.

Thus, in core heatup accidents without RCCS the peak fuel temperatures are only about 30°C higher than with RCCS. However, the vessel temperatures as well as the concrete silo temperatures are much higher, and the ultimate cooldown is exceedingly slow.

The next section will present a parametric evaluation of the effects of concrete and soil properties and configuration on the peak fuel and vessel temperatures, as fuel and/or vessel failure are the major items of concern. The section thereafter discusses the margins from the best estimate evaluations, i.e., to temperature levels at which significant failures must be expected.

4.2 Parametric Evaluation of the Effect of Concrete and Soil Configuration and Properties

Several parametric variations of this accident scenario are summarized in Table 4-1. As shown in Figure 4-1, the base configuration of heat rejection via concrete sidewalls and across side cavities to the outer walls applies over a larger part of the perimeter and is more representative than the case of direct heat transfer to the 0.9 m outer concrete walls and surrounding soil. As Case 2, such heat transfer directly to outer walls and to the rather adverse clay soil of low thermal conductivity was evaluated. As expected, the peak core temperatures were not affected by this change, since the back sides of the concrete have not yet begun to heat up when the peak core temperatures are reached. However, the vessel in this case peaks much later, at 1105 hr and at a 13°C higher value of 767°C. In actuality, a combination of these two cases would best describe the actual transient. At the time scales considered here, there will be significant peripheral conduction in the vessel walls, and the actual peak vessel temperature will be between the values of Case 1 and Case 2. Both cases are very close in their peak vessel temperatures, but Case 2 results in a longer duration of the high vessel temperatures. Therefore, one can consider Case 2 as a more conservative evaluation, with the Base Case being more representative of a best estimate evaluation. In any case, a three-dimensional evaluation, considering a complete combination of both cases with peripheral vessel conduction is not justified, particularly in light of the significant uncertainties in concrete and soil properties.

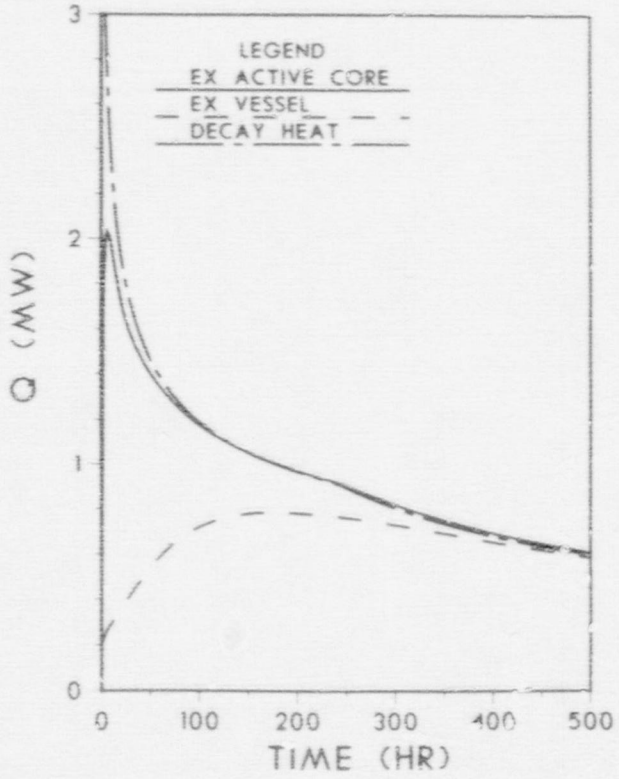

Figure 4-3 Decay Heat and Heat Flows During a Depressurized Core Heatup Accident Without Operating RCCS (Base Case)

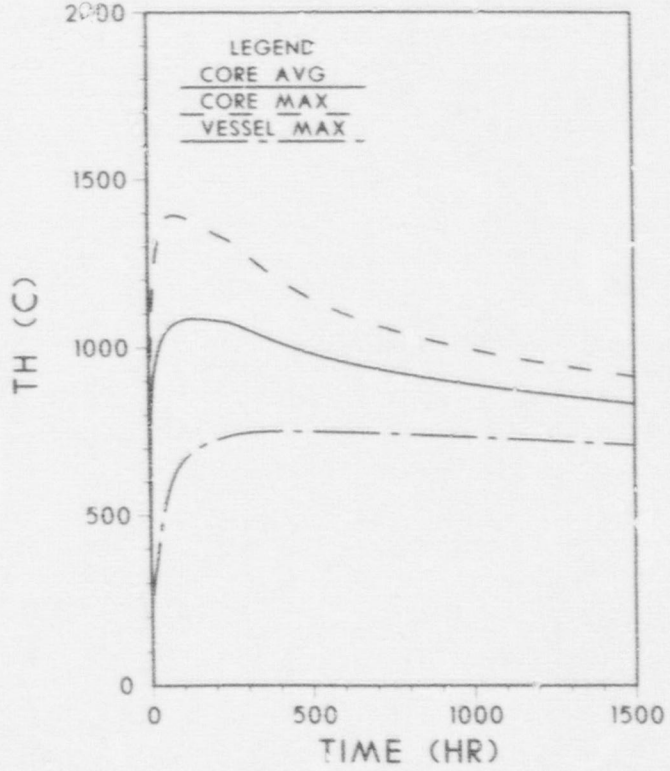

Figure 4-4 Core and Vessel Temperature During a Depressurized Core Heatup Accident Without Operating RCCS (Base Case)

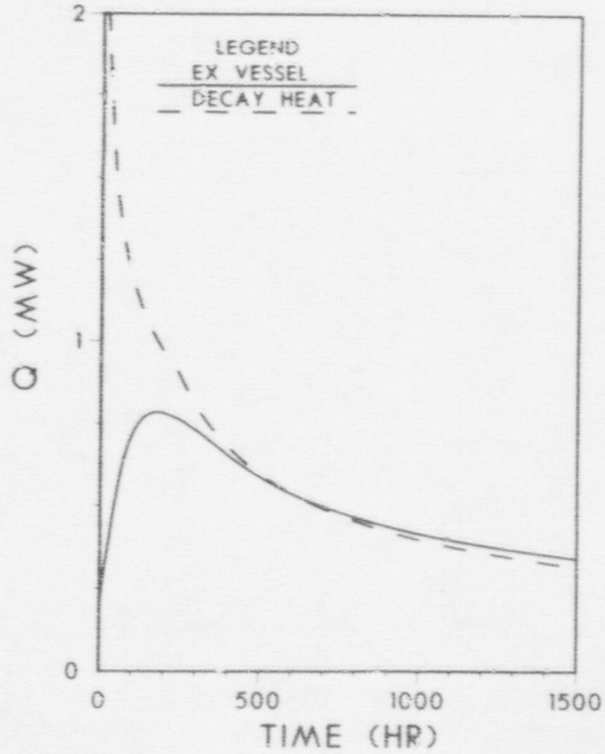

Figure 4-5 Decay Heat and Heat Flows During a Depressurized Core Heatup Accident Without Operating RCCS (Base Case)

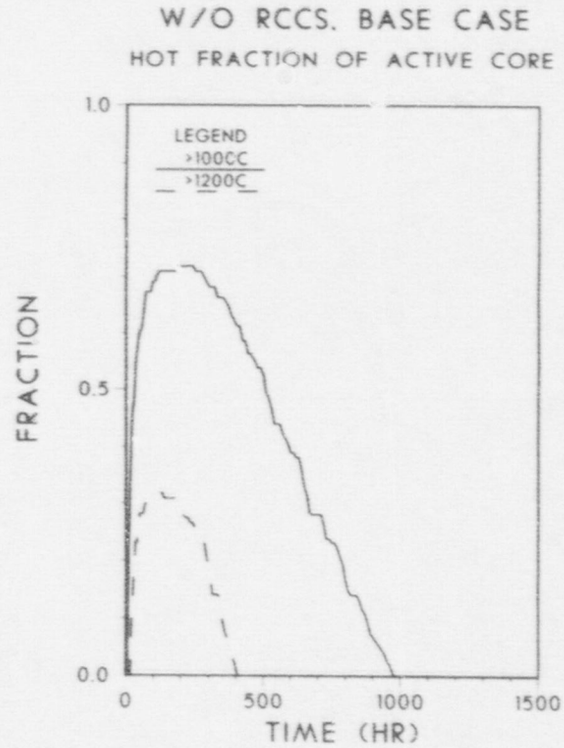

Figure 4-6 Fraction of Active Core Exceeding Specified Temperature Limits During a Depressurized Core Heatup Accident Without Operating RCCS (Base Case)

Table 4-1 Parametric Comparison of Depressurized Core Heatup Transients without Operating RCCS

Case No.	Description	Peak Fuel Temperature			Peak Vessel Temperature			Vessel Cross Over Time* hr	Maximum Core Temp. at 1500 hr	Maximum Vessel Temp. at 1500 hr
		Value °C	At Time hr	Variation From Base Case °C	Value °C	At Time hr	Variation From Base Case °C			
1	Best Estimate Case	1393	78	----	754	425	---	610	914	710
2	Heat Transfer to Exterior Concrete Wall and Clay Soil	1393	78	0	767	1105	+13	1250	966	764
3	Concrete Properties of Ref.4 without Assuming Reduced Thermal Conductivity with Dryout	1393	78	0	739	310	-15	345	**	**
4	As Case 2, but Surrounding Soil Thermal Conductivity Reduced by 50%	1393	78	0	793	1680	+39	1790	994	792
5	Conservative Decay Heat	1636	125	+243	964	1015	+210	1150	1200	956
6	Average Soil and Concrete	1378	62	-15	647	315	-107	350	**	**

* Time at which heat leaving vessel exceeds decay heat, i.e., net cooldown of reactor vessel and internals begins.

** Case was not run to 1500 hr.

Our Base Case and Case 2 evaluations assume a reduction of concrete thermal conductivity with dry out. This conservative assumption was not included in the DOE evaluations. Case 3 uses the Base Case geometry and the GA-A15000 concrete properties without such dry out. In this case, the vessel temperature peaks earlier, at 310 hr and at 739°C, i.e., 15°C below the Base Case.

As the soil properties are not controlled, even worse soils than low conductivity clay may be encountered. In Case 4 this effect is shown, by arbitrarily lowering the soil conductivity to 50% of its Base Case value of 1.28 W/mK. This will increase the peak vessel temperatures by only 39°C, but it should be noted that the cooldown will be much slower with core and vessel temperatures about 80°C higher than the Base Case at 1500 hr (2 months from scram).

Using LTR-4 decay heat [Sund, 1973], significantly higher core and vessel temperatures are indeed obtained. Peak fuel temperatures of 1636°C at 125 hr and peak vessel temperatures of 964°C at 1015 hr (six weeks) were computed. However, the arbitrary use of this decay heat may not be realistic. Over the first 100 hr it releases 28% more in energy than the best estimate data indicate, and over 1500 hr the increase amounts to 38%. Results for this case are shown in Figures 4-7 through 4-11.

Thus, with best estimate decay heat data and for several fairly conservative concrete and soil configurations, the peak core temperatures were found to be about 1400°C at about 80 hr, and the peak vessel temperatures ranged from 740°C to 795°C. However, the transient would take months, and for less favorable concrete and soil conditions it would proceed significantly slower.

The concrete at the center of the cavity can reach very high temperatures. In the Base Case it peaked at 605°C at 1200 hr. In Case 2 it reached 673°C at 1500 hr and was still rising slowly. In Case 5, with a very conservative soil property assumption, it was 710°C at 1500 hr, and still rising, although slowly. Such temperatures would cause loss of most or all bound water, and, for most concretes, would result in a loss of strength and cracking. These peak concrete temperatures, occuring at the inside reactor cavity wall surface, roughly at the mid-elevation of the vessel, are included as "side max" in Figures 4-12 and 4-13 for the Base Case and for Case 2.

It was also observed that the concrete of the operating floor above the reactor cavity was getting rather hot. For instance, in the Base Case it peaked at about 1100 hr with temperatures from 110°C at the top surface to 480°C at the bottom surface of the 0.9 m thick floor. Whether structural integrity of the floor can be assured at such temperatures may not be assured. It should be noted, however, that our modelling and nodalization, as well as assumptions on thermal insulation for the top region, were not as refined as for the center portions of core and reactor vessel, which constituted our major concern. Thus, if this region were to be of concern, our modelling of it should be improved before significant conclusions are drawn. Nodal peak temperatures of the top floor and the average top floor temperature are included in Figures 4-14 and 4-15 for the Base Case and for Case 2.

The concrete temperatures in the region of the vessel supports were also fairly high, 450°C in the Base Case and 500°C in Case 2, and still rising in both cases. These data are also included in Figures 4-14 and 4-15.

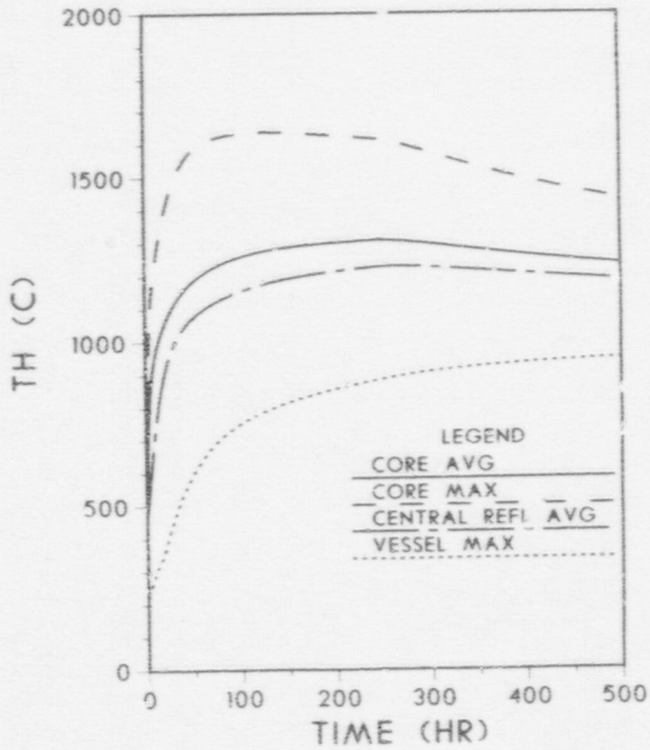

Figure 4-7 Core and Vessel Temperatures During a Depressurized Core Heatup Accident Without Operating RCCS (LTR-4 Decay Heat)

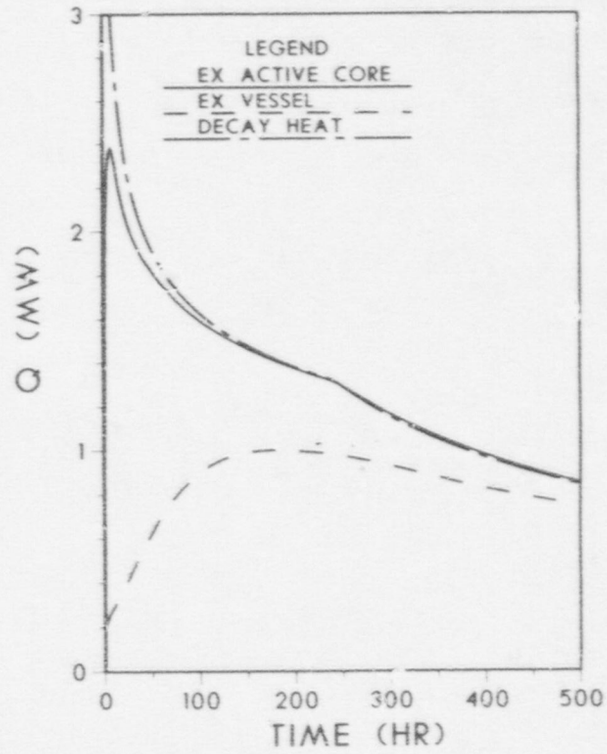

Figure 4-8 Decay Heat and Heat Flows During a Depressurized Core Heatup Accident Without Operating RCCS (LTR-4 Decay Heat)

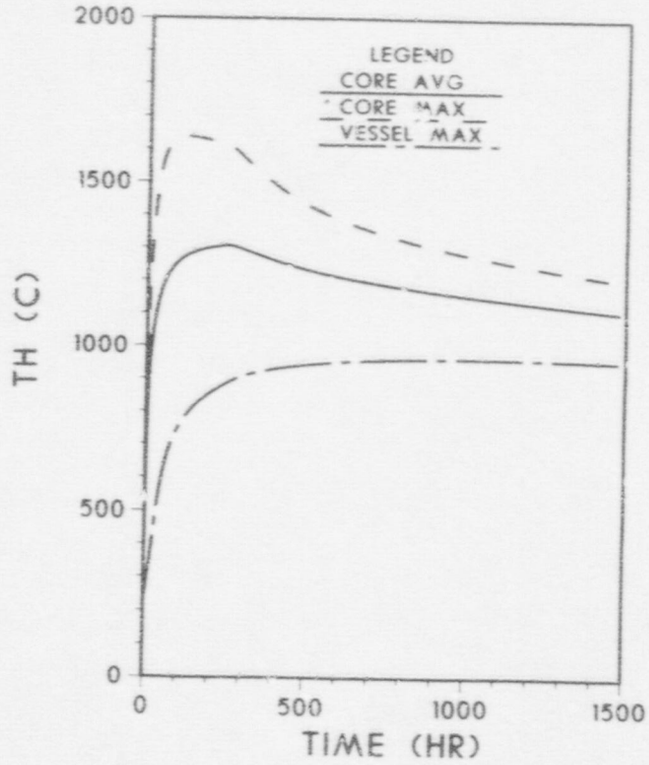

Figure 4-9 Core and Vessel Temperature During a Depressurized Core Heatup Accident Without Operating RCCS (LTR-4 Decay Heat)

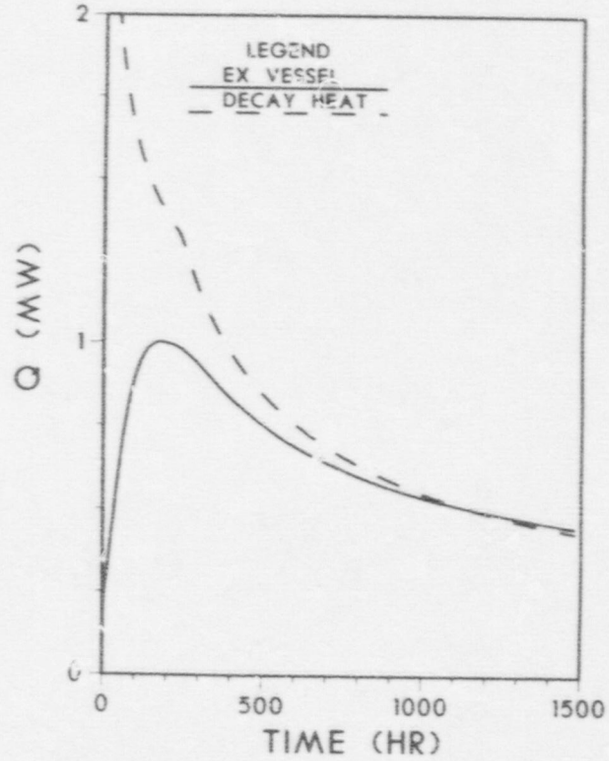

Figure 4-10 Decay Heat and Heat Flows During a Depressurized Core Heatup Accident Without Operating RCCS (LTR-4 Decay Heat)

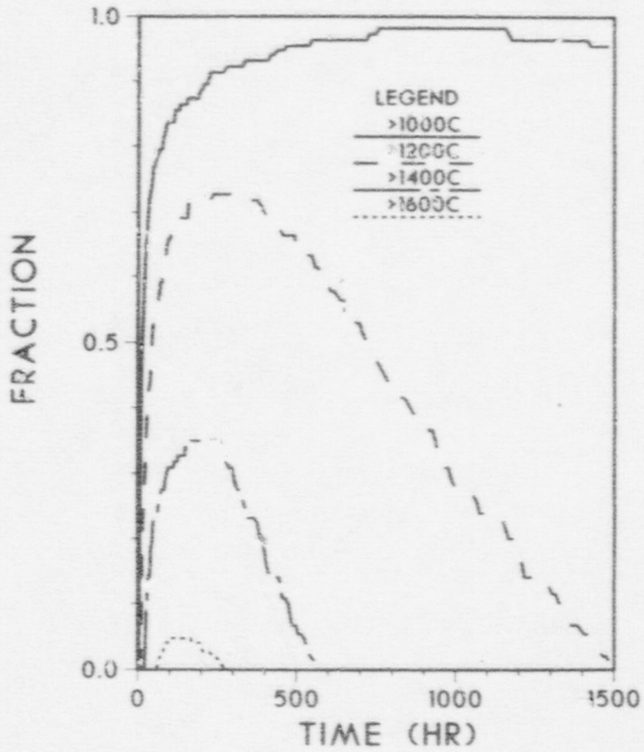

Figure 4-11 Fraction of Active Core Exceeding Specified Temperature Limits During a Depressurized Core Heatup Accident Without Operating RCCS (LTR-4 Decay Heat)

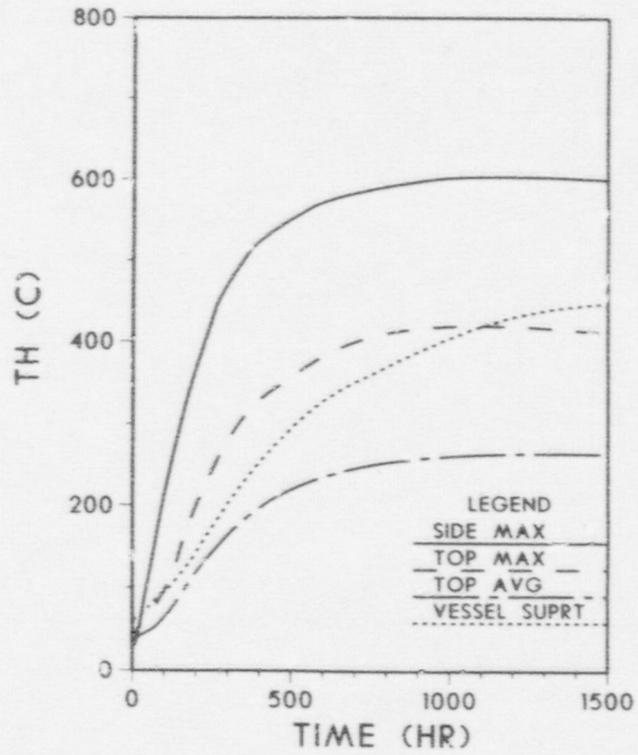

Figure 4-12 Concrete Temperatures in the Reactor Silo During a Depressurized Core Heatup Accident Without Operating RCCS (Base Case)

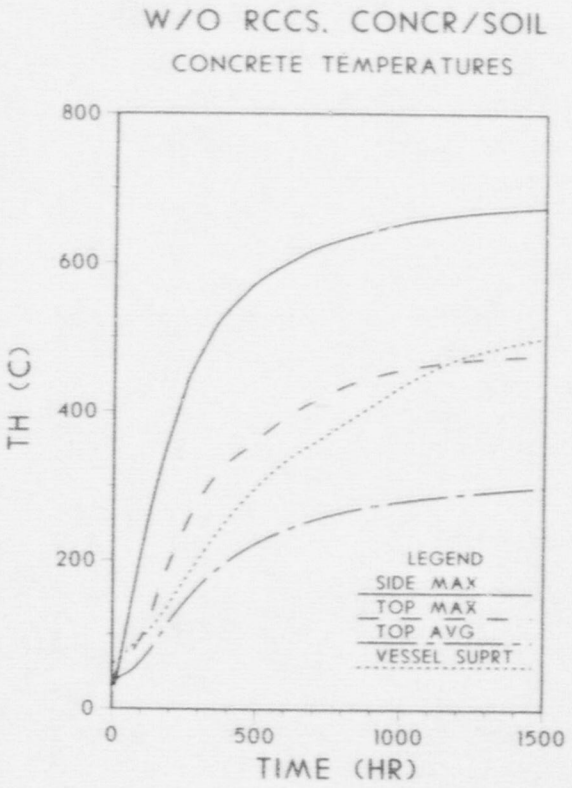

Figure 4-13 Concrete Temperatures in the Reactor Silo During a Depressurized Core Heatup Accident Without Operating RCCS (Case 2; Direct Heat Conduction to Outside Wall and Soil)

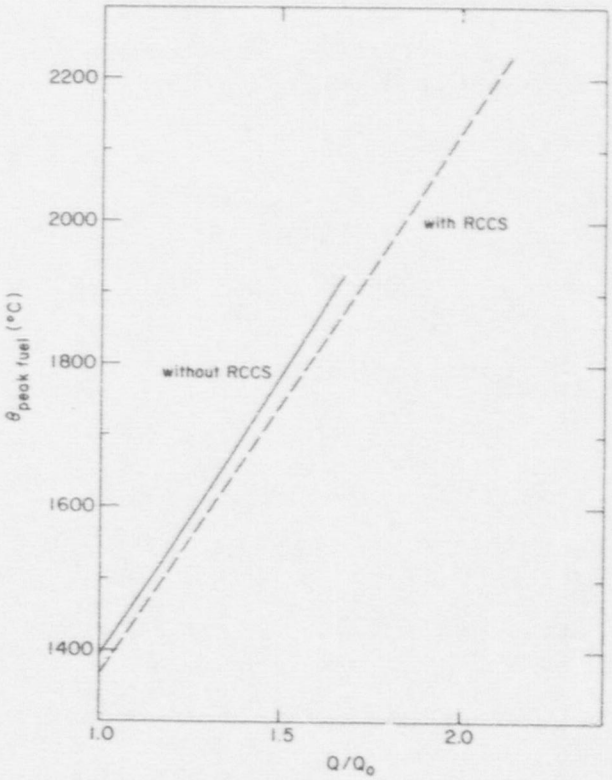

Figure 4-14 Peak Fuel Temperatures as Function of Increased Decay Heat Generation

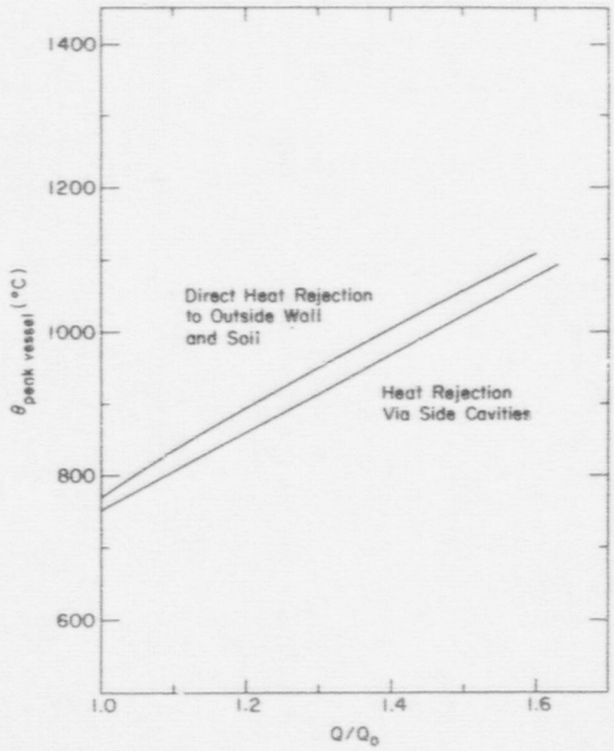

Figure 4-15 Reactor Vessel Peak Temperatures as Function of Increased Decay Heat Generation

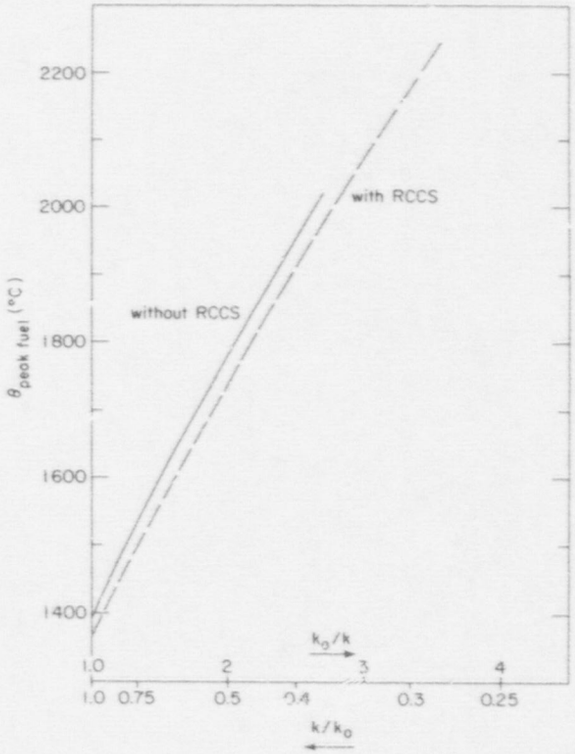

Figure 4-16 Peak Fuel Temperature as Function of Reduced In-Core Effective Thermal Conductivity

Another possible area of concern is the metal core support structure. In the Base Case 1 its peak temperature was about 650°C at 1200 hr. It varied by less than 10°C from the centerline to the area of attachment to the reactor vessel. These values agree fairly well with thos reported by the DOE team, which stated that only minor creep would be expected at such temperatures.

To establish whether the reactor cavity could be designed to withstand even these core heatup accidents without functioning RCCS, an evaluation was made in Case 6, using more average rather than conservative concrete and soil properties and removing the thermal insulation within the RCCS (this insulation is not really required for the RCCS to function properly under normal operation or under design basis accident conditions). In this case, the vessel temperatures peaked at 647°C, about 100°C lower than in the preceding cases, and the peak concrete temperatures at critical areas peaked near 260°C. One local peak concrete temperature at the side wall surface reached 500°C. Thus, a "hardened" reactor silo design, showing significantly lower vessel and concrete temperatures under such severe accident scenarios, may be achievable with appropriate design modifications, i.e., elimination or reduction of insulation and proper selection of concrete and backfill soil.

Thus, in summary, under best estimate decay heat conditions, it appears that there will be no significant core temperature excursions and that core and vessel integrity remain intact. The ultimate core cooldown would take many months. Concrete temperatures at the side of the reactor silo would be in the range of 600°C, which would result in release of bound water and loss of strength. If operating floor temperatures of 100 to 500°C become reason for concern, more detailed modelling of those areas should be implemented.

4.3 Evaluation of Safety Margins in Decay Heat and Core Properties on Reactor Peak Temperatures

As in Section 3-3 the decay heat was raised to establish the effect of uncertainties in the given best estimate data. The results are summarized in Table 4-2 and in Figures 4-14 and 4-15. Peak fuel temperatures are again largely independent of concrete and soil configuration and property effects, as only small portions of the concrete have begun to heat up at the time of the peak fuel temperatures of 70 to 80 hr.

Figure 4-14 shows that a 27% increase in decay heat would bring peak fuel temperatures to 1600°C. It also shows that the peak fuel temperatures remain about 30°C to 40°C above those with operating RCCS. Thus, failure of the RCCS does not have a major impact on the peak fuel temperatures.

Effects of decay heat variation in vessel temperature are shown in Figure 4-15. A 40% increase in decay heat would result in peak vessel temperatures above 1000°C more than 1000 hr (6 weeks) after the beginning of the accident.

While there is no specific vessel temperature at which failures are certain, at 1000°C vessel integrity can most likely not be assured. At the same time the peak fuel temperature at such decay heat levels are about 1780°C, with only 19% of the core ever exceeding 1600°C, in the time range from 24 to 330 hr. At the time of peak vessel temperatures, core average and peak temperatures are 1215°C and 1320°C respectively. Thus, at such increased decay

heat levels, cases are conceivable, where some fuel failures occurred at about 100 hr, with subsequent vessel failures after several weeks, when core temperatures have already returned to the 1200°C to 1300°C range.

The effect of variation in core thermal conductivities is shown in Figure 4-16, and is included in Table 4-2. The resulting peak fuel temperatures are again about 30°C higher than those for the corresponding cases with RCCS. A loss of 33% in thermal conductivity would be required to reach a peak fuel temperature of 1600°C. As reduced core thermal conductivities had only very minor effects on the vessel temperatures, these cases were not extended to longer times or to other concrete/soil variations.

Thus, in summary, the decay heat and thermal conductivity margins for fuel failures are very close to those for cases with RCCS. However, higher decay heat levels can affect the peak vessel temperatures negatively, possibly resulting in some structural failures at very long times into the transient, again pointing to a need for high confidence in the provided decay heat data.

Table 4-2 Parametric Evaluation of Safety Margin During Core Heatup Scenarios without RCCS Operation

Case No.	Description	Peak Fuel Temperaturen		Peak Vessel Temperature	
		Value °C	At Time hr	Value °C	At Time hr
	Increased Decay Heat Heat Rejection Via Side Cavities To Soil Q/Qo				
11	1.0 (Base Case)	1393	78	754	420
12	1.2	1545	72	859	780
13	1.5	1778	76	1023	1220
	Increased Decay Heat Heat Rejection Directly To Outside Wall and Soil Q/Qo				
21	1.0 (Case 2)	1393	78	767	1100
22	1.2	1545	72	894	1470
23	1.5	1778	76	1055	1500
	Decreased Core Thermal Conductivity Heat Rejection via Side Cavities to Soil k/ko				
11	1.0 (Base Case)	1393	78	754	420
31	0.6	1659	90	758	430
32	0.4	1951	116	759	460

5. AIR INGRESS DURING DEPRESSURIZED CORE-HEATUP ACCIDENTS WITH FAILED CROSS DUCT AND/OR FAILED REACTOR VESSEL

The low probability accident scenario which has always raised significant concern in gas-cooled reactor concepts is an air ingress accident with significant graphite oxidation. So-called graphite fires are virtually precluded by the current MHTGR design. The air ingress scenarios considered here are of extremely low probability, but could lead to the formation of combustible gases and, if allowed to persist for a long time, to a weakening of the core structure. Furthermore, if the exothermal graphite oxidation with air could increase the fuel temperatures sufficiently, fuel failures and fission product release could result.

As in previous designs, the MHTGR precludes significant air ingress from being a credible event. It would require the simultaneous failure of the reactor vessel at both, top and bottom locations, or a complete double guillotine break of the short cross duct, which is built to vessel specifications. While such scenarios, like shearing the cross duct but leaving the reactor and its internal components intact, may not be credible events, they can serve as an upper bound for potential air ingress scenarios, establishing bounding consequences. It was therefore assumed here, that the cross duct has failed catastrophically and yet remains fully open for gas flow into and out of an intact reactor vessel.

Following such a cross duct break, gas would enter the inner section of the annular cross duct, flowing by natural convection upward through the core, then downward at the core barrel, to discharge through the outer annulus of the cross duct. Significant gas recirculation would occur at the exit, with part of the inflowing gas being exhaust gas. Again, this recirculation, as well as the fact that the fresh air inventory in the silo cavities is very limited, are being disregarded. Rather, non-mechanistically, pure air inflow into the inner section of the cross duct is generally assumed.

Subsequent to such a break the reactor would experience a core depressurized heatup transient with decay heat rejection to the passive Reactor Cavity Cooling System, as described in Section 3. The natural convection gas flow through the reactor, coupled with the mass transfer and chemical reaction between the incoming oxygen and the core graphite will be analyzed in this Section.

5.1 Flow and Chemical Reaction Models

The transient reactor temperature field is computed by the THATCH code, as described in Section 3. In computing the core temperatures, the additional heat generation from the chemical reactions of graphite and oxygen was found to be small, and was initially neglected. In more recent runs, this effect was included by coupling the THATCH code and the flow and oxidation computations to be described here.

Based on the above temperature history, the THATCH flow module, FLOXI, evaluates the gas flow through the reactor coupled with the graphite/oxygen chemical reaction. The code represents several parallel flow channels through the core and one flow channel at the core barrel. Generally, the flow will be

upward through the core and downward in the outer core barrel channel. Typically, the FLOXI parallel flow channels follow the THATCH radial nodalization, and six parallel flow channels were employed here. Axially, each flow channel had 28 nodes, of which 20 were in the active core.

The gas flow through the reactor is modelled by a quasi-steady momentum equation, primarily balancing buoyancy and friction forces. The gas temperature is assumed to follow the temperature of the solid structures, which is believed to be a good assumption in the core during these very slow transients with a low thermal capacitance gas flowing through a structure of very large thermal capacitance. Alternately, the gas temperatures can be computed, modelling the convective heat transfer between the solid structures and the gas. This was done in some of the later runs for the core barrel region, resulting in more accurate flow computations, which typically yield 10% lower core gas flows. Gas properties are evaluated for the prevailing mixtures, permitting O_2, N_2, CO, CO_2, H_2O, H_2 and He as gas components. The flow computations include the effect of gas expansion resulting from the chemical reaction and its effect on the increased friction pressure drop.

In all cases the core flow was found to be laminar, with Reynolds number generally between 5 and 50, and with gas velocities between 0.1 and 0.4 m/s.

The graphite oxidation process is a function of the temperature regime. At low temperatures, the carbon/oxygen reaction kinetics control the reaction rate. At intermediate temperatures, the in-pore diffusion is controlling, while at high temperatures the coolant to surface mass transfer by diffusion, here in a laminar flow field, is controlling.

To consider all three regimes a model including external mass transfer, in-pore diffusion, and chemical reaction kinetics would be required, as is done, for instance in the Oxide-3 code [Peroomian et al., 1974]. For the current initial applications it was decided to use a simpler approach, combining the in-pore diffusion and chemical reaction process into a single Langmuir-Hinshelwood type semi-empirical equation as done, for instance, by Moormann and Petersen [1982]. This equation is

$$R = \frac{k_1 e^{-c_1/\theta} \, p_{O_2 w}}{1 + k_2 e^{c_2/\theta} \sqrt{p_{O_2 w}}} \cdot \sqrt{\frac{D}{D_o}} \quad \left[\frac{\text{Moles } O_2}{m^2 s}\right] \qquad (1)$$

where R is the oxidation rate per unit surface area, p_{O_2} is the partial pressure of oxygen and D is the binary diffusion coefficient of oxygen in the gas mixture. θ is the gas temperature, k_1, k_2, c_1 and c_2 are constants. D_o is the binary diffusion coefficient at reference temperature and pressure. This relationship is solved simultaneously with the coolant to surface mass transfer relationship

$$R = \frac{\beta}{R\theta} \left(p_{O_2 str} - p_{O_2 w}\right) \quad \left[\frac{\text{Moles } O_2}{m^2 s}\right] \qquad (2)$$

where the mass transfer coefficient β is computed from the Sherwood number correlation

$$Sh = \frac{\beta d}{D} = f\left(Re, \frac{\nu}{D}\right) \tag{3}$$

and for purely laminar flow

$$Sh = \frac{\beta d}{D} = 4.3 \tag{3a}$$

$\hat{R}$ is the universal gas constant, d the coolant hole diameter, Re the Reynolds number and ν the gas viscosity. The subscripts w and str refer to wall and bulk stream values, respectively.

The shortcoming of this model is that for the in-pore diffusion regime it cannot predict the lateral distribution of the oxidation process, i.e., the depth of the reaction zone. (In the chemical reaction controlled regime the burn-off is essentially uniform throughout the graphite, while for the coolant to surface mass transfer controlled regime essentially all the oxidation occurs at the surface.)

As will be shown below, the temperatures in the center of the core virtually always extend well into the mass transfer controlled regime, and essentially all incoming oxygen will react. Therefore, the total amount of carbon reacting is determined by the gas inflow rate, which in turn is limited by the high core friction pressure drop. Thus, this model is sufficient for our current evaluations.

The binary diffusion coefficients for various non-polar gas mixtures were computed based on the Chapman-Enskog kinetic theory [Bird et al., 1960].

For most of the current evaluations it was assumed, conservatively, that the gas inflow at the cross duct was pure air. Therefore, as most representative, the binary diffusion coefficient of oxygen in nitrogen was used.

For the Best Estimate Case the reaction rate constants of Katcher and Moormann [1986] for A3-3 graphite, a typical core graphite, were used, since these reaction rate constants were readily available in the required format. Corresponding data representative of U.S. core graphite will be used in future work. However, parametric variations of the rate constants by one order up and two orders down will show below, that the total oxidation is strictly gas flow limited.

Only the reaction

$$C + \frac{1}{2} O_2 \rightarrow CO$$

was considered here. While it is possible that initially some CO_2 is formed in the cooler bottom regions of the core, this CO_2 would then react in the hotter core regions with carbon to CO. For the amount of combustible gases formed, and for the total burn-off, the assumed reaction is conservative. If

any significant amounts of CO_2 were to leave the reactor this would result in a higher chemical energy release from the oxidation. But even if, hypothetically, all oxygen would react to CO_2, the effect of this chemical energy release would still be small in comparison to the decay heat.

5.2 Best Estimate Evaluation

Initially, after scram from full power operation, the bottom regions of the core were the hottest (about 690°C), and assuming pure air inflow at the break, some of the entering oxygen did not react. The volume fraction of air leaving the core was 6% at the beginning of the transient. However, within a few hours, the temperatures at the center of the core rose, and the incoming gas flowed into hotter regions, where it reacted fully. Using best estimate chemical reaction rates, most of the oxidation occurred in the very bottom regions of the core, where the in-pore diffusion process was still controlling. In addition to the increase in temperatures, the total coolant to graphite exposed surface area also increases very markedly in the upflow direction from the lower plenum post blocks, to the flow distribution blocks, and to the bottom reflector blocks, thus further increasing the reaction rate per unit length of core flow channel.

The best estimate run was established by iterating between the THATCH and FLOXI code to include the effect of chemical reaction heat on the core temperature field. This additional energy release amounted to about 10% for the first 100 hr. However, since it remains primarily concentrated in the lower reflector regions, the peak core temperatures rose by only 16°C to 1382°C, when compared to the best estimate case without air ingress of Section 3 (Note that comparison is to the case with uniform radial after heat distribution).

The air inlet flow and the amount of core graphite oxidizing are shown in Figure 5-1. The air flow decreased early in the transient from about 800 kg/hr to about 260 kg/hr for most of the transient. In the laminar flow regime, as core temperatures rise, the increased in core friction pressure drop is more pronounced than the increase in buoyancy, thus leading to a flow reduction as the core heats up and a later slight flow increase, as the core begins to cool down.

When all oxygen was consumed in the lower portion of the core, after the first two to three hours, the gas mixture through most of the core was about 35 vol % CO and 65 vol % N_2. The amount of graphite oxidized, as shown in Figure 5-1, decreased proportional to the air inflow from 150 kg/hr early in the transient to about 45 kg/hr for most of the transient.

As the total initial air inventories in the reactor and steam generator cavities are of the order of 500 kg air each, it is clear that a sustained pure air inflow is physically impossible as long as the Reactor Building remains intact. Even with an unlimited air supply, significant recirculation would occur at the break between the gas entering through the inner section of the cross duct and the gas leaving through the surrounding annular section of the cross duct, and the assumption of pure air inflow again constitutes an upper limit.

In an intact reactor building, the available air would be converted within a few hours to CO and N2. In particular, if the He concentration in the

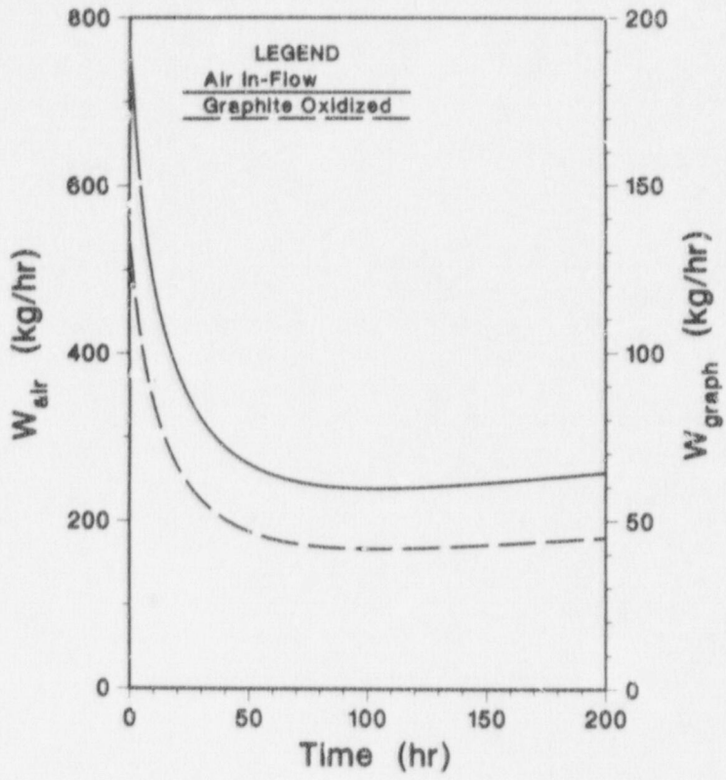

Figure 5-1 Air Inflow and Graphite Oxidation Rate Subsequent to Double Guillotine Cross Duct Break with Unlimited Air Inlet Supply

affected cavities after blowdown is sufficiently low, combustible gas mixtures of CO and air could be formed temporarily, and local burning in the reactor building outside of the primary loop would be possible.

5.3 Parametric Variation of Reaction Rate Constants

To assess the effects of uncertainties in graphite oxidation rates and gas diffusion coefficients a set of parametric evaluations were made. These evaluations used an earlier decay heat function which exceeds the current best estimate decay heat function by 28%. The resulting peak core temperatures were about 1600°C, and for this hotter core the predicted gas flow rates were about 5 to 10% lower than in the current best estimate case.

Varying the graphite reactivity, the rate constant k_1 of Equation (1) was raised from its base value of 2.34 by one order and lowered by two orders.

As the results in Table 5-1 show, the only effect of drastically lower reactivity is a relatively minor upward extension of the oxidation region. It has virtually no effect on the total amount of graphite oxidized. The total amount of graphite oxidized actually increases very slightly with decreasing reactivity, since the coolant average density is affected by the changing gas composition, and less of the total core flow path has to carry the increased mass flow after reaction, thus resulting in a slightly lower friction pressure drop, and a higher gas inflow. As seen from the oxygen partial pressures at the core inlet, the in pore diffusion and chemical reaction are the controlling effects at the core inlet. Generally the reaction was found to be completed before the hotter core regions were reached, where the coolant to surface mass transfer would be limiting.

The above evaluations used a binary diffusion coefficient of oxygen in nitrogen, computed from the Chapman-Enskog model. To assess the effect of uncertainty in this coefficient, a run with a two orders lower diffusion coefficient was made. In this case, with greatly increased coolant to surface mass transfer resistance, the oxidation process was generally controlled by the mass transfer resistance and some of the oxidation did occur in the center of the core. Beyond the first few hours, most, but not all, of the oxygen reacted in this case.

Table 5-2 compares the gas flow rates and carbon burnt for the case of reduced gas diffusion coefficient against the base case. Again, the delayed chemical reaction results in a slightly higher mass flow through the core and a slightly higher total core graphite oxidation rate during most of the transient. But the result indicates that uncertainties in the diffusion coefficients have very little effect on the total amount of carbon reacting.

Also included in Table 5-2 are the results for a case where the inflowing gas composition is a 50/50 mixture by volume of helium and air. This would be more typical of potential gas ingress scenarios, subsequent to a blowdown, than the more hypothetical but also more limiting case of pure air inflow. As the helium contribution reduces the total core mass flow to about one-third of that for pure air inflow, the amount of carbon burnt is also reduced to about one third of the base case burn-off.

Table 5-1 Oxidation Results at 20 hr for Core Hot Channel

k_1/k_1 base	0.01	0.1	1.0	10
ΔZ (m)	7.75	5.4	3.7	3.0
Total Core Gas Inflow (kg/hr)	401	383	376	373
Total Core Carbon Reacting (kg/hr)	69.9	67.0	65.7	65.2
$p_{O_2\ str}$ (bar)	.2100	.2100	.2096	.2064
$p_{O_2\ w}$ (bar)	.2100	.2099	.2088	.1987

Legend:

k_1 = rate constant of Equation (1)

ΔZ = vertical distance, from entry to bottom reflector post block, at which all oxide is consumed

$p_{O_2\ str}$ = partial pressure of O_2 in coolant stream in post block

$p_{O_2\ w}$ = partial pressure of O_2 at coolant/graphite surface of post block

Table 5-2 Core Gas Inlet Flow and Total Graphite Oxidation Rate for Best Estimate Case, Case of Reduced Binary Diffusion, and Case of Helium-Air Mixture Entering Core

Time hr	Inlet Gas Flow kg/hr			Total Core Graphite Oxidation Rate kg/hr			Fraction of Oxygen Reacted			Energy Release due to Graphite Oxidation as Fraction of Decay Heat
	Base Case	Reduced Diffusion Coefficient	Air Helium Mixture	Base Case	Reduced Diffusion Coefficient	Air Helium Mixture	Base Case	Reduced Diffusion Coefficient	Air Helium Mixture	Base Case
0	688	894	246	112	20	38	.929	.129	.996	.013*
20	376	402	138	66	67	21	1.0	.959	1.0	.070
40	289	302	107	51	52	16	1.0	.988	1.0	.063
80	240	248	89	42	43	14	1.0	.996	1.0	.060
120	233	241	87	41	42	13	1.0	.997	1.0	.065
160	238	246	89	42	43	14	1.0	.996	1.0	.071
200	248	257	92	43	45	14	1.0	.995	1.0	.078

* using 6% decay heat at time zero

Also included in Table 5-2 is the ratio of chemical energy release from graphite oxidation to CO as fraction of the decay heat at that time. The contribution from this chemical energy release remains around 6 to 8% of the decay heat, and is, therefore, not a major effect, particularly since the results of this subsection were obtained using a very conservative decay heat function.

5.4 Conclusion

In case of a massive break in the coolant pressure boundary, such as the case of a double guillotine cross duct break, permitting external gas ingress into the core, the resulting natural convection flow through the core remains limited by the in-core friction pressure drop in the coolant hole passages. The flow is always laminar, with typical Reynolds numbers remaining well below 100.

With core temperatures rising during the subsequent core heatup, any oxygen entering the core will be oxidized, and at the prevailing core temperatures virtually all of it will leave as CO. Thus, the graphite oxidation rate in case of such a massive failure is limited by the possible gas flow through the core and not by the chemical reactivity or mass transfer processes.

In an intact reactor building some temporary local burning could occur, with the CO exiting from the primary loop reacting with some of the remaining air in the reactor building.

As long as the total air available remains limited to the initially available air of the reactor and/or steam generator cavity, its oxygen would be consumed within a few hours, resulting in a few hundred kg of graphite in the lower portions of the bottom reflector and core structure having been oxidized. The mass of graphite in the active core is about 8000 kg/m. Thus even under these severe conditions the fraction of graphite reacted would remain in the range of a few percent.

Only if an unlimited air supply were available, for instance after destruction of the Reactor Building, and the 60 kg/hr oxidation rate were sustained for days, would a significant loss of graphite and loss of structural integrity become a possibility.

Thus, even under the above extreme assumptions, such an accident would not lead to any rapid destruction of the core or to any significant additional fission product releases.

As the lower plenum core support posts and the post blocks and flow distribution blocks are made out of 2020 stack pole graphite, these results will be reviewed using data for 2020 graphite in order to determine whether any preferential oxidation in the originally hot lower plenum region could be of further concern. In particular, since the exposed surface area of graphite in this part of the reactor is small with respect to the core, we do not anticipate that there will be any significant concern in this area.

6. WATER INGRESS SCENARIOS

Water ingress scenarios in connection with depressurized core heatup transients were considered briefly in connection with the SRDC-6 and 7 scenarios of Chapter 15 of the PSID. The more severe Bounding Event Sequence BES-4 remains to be considered in the future. The main emphasis was to determine whether significant graphite oxidation or the accumulation of combustible gases would have to be expected.

The computations were made with the THATCH/FLOXI code, using the same modelling as described in Section 5 for the case of air ingress, except that water properties and the water/graphite chemical reactions were applied here.

These accident scenarios include scram and depressurization early in the transient, followed by a depressurized core heatup transient. The chemical reaction between steam and graphite is endothermal, but its energy consumption remains very small compared to the core decay heat, and the thermal transient was assumed to proceed identical to the basic depressurized core heatup transients of Chapter 3.

The in-core gas after depressurization can include significant concentrations of H_2O, since several tons of water were released into the primary loop during SRDC-6 scenarios. For the current evaluation a mass fraction of 50% H_2O and 50% He was assumed, corresponding to 18 volume % of H_2O.

As the HTS is lost, the main loop shutoff valve closes, thus restricting flow between the steam generator and the reactor vessel. However, the valve is designed to permit a bypass flow of about 10% of the core flow during normal SCS operation. Thus, some flow through the steam generator must also be expected in the current depressurized core heatup scenario. Scaling from SCS operating conditions, one finds that the pressure drop loss coefficient for the flow path through steam generator and main loop valve should be about 80 to 100 times the corresponding coefficient for the core. However, such scaling from forced flow conditions to natural flow conditions at about 3 orders lower flow rates is questionable. Figure 6-1 shows the in-core gas flows as functions of the MLSV flow resistance. (This "equivalent flow resistance" has such high values, since it includes a factor of flow cross section areas $(A_{core\ barrel}/A_{valve})^2$, which is very large for a nearly closed valve.) For an open MLSV ($K_{v\ equiv}$ in the range from 10 to 100) the gas flow through the primary loop is about 22 kg/hr at 20 hr into the transient, and no flow recirculation occurs in the core. At $K_{v\ equiv} \approx 5 \times 10^5$ in-core recirculation begins, and the flow from the steam generator decreases to a few kg/hr. Scaling from the flow distributions during SCS operation would result in a "best estimate" equivalent K_v value of about 10^7. At that value, the gas flow from the steam generator is about 1 kg/hr with an in-core up-flow of close to 3 kg/hr and an in-core down-flow of less than 2 kg/hr. For a hermetically sealed MLSV, one would obtain an in-core natural circulation flow of about 2 kg/hr.

Thus, even with an open MLSV, the in-core flow of helium gas mixture would be lower than those encountered during air ingress, primarily due to the lower molecular mass. While it is not certain without more detailed valve data where flow rates for closed MLSV would lie, they will be significantly lower, and can be expected to be about an order of magnitude lower than those with an open

(a)

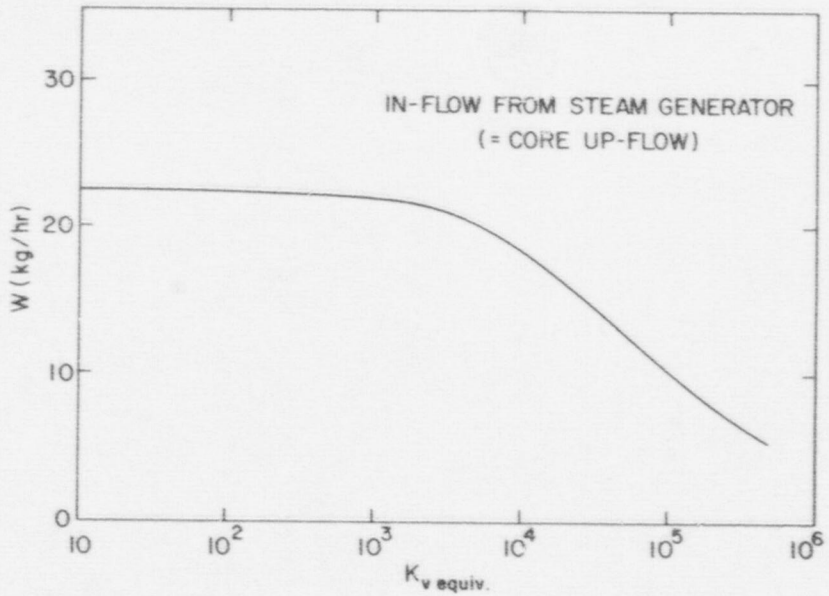

(b)

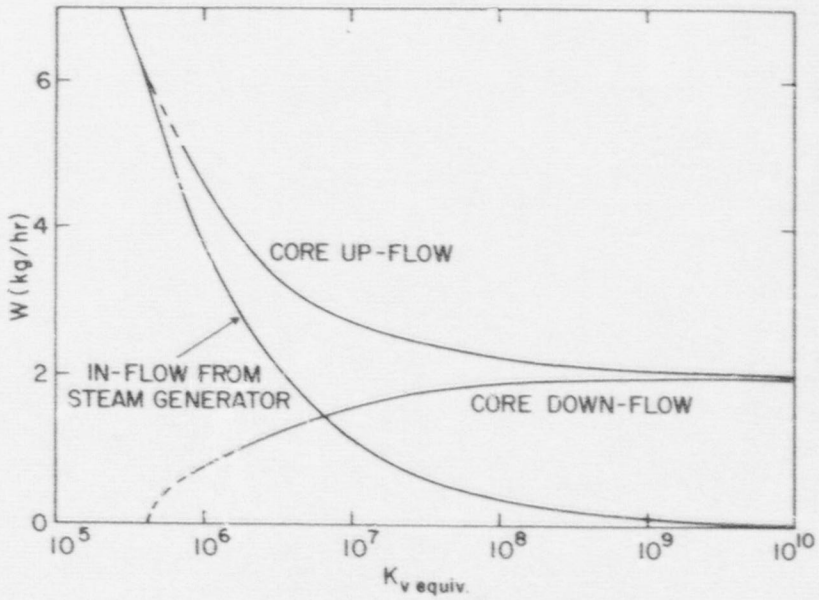

Figure 6-1 In-Core Gas Flows during a Depressurized Core Heatup Accident with Preceding Water Ingress as Function of Main Loop Shutoff Valve Flow Resistance (t = 20 hr)

MLSV.

Actual gas in-flow rates during the transients and the amount of graphite oxidized are shown for the case of an open MLSV in Figure 6-2, and for a closed valve in Figure 6-3. Figure 6-4 shows the in-core recirculation flows for the best estimate closed valve condition. As in the case of air ingress, it was found that except for the first few hours, all entering H_2O will react, forming CO and H_2, but that the actual amounts of graphite oxidized remain very small. For the case of a closed valve, it amounted to about 0.3 kg/hr, and even if the MLSV were to remain open, the graphite oxidation rate amounted to about 5 kg/hr over most of the transient.

Cases of more massive tube breaks, such as BES-4, will be evaluated in the future. However, since the gas flow rates after depressurization cannot be much larger than the ones encountered here, it is not anticipated that this will lead to much higher graphite oxidation rates.

The effect of the available steam on fuel kernel hydrolysis resulting in some additional fission product releases will also be incorporated into the FLOXI module, and will be evaluated later.

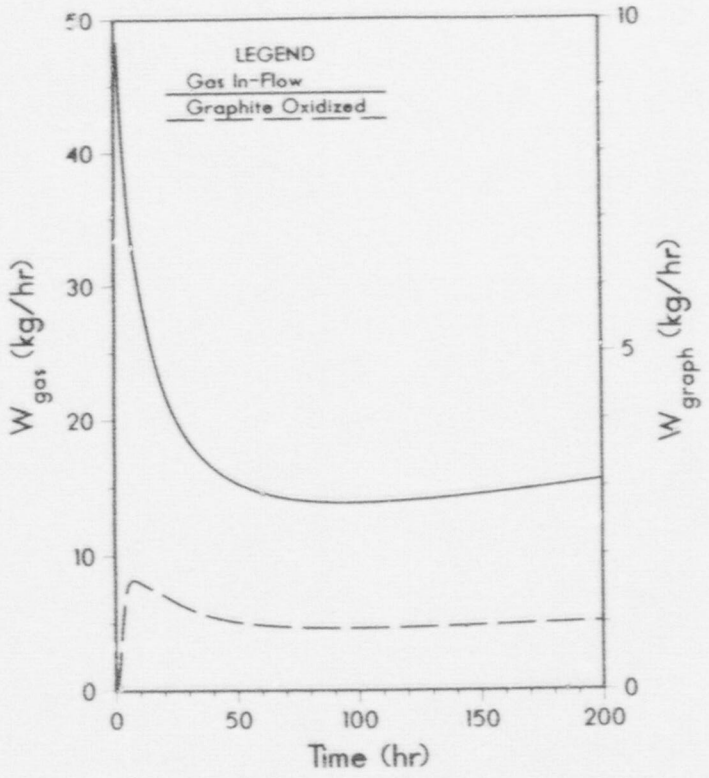

Figure 6-2 Gas Flow into Core, and Graphite Oxidized during a Depressurized Core Heatup Accident with Preceding Water Ingress with Open Main Loop Shutoff Valve (MLSV)

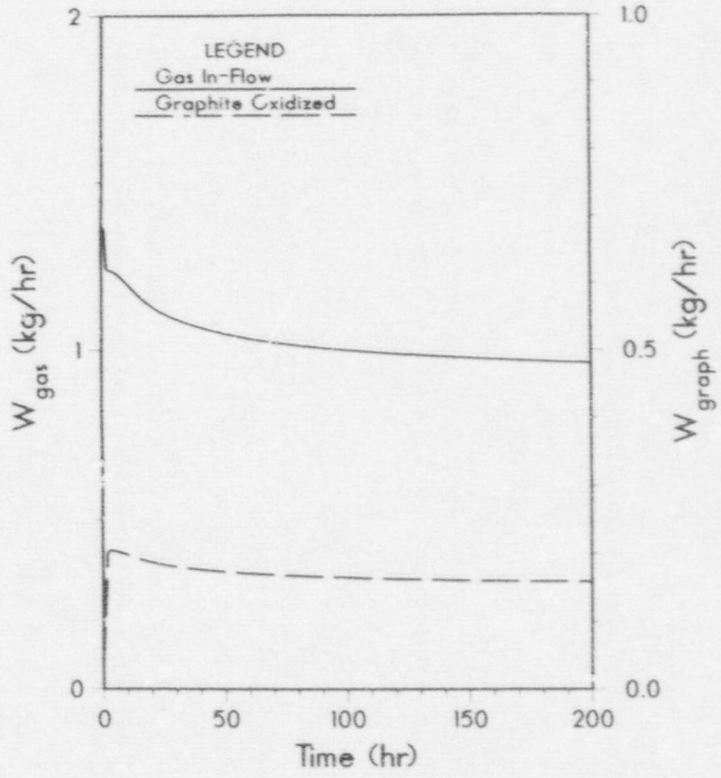

Figure 6-3 Gas Flow into Core, and Graphite Oxidized during a Depressurized Core Heatup Accident with Preceding Water Ingress with Closed Main Loop Shutoff Valve (MLSV)

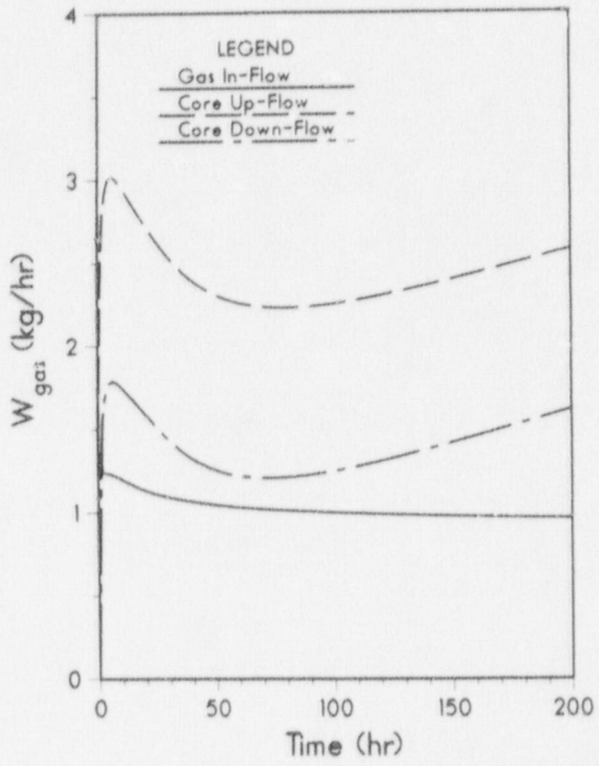

Figure 6-4 In-Core Gas Flows during a Depressurized Core Heatup Accident with Preceding Water Ingress with Closed Main Loop Shutoff Valve (MLSV)

7. CORE HEATUP ACCIDENT SCENARIOS WITHOUT FORCED COOLING AND WITHOUT SCRAM

If all forced cooling is lost, the reactor is to be scrammed and decay heat is to be removed by the passive RCCS. In case of failure of the scram system, the reserve shutdown system should be activated to cause neutronic shut down, and to keep the reactor subcritical.

This section evaluates accident scenarios where, after loss of all forced circulation, neither of the two scram systems succeeds in shutting down the reactor. Most of this analysis was done for the case of the RCCS operating and with primary loop depressurization early in the accident scenario. An extension to the corresponding accident without functioning RCCS, and to the case of pressurized conduction cooldown, will be discussed qualitatively.

7.1 Reactor Kinetics and Xenon Decay

During conduction cooldown scenarios without scram, the core will initially heat up, resulting in a rapid power decrease due to the negative Doppler feedback. Additionally, the Xenon-135 concentrations will rise, and the reactor will remain subcritical. After about two days the Xenon concentration has decreased sufficiently that recriticality becomes possible, resulting in power oscillations with a period of about one per hour, decaying to a final quasi-steady level, where positive reactivity, due to low xenon levels, just balances the negative reactivity, due to elevated fuel temperature.

To model these effects, a point kinetics model with six delayed neutron groups [Cheng, 1976] was adapted and incorporated into the THATCH code, together with a Xenon decay model [Knief, 1981]. Details of the model are summarized in Appendix C.

7.2 Depressurized Core Heatup Transient with Functioning RCCS

Using the neutron kinetics data mostly provided by GA and included in Appendix C the resulting best estimate depressurized core heatup transient with function RCCS was evaluated.

Assuming and instantaneous loss of forced circulation at time zero and no scram, the core begins to heat up, resulting in a negative reactivity insertion and loss of power. Within 200s the neutronic power is reduced to 1% of full power level, with the total power being produced during this period corresponding to about 38 full power seconds. During this time the peak active core temperature rose by 46°C, while the average core temperature rose by 120°C, with the temperature rise being most pronounced in the colder upper regions of the core, where the cooling by cold inlet helium was interrupted. As the xenon concentration increases with decreasing power, additional negative reactivity is inserted. At 200s this amounts to 20% of the total negative reactivity.

The xenon concentration peaks at 10 hr, reaching about four times the full power equilibrium level. At about 40 hr the xenon concentration drops below its full power equilibrium value, while the average active core temperatures have nearly reached their peak values and are relatively constant at

1030 °C. As the xenon concentration decreases further, the net reactivity becomes positive at about 49 hr, resulting in the onset of power oscillations, with the first four peaks as listed below:

Peak No	Time [hr]	Power [MW]
1	49.8	16.9
2	50.9	8.7
3	51.7	5.7
4	52.4	4.4

Decay heat and total power for this period are shown in Figure 7-1. As the oscillations subside, a quasi-steady level is reached, where the power just keeps the xenon level at a value to balance the negative reactivity due to elevated fuel temperatures. After this state is established, the reactor temperatures remain virtually constant with a peak active core temperature of 1760°C being reached at about 95 hr. The core average temperature remains about constant at 1315°C.

Typical results for this transient are shown in Figure 7-2 to 7-5. Up to about 50 hr the transient proceeds similar to the case with scram, except that, due to power input of the first few minutes, the effective initial temperatures are about 120°C higher. At about 50 hr, as peak core temperatures are being approached, the power oscillations begin (In the 50 to 60 hr range, the plot points supplied in Figure 1-3 were too coarse to produce the correct oscillations, which are shown correctly, however, in the expanded scale of Figure 7-1). Subsequent to the power oscillations, the total core power settles at about 2.8MW at 57hr, decaying slowly to about 2.1 MW at 100 hr, remaining roughly constant thereafter.

Due to this increased core power, core temperatures begin to rise again at 49 hr and reach their final plateau at about 100 hr, with peak and average core temperatures of 1760°C and 1310°C respectively. In 18% of the core the temperatures exceed 1600°C. The reactor vessel temperatures reach the ASME code limit value of 480°C (900°C) at 75 hr and remain close to 550°C beyond 130 hr. The RCCS can successfully absorb the heat load of 2.1 MW with an air exit temperature of 165°C. As the temperatures in the core exceed 1600°C beyond 60 hr, remaining indefinitively at this level, additional long term fission product releases, after maybe 100 hr, from the fuel to the reactor vessel atmosphere would have to be anticipated. However, with little or no gas expansion in the primary loop, not much of this release would be expected to escape from the reactor.

As the indicated peak vessel temperatures exceed the projected ASME code limit of 480°C, a re-use of the reactor vessel, subsequent to the accident, would be precluded.

Without scram the above accident temperatures would persist indefinitely and a successful scram would be required to initiate a final core cooldown.

The final core temperature level during this accident scenarios is dictated by a balance between negative fuel temperature coefficients,positive reactivity from moderator and reflector, and reduced xenon concentrations.

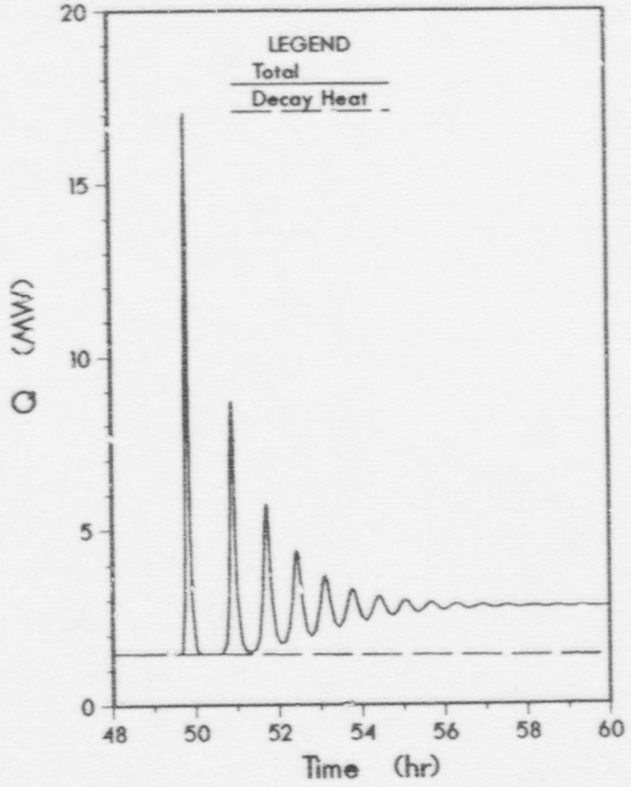

Figure 7-1 Decay Heat and Total Power During Onset of Recriticality During a Depressurized Core Heatup Accident with Functioning RCCS but Without Scram

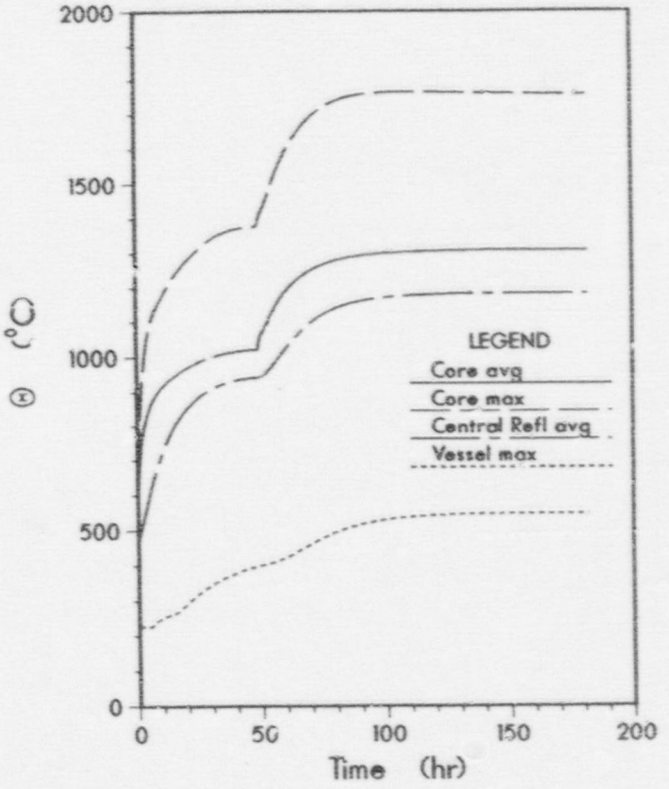

Figure 7-2 Core and Vessel Temperatures During a Depressurized Core Heatup Accident with Functioning RCCS but Without Scram

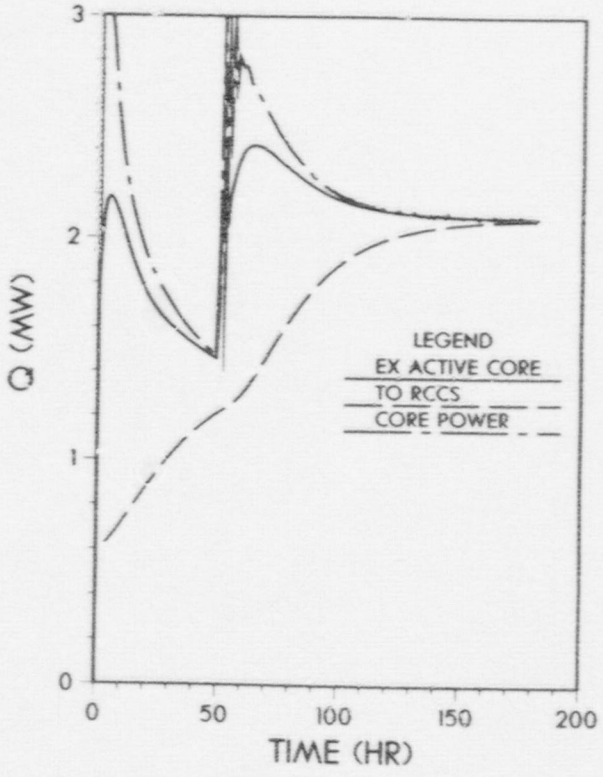

Figure 7-3 Core Power and Reactor Heat Flows During a Depressurized Core Heatup Accident with Functioning RCCS but Without Scram

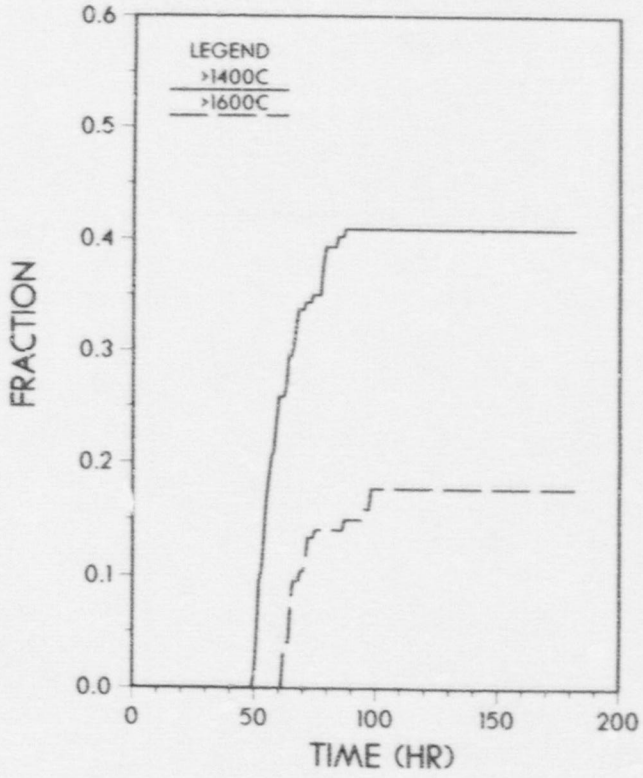

Figure 7-4 Volume Fractions of Active Core Exceeding Indicated Temperature Limits During a Depressurized Core Heatup Accident with Functioning RCCS but Without Scram

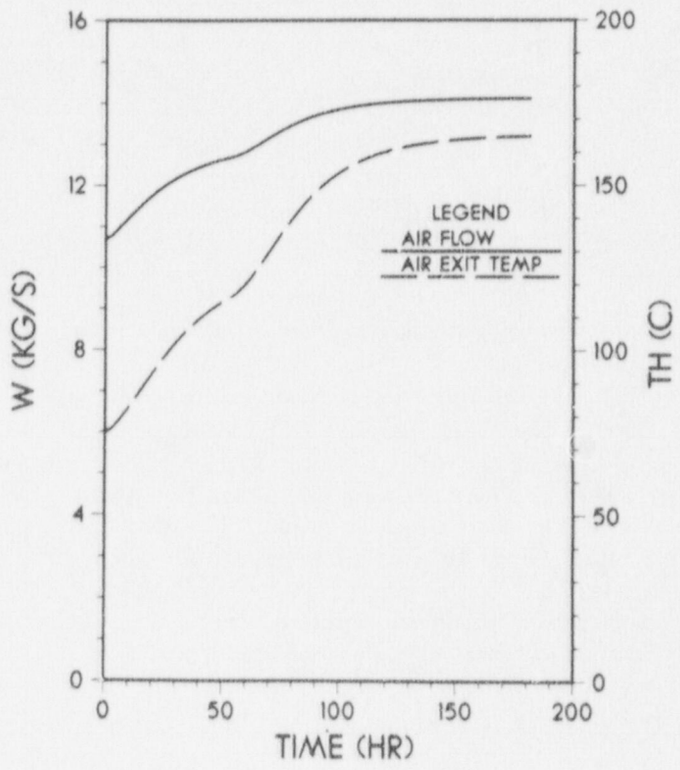

Figure 7-5 RCCS Performance During a Depressurized Core Heatup Accident with Functioning RCCS but Without Scram

All these values depend on the total reactor temperature field, as well as on the microscopic Xenon-135 cross section and the macroscopic fission cross sections. Best estimates of these values were used here. However, to establish more confidence in the quantitative results, a further sensitivity study is planned in order to identify any possible uncertainties in the resulting peak fuel temperatures. This is essential, since the peak fuel temperatures are strongly dependent on the Doppler feedback coefficient.

Initial variations indicate that using a lower Xenon microscopic cross section of 1.4×10^6b (flux weighted value, typically used in LWR applications), rather than the "Barn-book" value of 2.65×10^6 b, results in recriticality occurring about 41 hr, i.e. about 9 hr earlier than in the Base Case.

7.3 Extension to Pressurized Core Heatup Transient Without Scram

This case has not been evaluated yet, but future evaluations are planned. With the above mechanism for core heatup transients without scram, one can anticipate that the transient will proceed very similarly to the depressurized case, although with slightly lower peak core temperatures.

This case is particularly important, since it could lead to the only mechanistic accident scenario with significant fuel failures, even though its probability may be vanishingly small.

Assume loss of all forced circulation and no scram. The system remain pressurized and decay heat removal via RCCS begins. Recriticality occurs around 50 hr. Fuel failure temperatures are reached at 60 hr, with peak fuel temperatures above 1700°C lasting for days. The expected peak vessel temperatures, above 500°C, are well beyond the design limits for an extended period of time. Ultimately vessel failure and depressurization would have to be expected, for instance at 120 hr. The primary coolant then released to the atmosphere would have a much higher fission product concentration than those of the other accident scenarios considered so far. While this scenario may have an extremely small probability, these considerations indicate the desirability of scram systems of high reliability and redundancy.

7.4 Extension to Core Heatup Transients Without Scram and Without Functioning RCCS

This case has not been evaluated yet, but future evaluations are planned. Qualitatively, we can again expect a transient very similar to the transient with functioning RCCS, most likely with very similar peak core temperatures and slightly higher long term vessel temperatures, due to the less efficient vessel to cavity heat transfer conditions. For the first 100 hr the transient should proceed very close to the corresponding case with RCCS.

8. REDUCTION IN REACTOR CAVITY HEAT TRANSFER DUE TO H_2O AND/OR CO_2 ACCUMULATION

Water vapor, carbon dioxide and, to a lesser extent, also carbon monoxide are gases which absorb radiation at certain wave lengths. Ingress of such gases into the reactor cavity could therefore reduce the predominantly radiant heat transfer from the reactor vessel to the RCCS panels and raise the peak vessel temperature. But it would have only a very minor effect on the peak fuel temperatures. The absorption of radiant heat transfer is strongly dependent on the partial pressure of the gases.

Ingress of CO_2 or CO into the reactor cavity could only occur after a significant ingress of air or water into the primary loop has taken place. And even then a theoretical upper limit for the CO_2 partial pressure would be 0.21 atmospheres, if all O_2 were replaced by CO_2, with no other gases like helium remaining. The probability of such an event would have to be minute. However, H_2O could enter the reactor cavity without any chemical reactions in the core, just due to some massive steam side break, for instance in the steam generator cavity. And at the prevailing reactor cavity temperatures, H_2O could exist at a partial pressure of 1.0 atmospheres. Water ingress is, therefore, the scenario of more concern.

Radiant heat transfer across H_2O and CO_2 is strongly "banded", i.e., absorption only occurs over certain wave lengths. The temperature range in the reactor cavity of 100 to 500°C is significantly lower than the area of most interest in gas radiation, and the commonly used emittance data are known to be inaccurate in the low temperature range [Sparrow and Cess, 1966]. Therefore, the spectral nature of the CO_2 and H_2O absorption should be considered in any accurate assessment of the effect of these gases on the reactor cavity heat transfer.

At this time, an initial estimate of this effect was made by using the band approximation model suggested by Sparrow and Cess, 1966. Details of the model are given in Appendix D. The results obtained there indicate that the effect of replacing all air in the cavity with water vapor would reduce the radiative heat transfer by about 32%. Currently, vessel and RCCS panel emissivities of $\varepsilon = 0.8$ are used in our THATCH models as best estimate values, corresponding to an overall reactor cavity emmissivity $\varepsilon_{1,2} = 0.69$. To simulate this reduction in heat transfer of 32% in our current THATCH model, the above component emissivities were lowered from 0.8 to 0.61 yielding an overall value $\varepsilon_{1,2} = 0.470$. THATCH runs with such reduced emissivities resulted in a peak vessel temperature of 469°C, i.e., 45°C above the best estimate values of Section 3. As pointed out in Section 3, the effect of reduced emissivities on the fuel temperatures remains very minor.

If normal steady state operation were maintained during such a scenario of water ingress into the reactor cavity, a vessel temperature increase of about 40°C from 220°C to 260°C would be encountered.

It should be emphasized that these are initial estimates, and that more detailed evaluations should be performed. However, it can also be noted that the current estimates include some conservatism. If the cavity were to fill with water vapor, the convective heat transfer, which currently contributes

only 5-10% of the total heat transfer would be enhanced, possibly even including some condensation and vaporization on the RCCS panels. Furthermore, the estimation of heat transfer reduction in Appendix D assumed black surfaces, and the fractional reduction for grey surfaces would be expected to be slightly lower.

At this time, indications are that the peak vessel temperatures under such a scenario would increase measurably, yet remain below the permissible values of 480°C (or 540°C).

9. TEMPERATURE TRANSIENTS SUBSEQUENT TO A COLLAPSE OF THE CORE SUPPORT STRUCTURE

As the core geometry subsequent to a collapse of the core support structure is not defined, the evaluation of such scenarios remains rather uncertain. However, some qualitative features can be pointed out. The current analysis considered here is only a preliminary step, and more comprehensive evaluations of further scenarios should be conducted at a later time.

In the hypothetical event of a complete collapse of the core support structure, the fuel and reflector elements could fall and fill up some of the bottom plenum space. Figure 9-1 (Figure 4.3-6 of the PSID) shows the location of the active fuel elements, surrounded by layers of reflector elements on all sides. The figure clearly shows that even if such a collapse of the core support structure were to occur, it would be extremely unlikely that any fuel elements could find their way to the vessel walls. Nevertheless, the current analysis evaluates the ranges of fuel and vessel temperatures to be expected if individual fuel elements should rest next to the vessel wall.

The fuel elements, hexagonal prisms, can never touch the cylindrical or spherical vessel walls at all of their surface, i.e., gaps must remain between fuel elementa and the vessel surface, except at local points. With these uncertainties in mind, several simplified geometric configurations with simplified fuel element, vessel and gap geometry were investigated. The fuel element was modelled as a cylinder having about the same volume and thickness as an actual fuel element, as well as the same decay heat power density. The element was considered to be surrounded by reflector elements, except for its bottom face, which was facing either the steel vessel surface, or a concrete surface. The outer surface of the steel vessel faced an air gap of 2m and then thermal insulation, and shielding, with concrete below these layers, typical of the bottom region of the reactor building.

In the Base Case, assuming a collapse of the core structure as initiator of the accident, a hot fuel element of 800°C average temperature is assumed to rest against the vessel walls with an average gap width of 2 cm. The vessel is initially at 220°C, and the surrounding reflector blocks are at 700°C. The maximum and average temperatures for this case are shown in Figures 9-2 and 9-3. Initially, the inner sections of the fuel element experience a slight temperature rise, peaking after 17 minutes at 835°C and then decreasing to about 690°C, while the fuel element average temperature decreases from the beginning, settling after about 5 hr at about 670°C.

The vessel maximum and average temperatures rise to their respective peak values of 665°C and 645°C over a period of about 25 hr, and remain virtually constant thereafter up to 100 hr.

The fuel temperatures in this case do not come anywhere near the values of 1300 to 1400°C, which are encountered in the core heatup accident scenarios discussed in Chapter 3. The local vessel temperatures e.g., under the fuel element, get much hotter than in core heatup scenarios, and one might have to consider whether at these temperatures the vessel (locally) could continue to hold the load that it is subjected to.

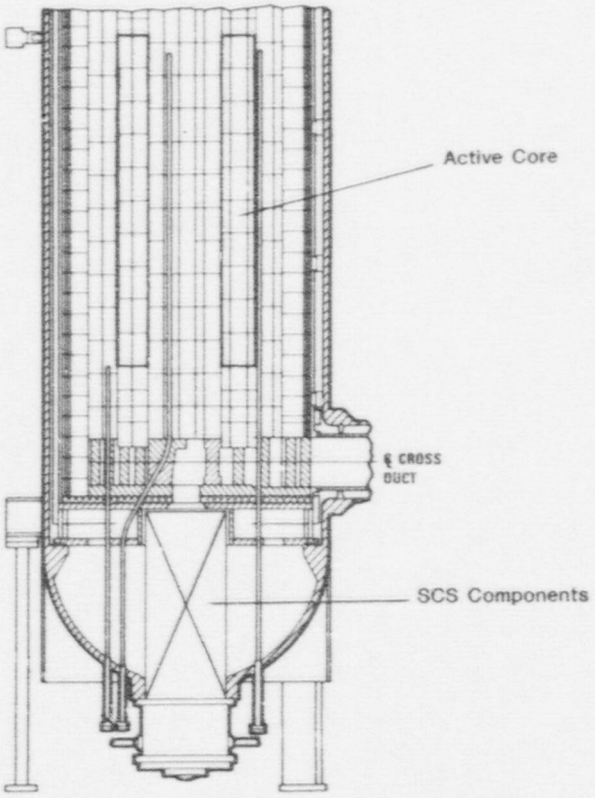

Figure 9-1 Active Core in Relation to Other Reactor Vessel Components

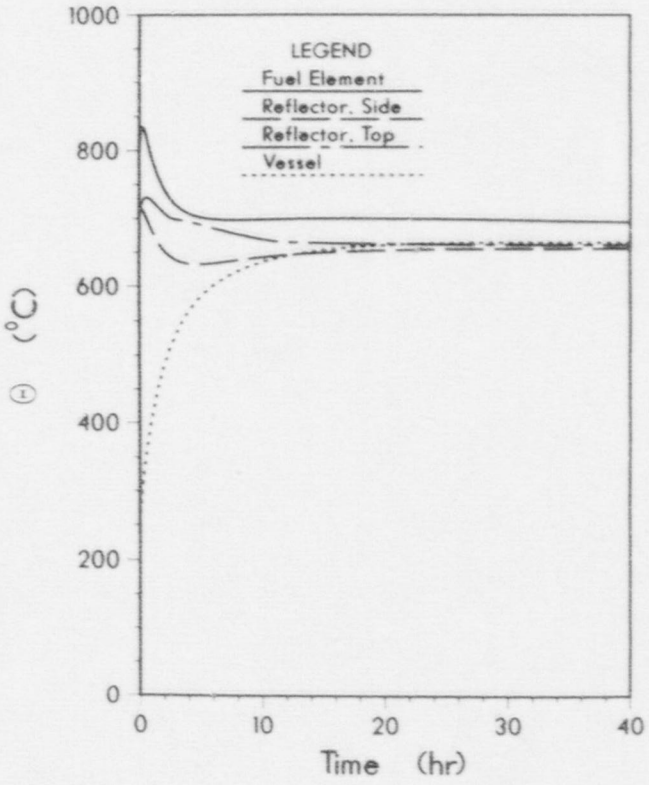

Figure 9-2 Maximum Temperature of Fuel Element Reflector and Vessel for a Single Fuel Element Resting at the Vessel Surface

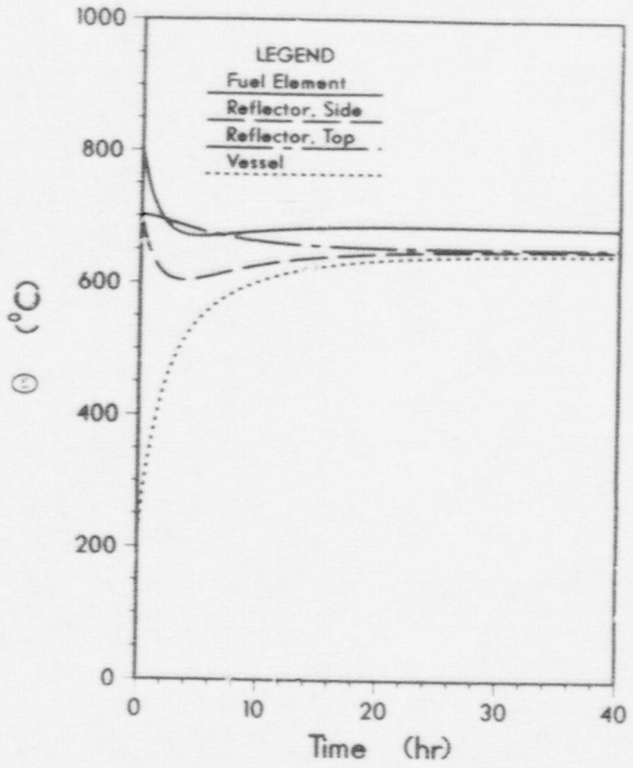

Figure 9-3 Average Temperatures of Fuel Element Reflector and Vessel for a Single Fuel Element Resting at the Vessel Surface

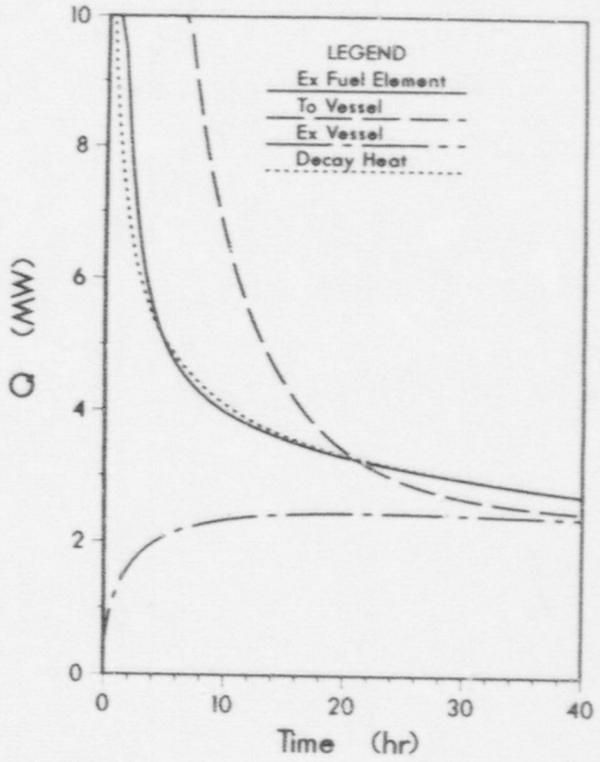

Figure 9-4 Heat Flows for a Single Fuel Element Resting at the Vessel Surface

Figure 9-4 shows the heat flows for this scenario. The decay heat and heat flow of the fuel element remain closely matched after the first few hours, resulting in a virtually constant fuel element temperature. For the vessel, the "cross over point", where heat loss to the concrete exceeds heat gain from the fuel and reflector elements, is only reached after 80 hr. The figure also shows that the decay heat of a single fuel element corresponds to that of a 3 to 4 KW heater, which is a relatively small load.

Several parametric variations of this case are summarized in Table 9-1. The results indicate that the averaged gap size between the vessel surface and the fuel element has virtually no effect on the peak fuel or vessel temperatures, indicating that radiation heat transfer is dominant (Case No. 2). If the fuel element were insulated from the reflector elements, i.e., all heat were transferred directly from the fuel element to the vessel, about 80°C higher peak fuel temperatures and about 100°C higher peak vessel temperatures are possible (Cases 3 and 4). The availability of more reflector surface area around the fuel element hardly affected fuel or vessel temperatures (Case 5). To simulate a core support structure failure at about 50 hr into a core heatup accident, when core temperatures are close to their peak, a case with corresponding initial temperatures was run. This time the fuel element hardly exceeded its temperature at the time of failure and begins to cool down, while the peak vessel temperature reached a much higher value of 954°C (Case 6).

The case of a fuel element resting on concrete, surrounded by the same blocks of reflector material, was also evaluated. In this case, a peak fuel temperature of 835°C was reached after 20 minutes, while the peak concrete temperatures of 660°C were reached after about 3 1/2 hr, with a slow decrease in temperatures thereafter.

The above cases assume no RCCS cooling to be available after the catestrophic core support system collapse. And they also assume that the fuel element next to the vessel or concrete surface is sufficiently far away from the rest of the core to not be heated from the back. In a run applying heating of the fuel element by large masses of other fuel elements, significantly higher fuel and vessel temperatures were obtained At maximum fuel temperatures of 1360°C, representing a typical peak fuel temperature during core heatup scenarios, the peak temperature in the fuel element adjacent to the vessel reached 1295°C, and the peak vessel temperature was 1280°C. At such temperatures, vessel integrity could not be assured. However, additional fuel failures would still not be expected. Also, such a scenario of a single or a few fuel elements resting against the vessel and a heat source corresponding to an intact core behind them is an incredible, if not impossible, scenario.

The current conclusion from these evaluations is that a collapse of the internal core geometry cannot lead to fuel temperatures higher than those found in an intact core geometry. For every physically possible rearrangement of fuel elements their overall volume can only increase, resulting in a lower overall power density and larger exterior heat transfer area of the core envelope. Both factors lead to lower peak fuel temperature. However, it is possible to conceive highly improbable but physically not impossible scenarios, where fuel elements touching the vessel can cause local vessel hot spots which might induce further structural failures of the vessel.

Table 9-1 Peak Fuel and Vessel Temperatures for a Simulated Single Fuel Element Resting Against the Vessel Surface

CASE NO.	DESCRIPTION	GAP CONDITIONS			INITIAL TEMPERATURES			Peak Fuel Temperature °C	Peak Vessel Surface Temperature °C
		Fuel Element to Vessel	Fuel Element to Reflector Elements	Reflector Elements to Vessel	Fuel Element °C	Reflector Elements °C	Vessel °C		
1	Base Case	2 cm	2 cm	2 cm	800	700	220	835	666
2	Increased Gap Sizes	10 cm	10 cm	10 cm	800	700	220	835	666
3	Fuel Element Insulated from Reflector Elements	10 cm	insulated	10 cm	800	700	220	913	767
4	Fuel Element Insulated from Reflector Elements; No Gap Resistance between Fuel Element and Vessel	ideal contact	insulated	10 cm	800	700	220	857	756
5	As Case 1, but with Extended Reflector Regions	2 cm	2 cm	2 cm	800	700	220	835	661
6	Core Support Structure Collapses after 50 hr of Depressurized Core Heatup Transient	2 cm	2 cm	2 cm	1300	1100	300	1301	954

10. FUTURE WORK

The above work is based on the current MHTGR PSID and should be extended as the design is refined and more details become available. Further, at this preliminary level of the evaluation some items had to be left for future, more detailed evaluations. Suggested future efforts are listed below in the sequence of Sections 3 through 9, with new items to be added at the end. Some relatively minor items will be included for completeness.

10.1 Pressurized and Depressurized Core Heatup Scenarios

Modeling of core heatup scenarios with functioning RCCS is fairly complete and does not require much additional work, in particular since the THATCH code, coupled with the FLOXI module, can now solve pressurized as well as depressurized core heatup transients.

One of the Bounding Event Sequences formulated towards the end of the review process calls for loss of RCCS cooling for 36 hours with partial RCCS coolant flow restored after that time. Peak vessel temperatures would be the main item of interest in such a scenario. The modelling for the period after partial restoration of the coolant flow would have to consider the fact that the down-flow air passages and the concrete behind them have been heated substantially, resulting at least initially in much less buoyancy for the RCCS air flow. Thus, the convective heat transfer in the down-flow passages and heat exchange with the surrounding solid structures will have to be included in the model. This presents no significant difficulties, as our RCCS model (PASCOL) includes convection in the down-flow passages, and the transient conduction in the solid structures can be included by specifying the corresponding additional solid structures and gaps in the THATCH code.

Some refinement in the upper plenum shroud representation is of interest for the case of pressurized core heatup scenarios (a feature which only recently became operational for our THATCH code). This would help to demonstrate whether peak vessel temperatures might arise at this elevation due to the hot gas rising from the core. Similarly, some model refinements in the core support structure and the bottom plenum would be desirable, since the bottom plenum constitutes the largest gas volume, and more precise temperatures here would affect the gas inventory and gas exchange modelling between the reactor vessel and the surroundings during depressurized core heatup scenarios. All these improvements are minor in terms of effort required, and minor to moderate in their anticipated impact on the results.

If desired, the code could be extended to three dimensional analysis, to explore the potential for vessel hot spots during long term transients, in particular for scenarios of impaired RCCS performance.

10.2 Depressurized Core Heatup Transients without Functioning RCCS

Future work in this area can be pursued as questions arise or as the construction materials for the silo are specified. However, no further efforts are planned or suggested at this time.

10.3 Air Ingress Scenarios

The evaluations of Section 5 have been based on chemical reaction rate constants representative for H451 graphite. Variations of these constants by several orders of magnitude showed that all incoming air would be consumed, under virtually all conditions.

The core support structure and the lower reflector blocks (flow distribution block) are made out of Stackpole 2020 graphite which is expected to be more reactive than H451, possibly by a factor of 3 [GA, 1987-01]. On the other hand, temperatures in this region are much lower than in the core, and the exposed surface area is significantly lower than in the core. Nevertheless, future evaluations should be made to determine whether preferential oxidation in this lower region should be expected, and if so, whether it could cause any significant reduction in strength of the core support structure.

10.4 Water Ingress Scenarios

An evaluation of massive water ingress, as assumed in Bounding Event Sequence BES-4, should be investigated. This analysis can be conducted with the THATCH/FLOXI code, without model changes, for pressurized or depressurized core heatup scenarios.

Fission product release due to hydrolysis of failed fuel particles should be added to our chemical reaction models.

10.5 Core Heatup Transients without Scram

The evaluations of Section 7 have essentially confirmed the vendors accident description with recriticality in our evaluations coming at about 48 hr. Later extensions of our model have included the long-term buildup of samarium, using preliminary samarium cross section data. The addition of this effect appears to delay recriticality slightly, and to reduce the final peak fuel temperatures a little, but it does not change the basic features of this transient.

All no-scram evaluations of Section 7 were done with best estimate data for feedback coefficients and cross section data, as supplied by the vendor. Analogous to our work in Sections 3 through 5, parametric variations of these input data should be applied to establish the sensitivity of our results to possible uncertainties in the input data.

To date, all unscrammed scenarios have been run with functioning RCCS. Runs without functioning RCCS should be made following Bounding Event Sequence BES-5. Even though Response 15-8 of the PSID states GA's plans on sealing the reactor building, these runs should be run to about 120 hr when a final peak core temperature has been attained, so as to be cognizant of the effect of this scenario on peak fuel temperatures. Once the thermal RCCS restart transient mentioned in Section 10.1 has been modelled, an evaluation of this scenario would be routine and would not require any further model changes.

10.6 Reduction in Reactor Cavity Heat Transfer due to H_2O and/or CO_2 Accumulation

The current band model of Section 8 constitutes a preliminary and approximate evaluation of this effect. While the probability of significant CO_2 concentrations is extremely small, water vapor ingress into the reactor cavity is a much more likely event, and is, therefore, the more important scenario for which the analysis should be refined.

Our current estimates of the effect of such gases on the vessel temperatures agrees with those of GA, but this is most likely fortuitious, as our evaluations are indeed preliminary. At least for the case of H_2O, better modelling remains to be done.

A more appropriate band model, summing the heat transfer over the three essential H_2O radiation bands and the heat transfer across transparent gas for the remainder of the spectrum, has been outlined but was not yet programmed. Implementation of this model would provide a significantly higher confidence than that given by our current results, which indicate 40 to 50°C higher peak vessel temperatures due to water vapor accumulation in the reactor cavity.

10.7 Core Heatup Transients Subsequent to a Collapse of the Core Support Structure

Even though it is anticipated that peak fuel temperatures for such an event will remain below those for an intact core geometry, some runs with assumed altered core geometry should be made, particularly since such a hypothetical event could lead to increased peak vessel temperatures.

10.8 Gas and Fission Product Transport through the Reactor Building

During and subsequent to any depressurization, primary coolant and other gases are flowing through the various cavities of the reactor building, including gas exchange with the outside environment and heat exchange between the gases and the reactor building structures and equipment. With these gas flows, fission products are carried through the building and to the outside.

Our current code capabilities include the use of RATSAM, which has been extensively used and modified at BNL during the source term study [Kroeger et al., 1982 and Hsu et al., 1982]. This code is particularly well suited for rapid blowdown transients and is the only HTGR code that can treat the pressure waves of a rapid blowdown. It provides for representation of the local time varying shear forces in each node for use in fission product lift-off evaluations during blowdown transients. Thus, this code permits the estimation of fission product release from circulating inventory and plate out. A RATSAM model of the MHTGR should be set up and executed to obtain estimates of the fission product releases during blowdown transients and of the pressure forces between various sections of the primary loop. As new data and/or correlations for plate out distributions and lift off become available, these should be incorporated into our simulations.

For the long term reactor building transients subsequent to blowdown, the ATMOS code has been applied in some sample calculations to one of the early MHTGR configurations [Kroeger, 1986]. The gas and fission product exchange

between the reactor building and the environment after blowdown is strongly affected by the heating and cooling of the various cavities, and will include times of inflow from the atmosphere into the reactor building. It is a relatively minor effort to revise the current MHTGR model in ATMOS to correspond to the current reactor building design. Thereafter, we would have the capabilities to evaluate the anticipated gas exchange between the various parts of the building and the environment.

The modelling that remains to be included is the fission product transport during this long time transient, which is potentially affected by such phenomena as radioactive decay, plate out and deposition, as well as aerosol settling. GA currently uses the SORS code for this analysis. It is suggested to include models for the most important fission products and their transport phenomena into a module of the ATMOS code in order to obtain an independent capability to assess the fission product release for various accident scenarios. As further data and correlations for fission product transport become available from the Regulatory Technology Development Program, these should be factored into the code to improve our predictive capabilities.

11. REFERENCES

BECHTEL NATIONAL, Inc. et al., "HTGR, Concept Description Report, Reference Modular High Temperature Gas Cooled Reactor Plant", Report DOE-HTGR-86-118, October 1986.

BIRD, R. B., STEWARD, W. E., and LIGHTFOOT, E. N., "Transport Phenomena," John Wiley & Sons, 1960.

CHENG, H. S., "PKINS - A Point Kinetics Program", Brookhaven National Laboratory, April 26, 1976.

GENERAL ATOMIC, "HTGR Accident Initiation and Progression Analysis, Status Report; Phase 2, Risk Assessment", GA-A15000, April 1978.

GA TECHNOLOGIES, INC., "MHTGR Core Decay Heat", Report No. DOE-HTGR-86-109, Rev. 1, July 1987.

GA TECHNOLOGIES, INC., Letter to Mr. Tom King, NRC, dated April 3, 1987 (01).

GA TECHNOLOGIES, INC., Letter to Mr. Tom King, NRC, dated April 16, 1987 (02).

GA TECHNOLOGIES, INC., Telephone Transmittal F. Silady and R. Lane to P. G. Kroeger, BNL, November 3, 1987 (03).

HSU, C. J., KROEGER, P. G., and COLMAN, J., "The Effect of Prior Forced Circulation Coolings on the Thermohydraulics of an HTGR Primary Loop During Core Heat-Up Accidents," Brookhaven National Laboratory Informal Report, BNL-NUREG-32520, November 1982.

KATCHER, W. and MOORMANN, R., "Graphite Corrosion under Severe HTR Accident Conditions," IAEA Specialists Meeting on Graphite Component Structural Design, JAERI, Tokai-Muro, Japan, Sept. 1986.

KNIEF, R. A., "Nuclear Energy Technology", Hemisphere Publishing Corp.

KROEGER, P. G., COLMAN, J., and HSU, C., "Analysis of the Thermohydraulics Prior to Depressurization in an HTGR Primary Loop During Unrestricted Core Heat-Up Accidents," Brookhaven National Laboratory Informal Report, BNL-NUREG-31825, August 1982.

KROEGER, P. G., "Reactor Building Transients During Depressurized Core Heatup Accidents," Brookhaven National Laboratory Technical Report, A-3827, April 1986.

MOORMANN, R., and PETERSEN, R., "REACT/THERMIX; Ein Computercode zur Berechnungder Stoerfallbedingten Graphitkorrosion in Kugelhaufenreaktoren," Kernforschungsanlage Juelich GmbH, Juel-1782, April 1982.

PEROOMIAN, M. B., BARSELL, A. W., and SAEGER, J. C., "OXIDE-3: A Computer Code for Analysis of HTGR Steam or Air Ingress Accidents," General Atomic Company, GA-A12493 (GA-LTR-7), January 1974.

REILLY, H. J. et al., "Preliminary Evaluation of HTGR Severe Accident Source Terms", Idaho National Engineering Laboratory Report, EGG-REP-6565, April 1984.

SCHNEIDER, W., DIEDRICHS, V., and EHM, C., "Effect of Temperature on Steel and Concrete for PCRV's", Nuclear Engineering and Design, Vol. 67, 1981, pp. 245-258.

SPARROW, E. M. and CESS, R. D., "Radiation Heat Transfer," Brooks/Cole Publishing Co., Belmont, CA, 1966.

SUND, R. E. et al., "Afterheat Calculations for the HTGR", Gulf General Atomic, Report No. GA-A12499, November 1973.

APPENDIX A

SUMMARY OF INPUT DATA AND MATERIAL PROPERTIES FOR DEPRESSURIZED CORE HEATUP ACCIDENT ANALYSES

The reactor model used in the THATCH code to analyze the depressurized core heatup scenarios is primarily based on PSID data, augmented by data submitted by DOE during the review process.

The nodalization of the major reactor components is summarized in Table A-1.

The core material properties for graphite include a complete annealing model as specified by DOE [GA, 1987-01]. The data as implemented at BNL are given in Figures A-1 to A-5. The GA data for H451 were provided to 1800K and for Stackpole 2020 to 1073K. In some of the severe accident transients data beyond these temperatures were needed. Linear extrapolations were employed in those cases.

The best estimate decay heat data were provided by DOE in [GA, 1986-01]. Some of our earlier evaluations (as noted in Section 3) also used the more conservative PSID data [PSID, Table 4.2-15], or those of LTR-4 [Sund, 1973].

The PSID data of Figure 4.2-10 were used to obtain an average radial power profile for the six radial active core nodes, two nodes for each of the three rings of fuel elements. The PSID data of Figure 4.2-11 were used to supply the axial profile, using one averaged value for each of the three axial zones.

Heat transfer from the reactor vessel across the reactor cavity to the RCCS panels is by radiation and natural convection. Thermal emissivities of 0.8 were assumed for the vessel and for the RCCS panels. Radiation was by far the dominant mode of heat transfer in the reactor cavity. At the prevailing temperature levels and dimensions, the natural convection was found to be turbulent, but nevertheless, did not contribute more than 5 to 10% of the total heat transfer.

In general a one-dimensional radiation model was employed, which is slightly conservative with respect to peak vessel temperatures. For the later cases of non-functioning RCCS a two-dimensional radiation model for the reactor cavity was incorporated into the code, and was used for all cases of non-functioning RCCS. However, even at these higher temperature levels, the effect of the two-dimensional radiation model on the peak vessel temperatures was not very significant.

Table A-1 Reactor Nodalization

Block	Radial Nodes	Axial Nodes	Material
Central Reflector	6	28	Solid H451
Active Core	6	20	H451/fuel/coolant holes
Replaceable Side Reflector	3	28	Solid H451
Permanent Side Reflector	3	23	Solid Stackpole 2020
Top Reflector	6	3	H451/coolant holes
Upper Plenum Elements	6	1	Alloy 800 and graphite nodules
Bottom Reflector			
- upper	6	2	H451/coolant passages
- lower	6	2	Stackpole 2020/coolant passages
Core Barrel (with flow passages)	1	35	Alloy 800 and flow passages
Reactor Vessel			
- side	2	44	Medium carbon steel
- top	19	2	Medium carbon steel
bottom	19	2	Medium carbon steel
Upper Plenum Shroud			
- side	1	5	Kao wool and Alloy 800
- top	18	2	Kao wool and Alloy 800
Lower Plenum Floor	18	3	Alumina pads
Core Support Structure			
- upper	18	1	Medium carbon steel
- lower	18	1	Medium carbon steel
Upper plenum	Open Space		Gas, 2-d radiation
Lower Plenum	Open Space		Gas, 2-d radiation
Bottom Plenum (below core support structure; with SCS components)	Open Space		Gas, 1-d radiation

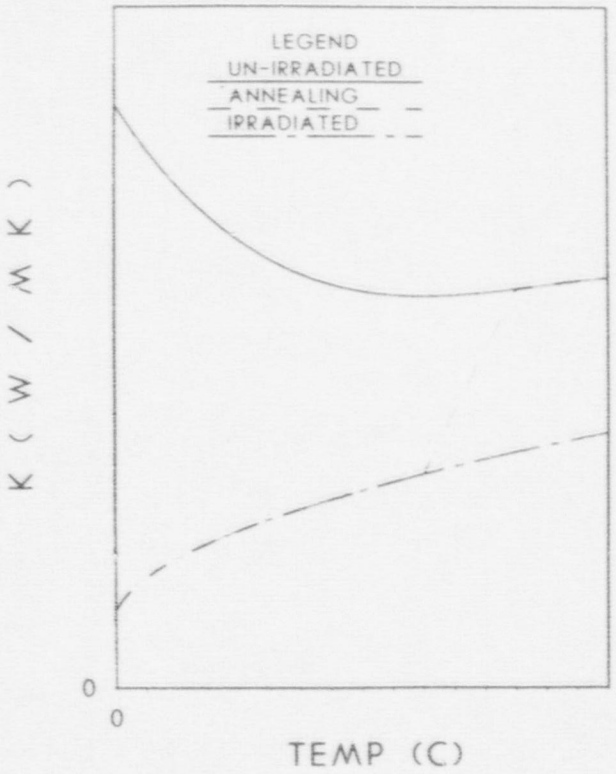

Figure A-1 Fuel Element Effective Radial Thermal Conductivity

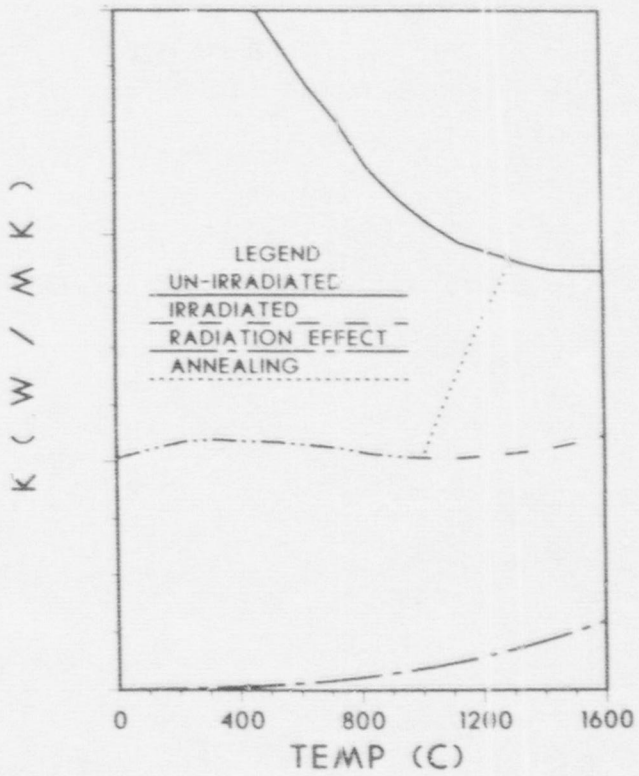

Figure A-2 Fuel Element Effective Axial Thermal Conductivity

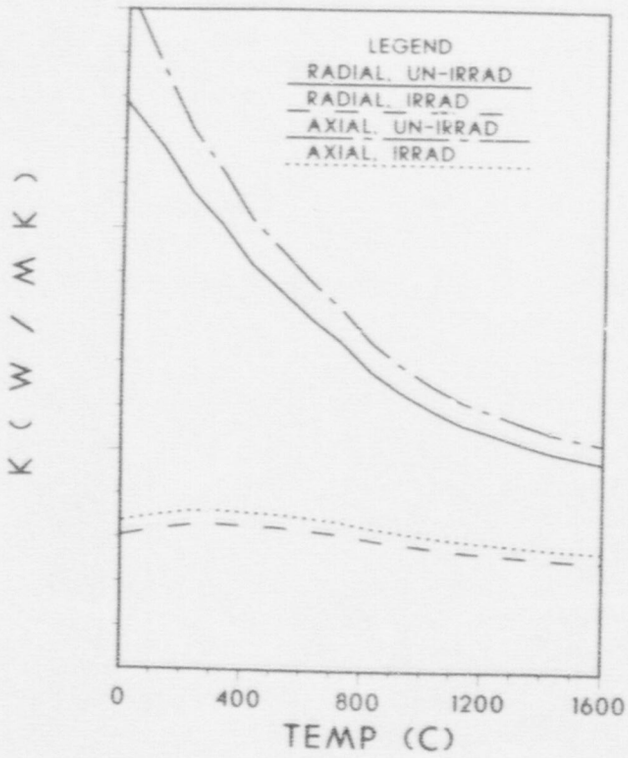

Figure A-3 Thermal Conductivity of H451 Graphite

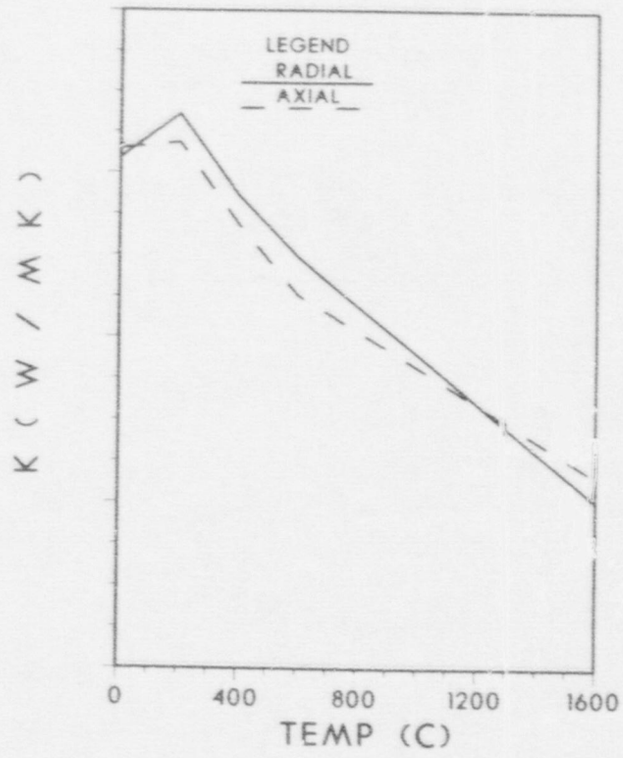

Figure A-4 Thermal Conductivity of Stackpole 2020 Graphite

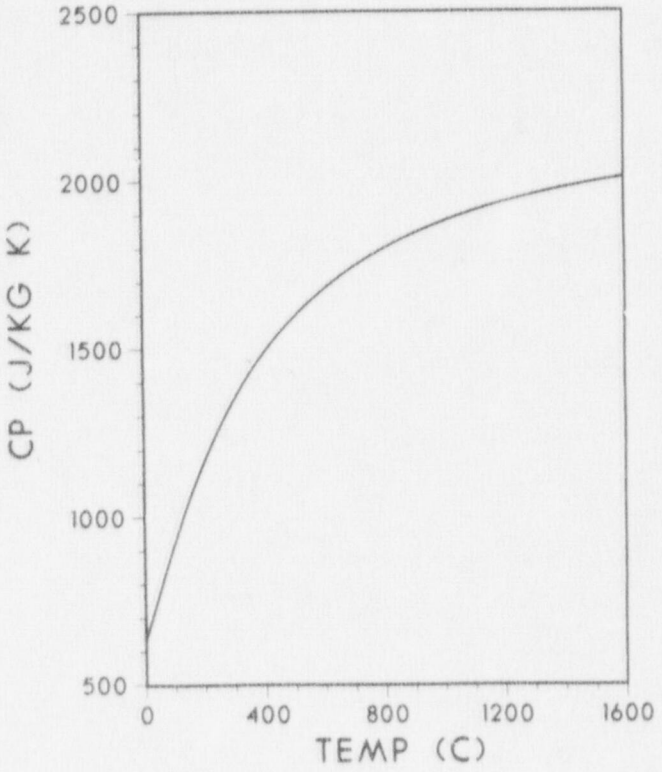

Figure A-5 Specific Heat of Graphite

APPENDIX B

RCCS PERFORMANCE EVALUATION

Most of the RCCS geometry is described in sufficient detail in Section 5.5 of the PSID.

The up flow channel of the RCCS contains internal fins as shown schematically in Figure B-1. The heat arriving from the reactor vessel at the RCCS front panel is distributed by conduction and radiation to the inside surface of the front panel, the fins, and the back panel. From all inside surfaces it is then transferred by convection to the upward flowing air.

The PASCOL code, which evaluates the performance of such passive air cooled decay heat removal systems, can (optionally) solve for simultaneous conduction and radiation in this finned channel, or can employ a user provided overall fin effectiveness factor Φ, which is defined as

$$\Phi = \frac{\text{Total Convective Heat Flow to Air}}{\text{Convective Heat Flow to Air from Unfinned Front Panel}}$$

Parametric evaluations were made to establish this fin effectiveness factor (FEF) as function of reactor vessel surface temperature, RCCS air temperature, mass flow of air and channel dimensions. As indicated in Figure B-2, it was found that the FEF was very insensitive to air temperatures and reactor vessel temperatures. Further results are, therefore, only shown for a representative air temperature of 100°C and a vessel temperature of 350°C.

Figure B-3 shows the effect of changing fin pitch and fin thickness. Closer fin spacing and thicker fins increase performance at a given mass flow. However, the main emphasis of this Figure is that the FEF of 4.5, used in DOE evaluations, is readily achievable with a base fin pitch of 2 in and a fin thickness of 0.25 in. Higher values would also be possible, in particular by reducing the fin pitch.

As set of parametric evaluations of steady state RCCS performance was made, using as base values an average reactor vessel temperature of 219°C, an air inlet temperature of 21°C, an effective stack height of 27.5 m. With the tortuous inlet and outlet paths of the air ducting, the inlet and exit losses are fairly high, estimated at about ten velocity heads each, (based on actual ducting cross section areas). As there are uncertainties in these estimates, the inlet and exit loss coefficients were usually treated as independent variable in these performance evaluations.

Figure B-4 shows air flow, air temperature rise and total heat removal as function of loss coefficients, evaluated for the fin thicknesses. While Figure B-3 showed that for a given mass flow performance would increase with greater fin thickness, the results here show, that for the RCCS system, under otherwise constant conditions, an increase in fin thickness does raise the air temperature rise. However, it also increases the flow resistance, and thus lowers the mass flow. Therefore, the net effect on the total energy being re-

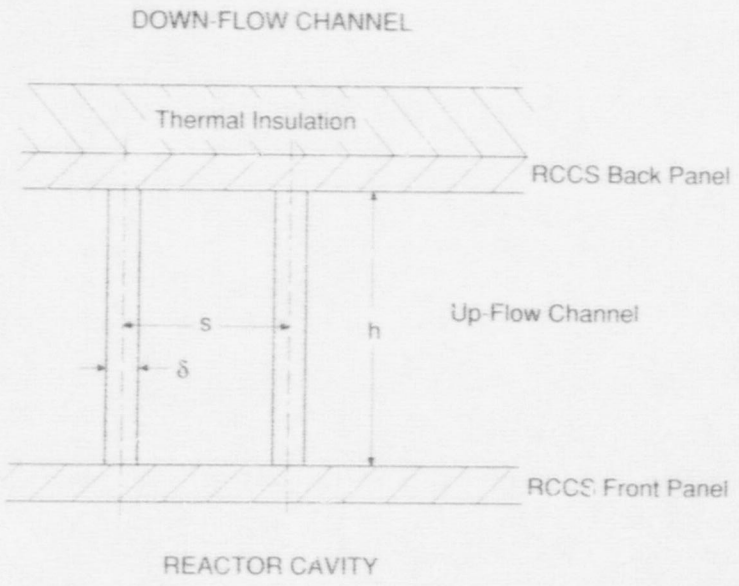

Figure B-1 Schematic of RCCS Up-Flow Channel

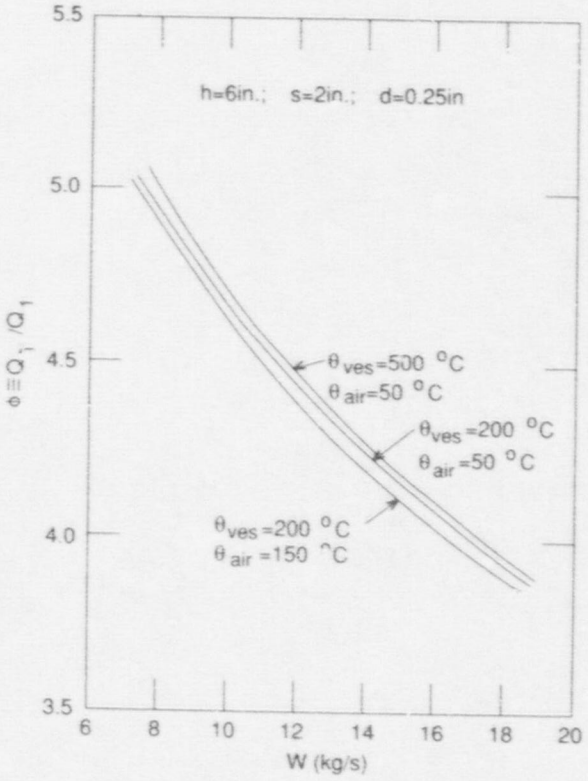

Figure B-2 Fin Effectiveness Factor at Base Channel Dimensions for Varying Air and Reactor Vessel Temperatures (h = 6 in.; s = 2 in.; δ = 0.25 in.)

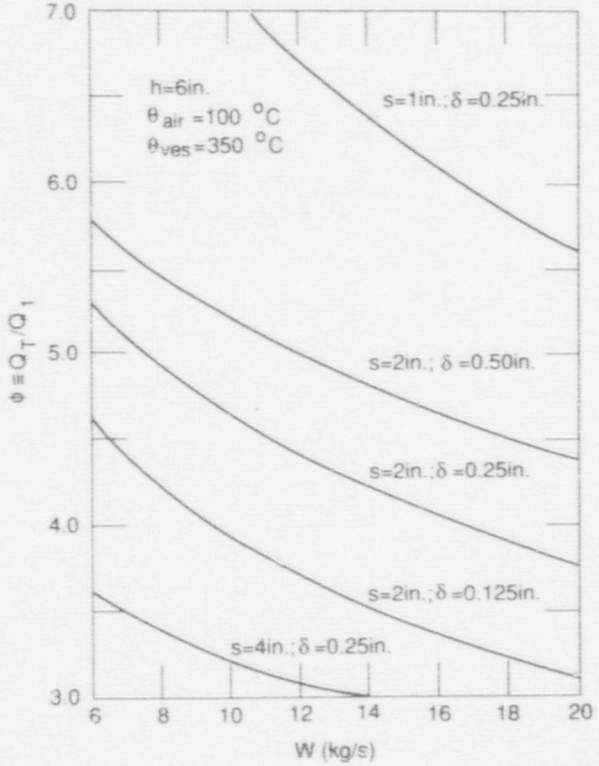

Figure B-3 Fin Effectiveness Factor as Function of Air Flow for Various Fin Spacing and Fin Thicknesses

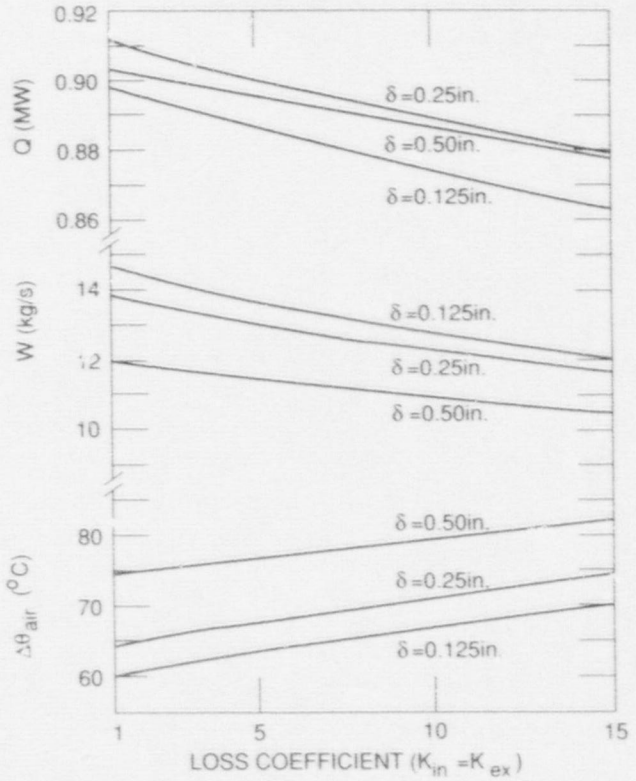

Figure B-4 RCCS Performance for Steady-State Full Power Production as Function of Ducting Pressure Drop Loss Coefficient for Various Fin Thicknesses (s = 2.0 in.; H = 27.5 m; θ_v = 219°C; $\theta_{air\ in.}$ = 21°C)

moved is an optimum at a fin thickness of δ = 0.25 in.

Considering the case of optimum fin thickness δ = 0.25 in, an increase in ducting losses from 1 to 15 velocity heads in each, the inlet and exit ducting (i.e. a total change from 2 to 30 velocity heads), results in a decrease of the air flow by only 16%. At the same time the air temperature rise increases by 14.8%, with a small net loss in energy removed of 3.5%. This tendency of RCCS system performance, of being rather insensitive to stack and ducting parameter changes, prevailed over most parametric variations.

The stack uses a "secondary chimney design" described in the PSID to reduce sensitivity of RCCS air flow to exterior wind effects. Intuitively this design appears to be well suited to such an application. However, its performance under actual operating conditions should be subjected to field testing. In the current design the lower stack inlet/outlet ports are about 17.5 m above the top of the RCCS cooling panels, and the top ports are 27.5 m above the top of the cooling panels. While the previous evaluations assumed full draft contribution from this upper stack section, this Base Case is being compared in Figure B-5 to a Case of a stack height of 17.5 m only, i.e. completely disregarding the upper stack section. The resulting loss in steady state performance amounts to about 11% less air flow, about 10% increased air temperature rise, with a net loss in energy removal of about 2.6%. Also included in Figure B-5 are the PSID performance predictions for normal full power operation. The PSID data generally tend toward slightly higher air flows and slightly lower air temperature rises, resulting in virtually identical energy removal rates.

Steady state performance is a very strong function of reactor vessel temperature, and an increase of only 6°C form 219°C to 225°C increased the RCCS energy removal by more than 5%. This means that under normal power operation any variations in flow resistance would be compensated for by minor adjustments in the vessel temperature. As was also pointed out in the accident analysis of Section 3, the reactor vessel and RCCS panel thermal emissivity are essential for good performance. An increase from ε = 0.8 to only 0.85 in the reactor cavity resulted in 6% higher energy removal. While emissivities of this order are readily achievable for steel surfaces, the surface emissivities ought to be controlled by technical specifications to avoid, for instance, inadvertent painting or polishing of these surfaces.

Based on the above parametric evaluations, an effective stack height of 22.5 m, a fin effectiveness factor of ϕ = 4.4, a thermal emissivity of 0.8, and a set of loss coefficients k_{in} = 16 and k_{ex} = 12 was generally used in our THATCH accident transients. (Test runs were also made with internally computed FEFs. However, values remained close to the above chosen level, and it was clearly more cost efficient to use a prescribed value of 4.4).

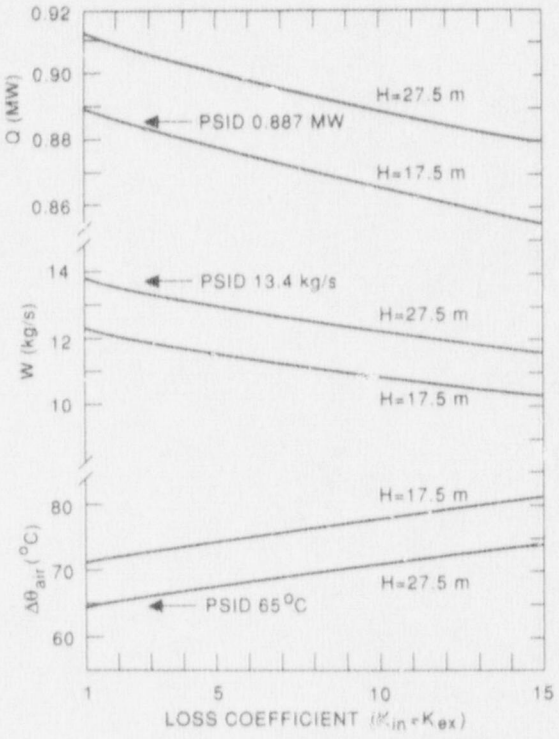

Figure B-5 RCCS Performance for Steady-State Full Power Production as Function of Ducting Pressure Drop Loss Coefficient for Various Stack Heights (s = 2.0 in.; δ = 0.25 in.; θ_v = 219°C; $\theta_{air\ in.}$ = 21°C)

APPENDIX C

REACTOR KINETICS AND XENON-135 MODEL FOR CORE HEATUP ACCIDENTS WITHOUT SCRAM

To model the neutronics and Xenon-135 concentrations during core heatup accidents without scram the following point kinetics model [Cheng, 1976] and Xenon-135 depletion model [Knief, 1981] were incorporated into the THATCH code.

The reactor point kinetics are modelled as follows using six delayed neutron groups:

$$\frac{d\tilde{P}}{dt} = \frac{\rho - \beta}{\ell^*} \tilde{P} + \sum \lambda \tilde{C} \qquad \text{(C-1)}$$

$$\frac{d\tilde{C}_i}{dt} = \frac{\beta_i}{\ell^*} \tilde{P} - \lambda_i \tilde{C}_i \qquad i = 1,6 \qquad \text{(C-2)}$$

where $\tilde{P} = P/P_O = N/N_O$, with P the reactor power, P_O the steady state full power level, N the neutron flux and N_O the neutron flux at steady state full power, and $C_i = C_i/N_O$.

Further

P = reactor Power

C_i = delayed precursor concentrations of group i

λ_i = decay constant of group i

β_i = delayed neutron fraction of group i

β = total delayed neutron fraction

ρ = total reactivity

ℓ^* = prompt neutron generation time

At initial steady state, $\tilde{P} = 1$ and $\rho = o$, with

$$\tilde{C}_i = \frac{\beta_i}{\ell^* \lambda_i} \; . \qquad \text{(C-3)}$$

The delayed group concentrations and decay times as well as the prompt neutron life time were taken from [GA, 1987-02] as follows

$\ell^* = 4.0 \times 10^{-5} s^*$

Delay Group	β_i	λ_i $[s^{-1}]$
1	2.140×10^{-4}	1.251×10^{-2}
2	1.424×10^{-3}	3.151×10^{-2}
3	1.273×10^{-3}	1.190×10^{-1}
4	2.567×10^{-3}	3.061×10^{-1}
5	7.470×10^{-4}	1.135
6	2.732×10^{-4}	2.876

The Xenon-135 concentration is obtained from the two following ODEs:

$$\frac{dI}{dt} = \gamma^{Te} \Sigma_f \Phi - \lambda^I I$$

and

$$\frac{dX}{dt} = \gamma^X \Sigma_f \Phi - \lambda^I I - X\sigma_A^X \Phi - \lambda^X X \qquad \text{(C-5)}$$

where

I I-135 concentration

X Xe-135 concentration

γ_{Te} fission yield of tellurium or iodine (due to short half-life of Te-135)

γ^X fission yield of Xenon-135

$\Sigma_f \Phi$ the fission rate [fission/m^3s]

λ^I, λ^X iodine and Xenon decay constante $[s^{-1}]$

σ_A^X microscopic Xenon-135 cross section $[m^2]$

The steady state full power concentration of iodine and xenon follow from the above equations as

$$I_o = \frac{\gamma^{Te}}{\lambda^I} (\Sigma_\phi \Phi)_o \qquad \text{(C-6)}$$

* Note apparent typographical error in [GA, 1987-02]

and

$$X_o = \frac{\gamma^{Te} + \gamma^{x}}{\frac{\sigma_A^x}{\Sigma_f} (\Sigma_f \Phi)_o + \lambda^x} \quad (\Sigma_f \Phi)_o \tag{C-7}$$

Using these to scale equations 4 and 5, one obtains

$$\frac{d\tilde{I}}{dt} = \lambda^I (\tilde{P} - \tilde{I}) \tag{C-8}$$

and

$$\frac{d\tilde{X}}{dt} = \frac{\lambda^x + G}{\gamma^x + \gamma^{Te}} (\gamma^x \tilde{P} + \gamma^{Te} \tilde{I}) - (G \tilde{P} + \lambda^x) \tilde{X} \tag{C-9}$$

where

$$\tilde{X} = X/Xo, \quad \tilde{I} = I/Io$$

$$\tilde{P} = P/Po = \Sigma_f \Phi / (\Sigma_f \Phi)_o$$

and

$$G = \left(\frac{\sigma_A^x}{\Sigma_f} \right) (\Sigma_f \Phi)_o = \left(\frac{\sigma_A^x}{\Sigma_f} \right) \left(\frac{P_o}{E} \right)$$

where

Σ_f is the macroscopic fission cross section, P_o the steady state, full power, power density and E the energy per fission.

The values used are

$\gamma^{Te} = 0.056$; $\gamma^x = 0.003$

$E = 200$ MeV/fission $= 3.2042 \times 10^{-11}$ J/fission

$P_o = 5.96$ MW/m^3

$\lambda^I = 2.9 \times 10^{-5}$ 1/s ; $\lambda^x = 2.1 \times 10^{-5}$ 1/s

The macroscopic fission cross section data were estimated by GA [GA, 1987-03] for a single group thermal cross section as follows:

$$\Sigma_f = 0.00251 \frac{1}{cm} \quad \text{(begin of cycle)}$$

$$= 0.00213 \frac{1}{cm} \quad \text{(end of cycle)}$$

The corresponding total macroscopic cross sections were given as

$$\Sigma_t = 0.00427 \quad \text{(begin of cycle)}$$

$$= 0.00380 \quad \text{(end of cycle)}$$

For the microscopic absorption cross section of Xenon a value of 2.65×10^6 barn ($=2.65 \times 10^{-22}$ m^2) was used for the base case calculations. The total change in reactivity is composed of the contributions from

fuel temperature change
moderator temperature change
reflector temperature change
xenon concentration change

and can be expressed as

$$d\rho = c_D d\theta_{fuel} + c_M d\theta_{moderator} + c_R d\theta_{reflector} + c_X dX \qquad \text{(C-10)}$$

The core temperature coefficients were given in Chapter 4 of the PSID and are tabulated in integrated form from a base cold temperature in [GA, 1987-02]. The Xenon coefficient is

$$C_X = - \frac{\sigma_A^e}{\Sigma_t}$$

where the above EOC values were used for Σ_t.

For typical ATWS transients, in particular in LWRs, transient analyses are extended over relatively short time spans. In contrast, for the core heatup accidents, to be considered here, several hundred hours of a transient must be considered. For such long time applications the typical implicit finite difference solution to the above set of nine simultaneous ODEs were found to be too time consuming and the DGEAR ODE solver of the IMSL library was employed. As the reactivity increases typically remained small, further simplifications of the currently used point kinetics equations could most likely be employed. This has not been done at this time.

APPENDIX D

INITIAL BAND APPROXIMATION MODEL FOR REACTOR CAVITY RADIOACTIVE HEAT TRANSFER IN THE PRESENCE OF PARTICIPATING GASES

To obtain an initial estimate of the effect of participating gases like H_2O and CO_2 on the radiation heat transfer from the reactor vessel to the RCCS panels, the Band Approximation Model, as described by Sparrow and Cess [1988], was applied (ibid Sec. 8.3).

As pointed out by Sparrow and Cess, this model "although crude at best, nevertheless constitutes a reasonable first approach" towards radiative heat transfer in non-grey gases.

For use of this method, the user must choose the band width of the various absorbing bands. Sparrow and Cess give in Section 1.3 integrated band absorption data for both H_2O and CO_2 and the approximate temperature and pressure dependence of these data. Only the results for H_2O will be given here, since that is the item of most concern.

The band widths were iteratively adjusted here such that over the temperature range of 400 to 800 K the total absorption of all bands matched the known Planck absorption coefficients as well as possible. The final band width selected in this way were:

Band (μ)	2.7	6.3	20
Lower Limit (μ)	2.50	5.00	20
Upper Limit (μ)	3.00	7.00	50

The 1.38 and 1.87 μ bands were included in the evaluation, but their contributions were found to be negligible in the current temperature range. With the above chosen band width the averaged absorption coefficients $\bar{\kappa}$ were computed and compared to the Planck mean absorption coefficient $\kappa_{p\ell}$ in Table D-1.[4]

Using these values, the radiative heat flux between two black surfaces of prescribed temperatures was evaluated, parametrically varying the hot surface (reactor vessel) from 450 K to 1000 K, but keeping the cold surface at 373 K, representative of RCCS panel temperatures. (Variations of the cold surface temperature were also applied and yielded about the same results.) Table D-2 gives the resulting optical thickness $\tau = \bar{\kappa} L$, where L is the cavity gap width. It also gives the dimensionless radiant heat flux $\bar{Q}$ which is the ratio of actual heat flux to heat flux across a transparent gas.

It is seen that the gas is optically thick ($\tau >> 1$). Furthermore, the dimensionless heat flow remains fairly constant over a wide temperature range,

[4] Note that by definition the average absorption coefficient must be larger than the Planck coefficient.

and even if our values of $\bar{\kappa}$ were inaccurate, this would not affect the results significantly, as shown by including values of $\bar{Q}$ evaluated for $\tau = 8$ and 1000.

Thus, the Band Approximation Model indicates that the participating gas H_2O in the reactor cavity will reduce the radiant heat transfer by about 32% since:

$$\bar{Q} = \frac{\text{Actual Radiant Heat Flux}}{\text{Transparent Medium Radiant Heat Flux}} \approx 0.68$$

This is the result to be applied in Section 8.

Table D-1 Averaged and Planck Mean Absorption Coefficients for H_2O

Temperature (K)	$\bar{\kappa}$ (1/m)	$\kappa_{P\ell}$ (1/m)
400	86.5	26.5
600	48.7	15.9
800	27.2	9.2

Table D-2 Optical Thickness τ_o and Dimensionless Heat Flux $\bar{Q}$ for Radiant Heat Transfer Between a Hot Surface at Θ_1 and a Cold Surface at 373 K

Θ_1 (K)	$\bar{\kappa}$ (1/m)	τ_o	$\bar{Q}_{\tau=\tau_o}$	$\bar{Q}_{\tau=8}$	$\bar{Q}_{\tau=1000}$
450	82.6	75.6	.690	.729	.685
600	60.9	55.7	.678	.717	.671
800	38.5	35.2	.673	.709	.661
1000	73.6	21.6	.660	.691	.640

NRC FORM 335 (8-87) NRCM 1102, 3201, 3202

U.S. NUCLEAR REGULATORY COMMISSION

BIBLIOGRAPHIC DATA SHEET

SEE INSTRUCTIONS ON THE REVERSE

1. REPORT NUMBER (Assigned by PPMB: DPS, add Vol. No., if any)
NUREG/CR-5261
BNL-NUREG-52174

2. TITLE AND SUBTITLE
Safety Evaluation of MHTGR Licensing Basis Accident Scenarios

3. LEAVE BLANK

4. DATE REPORT COMPLETED
MONTH: October
YEAR: 1988

5. AUTHOR(S)
P. G. Kroeger

6. DATE REPORT ISSUED
MONTH: April
YEAR: 1989

7. PERFORMING ORGANIZATION NAME AND MAILING ADDRESS (Include Zip Code)
Brookhaven National Laboratory
Upton, New York 11973

8. PROJECT/TASK/WORK UNIT NUMBER

9. FIN OR GRANT NUMBER
A-3827

10. SPONSORING ORGANIZATION NAME AND MAILING ADDRESS (Include Zip Code)
Division of Regulatory Applications
Office of Nuclear Regulatory Research
U.S. Nuclear Regulatory Commission
Washington, DC 20555

11a. TYPE OF REPORT
Technical

b. PERIOD COVERED (Inclusive dates)

12. SUPPLEMENTARY NOTES

13. ABSTRACT (200 words or less)

The safety potential of the Modular High-Temperature Gas Reactor (MHTGR) was evaluated, based on the Preliminary Safety Information Document (PSID), as submitted by the U.S. Department of Energy to the U.S. Nuclear Regulatory Commission.

The relevant reactor safety codes were extended for this purpose and applied to this new reactor concept, searching primarily for potential accident scenarios that might lead to fuel failures due to excessive core temperatures and/or to vessel damage, due to excessive vessel temperatures.

The design basis accident scenario leading to the highest vessel temperatures is the depressurized core heatup scenario without any forced cooling and with decay heat rejection to the passive Reactor Cavity Cooling System (RCCS). This scenario was evaluated, including numerous parametric variations of input parameters, like material properties and decay heat. It was found that significant safety margins exist, but that high confidence levels in the core effective thermal conductivity, the reactor vessel and RCCS thermal emissivities and the decay heat function are required to maintain this safety margin.

Severe accident extensions of this depressurized core heatup scenario included the cases of complete RCCS failure, cases of massive air ingress, core heatup without scram and cases of degraded RCCS performance due to absorbing gases in the reactor cavity. Except for no-scram scenarios extending beyond 100 hr, the fuel never reached the limiting temperature of 1600°C, below which measurable fuel failures are not expected. In some of the scenarios, excessive vessel and concrete temperatures could lead to investment losses but are not expected to lead to any source term beyond that from the circulating inventory.

Several future extensions of the current work are suggested.

14. DOCUMENT ANALYSIS - a. KEYWORDS/DESCRIPTORS
modular high-temperature gas reactor (MHTGR)
Preliminary Safety Information Document (PSID)
design basis accident

b. IDENTIFIERS/OPEN ENDED TERMS

15. AVAILABILITY STATEMENT
Unlimited

16. SECURITY CLASSIFICATION
(This page) Unclassified
(This report) Unclassified

17. NUMBER OF PAGES

18. PRICE

* U.S. GOVERNMENT PRINTING OFFICE: 1989-241-590:00020

UNITED STATES
NUCLEAR REGULATORY COMMISSION
WASHINGTON, D.C. 20555